Symmetry breaking in regenerating *hydra*: The role of fluctuations and cell mechanics

Dissertation

zur Erlangung des akademischen Grades
des Doktors der Naturwissenschaften
der Naturwissenschaftlich-Technischen Fakultät
der Universität des Saarlandes

von
Heike Linda Sander, geb. Wech
Eingereicht unter dem Namen Heike Dobicki

Saarbrücken, 2016

Tag des Kolloquiums: 17.03.2017

Dekan: Univ.-Prof. Dr. Guido Kickelbick

Mitglieder des Prüfungsausschusses:
Univ.-Prof. Dr. Albrecht Ott
Jun.-Prof. Dr. Franziska Lautenschläger
Univ.-Prof. Dr. Karin Jacobs
Dr. Martin Brinkmann

Eidesstattliche Versicherung

Hiermit versichere ich, Heike Dobicki, an Eides statt, dass ich die vorliegende Arbeit, "Symmetry breaking in regenerating hydra: The role of fluctuations and cell mechanics" selbstständig und ohne Benutzung anderer als der angegebenen Hilfsmittel angefertigt habe. Die aus anderen Quellen oder indirekt übernommenen Daten und Konzepte sind unter Angabe der Quelle gekennzeichnet. Die Arbeit wurde bisher weder im In- noch im Ausland in gleicher oder ähnlicher Form in einem Verfahren zur Erlangung eines akademischen Grades vorgelegt.

Unterschrift:

Ort und Datum:

"It's still magic even if you know how it's done."

– *Terry Pratchett*

UNIVERSITÄT DES SAARLANDES

Abstract

F7 Naturwissenschaftlich-Tech. Fakultät II
7.2 Biologische Experimentalphysik

Symmetry breaking in regenerating hydra: The role of fluctuations and cell mechanics

by Heike Dobicki

The transition from an isotropic tissue to an anisotropic one is one of the first steps in the development of multicellular organisms and not yet fully understood. While some keyplayers of the molecular processes after the initial polarization are well known, the discussion about the conclusive mechanism is ongoing. Here experiments investigating *de novo* symmetry breaking in hydra spheroids suggest a mechanical basis of the self-organized symmetry breaking process. Mechanical oscillations on several timescales, fluctuations of the main axis orientation, and scale free behavior are connected to symmetry breaking. The process is closely linked to the cytoskeleton. Especially the presence of polymerized microtubules is crucial during the establishment of the new symmetry. A self- organization process based on inherent mechanical abilities that is able to induce polarization and a link to the wnt-pathways that are known to play a role in establishment of polarization is proposed.

Symmetriebruch in regenerierender *Hydra*: Die Rolle von Fluktuationen und Zellmechanik

Der Übergang von einem isotropen in ein ansiotropes Gewebe ist noch nicht völlig verstanden. Während einige beteiligte genetische und molekulare Mechanismen der Polarisation bekannt sind, wird der zugrundeliegende Mechanismus des Symmetriebruchs noch diskutiert. In dieser Arbeit wird die Fragestellung mit Hilfe von regenerierenden Hydra Fragmenten untersucht. Es zeigt sich, daß mechanische Fluktuationen der Symmetrie und skalenfreies Verhalten im Zusammenhang mit dem Symmetriebruch auftreten. Der zugrundeliegende Mechanismus steht in engem Zusammenhang mit dem Vorhandensein von polymerisierten Mikrotubuli. Es wird ein mechanischer, selbstorganisierender Prozess des Symmetriebruchs vorgeschlagen und eine Verbindung zu den bekannten *wnt* pathways vorgeschlagen.

Acknowledgements

Many thanks to all the people who accompanied this thesis. Thanks to my supervisor Prof.Dr. Albrecht Ott. Thank you to Jun-Prof. Dr. Franziska Lautenschläger for fruitful discussions and for disentangling of loose ends. Thanks to my office mates and coworkers who kept me company and provided an open ear to share all complaints and happy times, and to the wonderful people working at the Lautenschläger Lab.
Thanks to Aravind, who was taking care of the *hydra*. A special **Thank You** goes to Mathias Sander and Henrietta, without whom this work would not have been possible, and to Birgit and Horst for continuous support.

Contents

List of Figures

List of Tables

Chapter 1

Introduction

Symmetry breaking and axis formation are among the first steps in evolution and embryonic development of multicellular organisms. All multicellular organisms originate from a hollow spherical isotropic tissue. During development, they break the initial symmetry and form an elongated, asymmetric body. This process is concluded by the formation of an organizing center that maintains the new symmetry. The formation of this organizing center requires a concerted action of tissue cells. Without superordinate structures, synchronization of the cells based on next-neighbor communication needs to take place. The decision process that induces symmetry breaking is not yet understood. Different species seem to have developed an individual solution to this decision problem, which appears counterintuitive from an evolutionary point of view. In *Xenopus*, the entrypoint of the sperm and the subsequent, microtubule mediated cortical rotation of the cytoplasm dictate the dorsoventral axis [1]. In *Drosophila*, the maternally transmitted asymmetry is irreversibly locked during oogenesis through a hierarchical series of symmetry-breaking steps[2].

The decision process of the localization of the organizer has been discussed using different models, as reaction diffusion, pre-patterning, asymmetric cell division, cell -migration and -sorting, or the position of the individual cell in the embryo [3]. However, there is no conclusive theory that describes the common mechanism on which all these symmetry breaking processes are based and whether one exists. Coherent understanding of all experimental findins, among them an observed stochastic fluctuations of RNA and Protein expression levels [4–6]. Recent publications [7, 8] suggest a mechanically induced symmetry breaking, driven by the cytoskeleton in tissue and cells. The cytoskeleton is an evolutionary very old structure found in all cells. A substantial part of the cytoskeleton, including tubulin structures, evolved before the last common prokaryotic ancestor [9]. The cytoskeleton is therefore a good candidate for a common element in symmetry breaking.

An important molecular component in cell and tissue polarization is the genetic wnt pathway, a complex signal transduction pathway which allows the cells to react to external influences. Brunet et al [7] showed that a cytoskeleton mediated mechanotransduction process can cause the activation of the canonical wnt pathway by activating a component downstream of wnt in zebrafish as well as *drosophila*. The canonical wnt pathway is conserved throughout the eukaryotic superkingdom. Wnt and its associated pathways play a role in both initial polarization and mesoderm invagination in *bilateria* and the setting up and maintaining of an organizer in *coelenterata* [10–12].

Here I investigate symmetry breaking using *hydra*, a member of the *coelenterata* and a model organism for early embryonic development[13]. The fresh-water polyp consists of a cell bilayer with a radial-symmetric body plan. Aggregates from single cells and sufficiently small tissue pieces form hollow spheres that undergo osmotically driven oscillations [14], break the initial symmetry and regenerate into fully functional, albeit small adult polyps with a head and a foot. The role of the canonical wnt pathway in the set up of the head organizer and in body plan maintenance of *hydra* has been quite well investigated [15–20].

However, there is no consensus about the exact mechanism how and why the wnt head organizing center is initially established at a specific location. In *Hydra*, the possibility of a self-organizing framework for this process has also been introduced [21]. Gamba et al. proposed a process based on self organized criticality that reproduces RNA expression fluctuations during regeneration as well as the influence of a temperature gradient on the axis orientation [22].

Soriano et al. [23] presented a Turing model driven by the mechanical stimulus provided by the osmotically driven oscillations. This approach has been refined by Mercker et al., who postulate a feedback loop between tissue stretching, resistance to lateral tissue stretch and the behavior of a head-defining morphogen [24]. This implies a connection between mechanical behavior and symmetry breaking in *hydra* regenerates. However, the exact nature and dynamics of the morphogen behavior is not settled yet. Turing mechanism, self organized criticality and curvature mediated approaches reproduce experimental results equally well. The unifying factor is the mechanical tissue stress, indicating a possible role of the cytoskeleton.

In this work, I investigate and confirm the hypothesis that the cytoskeleton plays a crucial role in symmetry breaking of *hydra* regenerates.

Using video microscopy I find that within the investigated size range, *hydra* regenerates adjust themselves to an ideal regeneration size. Below a critical size, symmetry is almost always lost. Besides large osmotically driven oscillations, fast rhythmical trembling and shape fluctuations play a role in symmetry breaking of *hydra* regenerates. $1/f$ noise and power law distribution of the fluctuations are observed. A local mechanical stimulus applied on the regenerate using a micropipette aspiration system determines axis

orientation.

Investigations using confocal microscopy and application of cytoskeleton drugs reveal the predominant role of microtubule polymerization. Large contractile actin structures need to be absent during the symmetry breaking moment, but seem to play a role in the subsequent elongation of the spheroid.

The results in this work imply a symmetry breaking process in *hydra* based on inherent polarizing properties of the microtubule cytoskeleton that is stabilized by the subsequent polarization of the actin cytoskeleton. From an evolutionary point of view, this suggests that the cytoskeleton substantially contributed to the emergence of complex body plans.

Chapter 2

Fundamentals

2.1 Early embryonic development of animals

The existence of the animal embryo starts with the fertilization of the oocyte by the sperm. First, a cleavage process, cell division without growth, occurs. This results in a dense sphere of 16 cells called the morula. The individual cells in the morula that are produced by cleavage are called blastomeres. After additional cell divisions and reorganization, the blastula, a hollow sphere consisting of a cell monolayer, emerges. The blastula undergoes a first symmetry breaking process that defines the mouth opening in diploblastic animals, like *hydra*. In triploblasts, after the emergence of a hollow cell bilayer sphere, gastrulation induces a mesodermal invagination at one specific location. This leads to the formation of a hollow bilayer sphere with one opening. For this invagination, a synchronized movement and deformation of cells is necessary. At this point the mechanical cues, among other signals, cause the differentiation of cells into different germ layers [25] (section 2.6.1). The embryonic cells undergo their first differentiation step. The role of the cytoskeleton in embryonic development is described in section 2.6.1 [26].

2.2 Symmetry breaking in development of organisms

Multicellular organisms have several organizing centers that establish the axes of the developing embryo [27]. The first organization step in embryonic development involves a polarization of an isotropic cell aggregate and the subsequent development of an organizing center. The outcome of these processes is conserved. However, the biochemistry and the mechanics of the process can vary, even within a phylum [28, 29].
Several mechanisms that lead to the emergence of the organizing centers have been proposed:
Pre-patterning presumes an external factor to dictate the axis orientation [26]. *Xenopus*, a frog, is an example for pre-patterning. The first body axis of the developing embryo is defined by the entrypoint of the sperm into the egg and the subsequent formation of the spermaster, which is a specialized centrosome. The consecutive spatio-temporal organization of the fertilized egg is promoted by the arrangement of microtubules, which establish dorso-ventral polarity [30]. Another example of pre-patterning is *Drosophila melanogaster*. Depending on the position of the oocyte in the maternal body, molecular determinants are asymmetrically localized within the oocyte and distributed differently among the daughter cells.
The **inside–outside model** [31] proposes that the position of the cells within the morula (section 2.1) determines their fate. Cells on the outside differentiate into the trophoectoderm, cells on the inside into endoderm. Mammalian embryos are completely symmetric until the 8 cell stage. All cells have the same potential and are genetically and morphologically indistinguishable [3]. They only differ in their position within the embryo. No biochemical signal is needed in this model, the positional information alone induces cell differentiation. However, the heterogeneity of cells in the morula cannot be explained by position alone [4].
The **cell polarity model** [3] is based on the asymmetry of blastomere membrane domains. Initially, the asymmetry stems from the orientation of cells within the division plane, leading to a polarization into an apical and dorsal domain. The cells are capable of dividing either symmetrically or asymmetrically, transmitting the apical domain to either both or one of the daughter cells. Cells that inherit the apical domain grow into trophoectoderm. However, no causal link between the orientation of the division plane and the cell fate specifications has been shown.
Recent experimental results demonstrate the importance of stochastic mRNA fluctuations during embryonic development and symmetry breaking [22, 32]. None of the presented models takes these processes into account.

In addition, all animals share a common ancestor that precedes the emergence of multicellular organisms, presuming a common mechanism underlying the breaking of symmetry.
Piccolo et al. proposed an explanation that the mechanics of embryonic development, specifically at the onset of gastrulation, is evolutionary conserved [29]. Cytoskeletal drugs (including nocodazole, section 2.7, and blebbistatin) can arrest the early steps of gastrulation in zebrafish as well as in *drosophila* [7, 33]. The effect can be rescued by mechanical stimulation in *drosophila* and zebrafish. Current knowledge states that early gastrulation is induced by the evolutionary highly conserved wnt pathways (see section 2.4). However, mechanical stimulus results in wnt independent nuclear translocation of β-catenin. This demonstrates that mechanical stimuli can have an effect on embryonic development and cell fate using a pathway that is evolutionary highly conserved. Mechanical stimulus is either independent or higher in the regulatory hierarchy (upstream) of known biochemical pathways that play a crucial roles in gastrulation processes (see section 2.4), [7].
It is unlikely that every organism developed its own symmetry breaking mechanism during evolution.
In support of this, van den Brink et al. observed that isolated aggregates of ≈300 mouse embryonic stem cells self-organize into polarized structures. These structures exhibit collective behavior including symmetry breaking, axial organization and axis elongation [34]. Self-organization may be an intrinsic ability of cells in a collective. This self-organized behavior has been linked to the wnt pathway (see 2.4). Krotov et al. postulated a self-organized system at criticality in the embryonic development of *Drosophila* [6]. To explain the early organization and polarization in regeneration, a self organization process involving mechanical forces on individual cells was postulated, which takes into account the different biochemical pathways [3].

2.2.1 Self-organization in biological systems

In physics and chemistry the term self-organization is an expression that refers to out-of-equilibrium processes. A self-organized out of equilibrium system continuously consumes and dissipates energy to maintain itself [35]. Self-organization leads to the emergence of complex patterns in systems from units of less complexity. No shaping external stimulus is necessary to determine the outcome of the patterns. Common features found in self- organized systems are non-linearity, breaking of symmetry and the emergence of patterns from stochastic fluctuations [36]. Examples of self organization in biological systems were first reported in 1790 by Immanuel Kant in his Critique of Judgement [37]. Self organization is found in Bird flocking, the formation of neuronal patterns and in

microtubule polymerization and depolymerization [38].
Self-organized criticality is a mechanism where a self-organized system develops towards criticality, a state where very small stimuli can determine the outcome of the system. Typical properties observed in self-organized systems close to the critical state are scale invariance, self similarity and 1/f noise [39].

2.3 *Hydra*

Hydra is a model for early embryonic development, especially the first symmetry breaking steps. It is a predatory fresh water polyp with a radial symmetry. It belongs to the phylum *Cnidaria*, class *Hydrozoa*, family *Hydridae* and genus *hydra*.
The size of the animals varies between 2 and 5 mm. The body plan of an adult *Hydra* (Figure 2.1) is a hollow tube with one main axis consisting of a head, body column and foot. The apical end exhibits a head with a hypostome and 3-12 tentacles arranged in a ring around the mouth opening. The foot or basal disc at the basal end produces a sticky substance that allows the animal to reversibly attach to different surfaces.
Hydra consist of two epithelial layers, the endoderm and the ectoderm, connected by the mesoglea (Figure 2.2). The mesoglea served as an attachment substrate for the cells and allows exchange of signals and nutrients (Figure 2.3). A third cell lineage, the interstitial cells, are multipotent stem cells [40] that differentiate into all non-epithelial cells within *Hydra* [41], including neurons, gland- and mucous- cells and the nematocytes, the distinctive characteristic of the cnidarians (section 2.3.5) [42, 43]).
The *hydra* species used in this work have strong regenerative capabilities due to its multipotent interstitial cells. The multipotent interstitial cells in *Hydra* are stationary [44] except during morphallaxis, the regrowth of a lost limb or body part. Migration of interstitial cells takes place to allow for a rapid position dependent nerve cell differentiation [45].
The current understanding of the body axis control and maintenance in the adult *hydra* is based on a model proposing two morphogens emerging in the hypostome: the head activator and the head inhibitor. Both are produced by the head organizer and form gradients along the body axis with the highest concentration at the head. The yet unknown morphogens are probably transported via gap junctions [46]. The operating distance of the inhibitor is shorter than of the activator, leading to the formation of new heads and subsequent buds in the lower third of the *hydra*. The molecular basis of the signals is unknown. However, wnt is a probable candidate for the head activator [27]. The head organizer is a structure in the hypostome that is molecularly similar to the embryonic Speman Organizer on a molecular level. The emergence of this organizer depends on *hydra*-wnt orthologues [17] (see section 2.4).
Hydra is flexible and reacts to its surroundings. A network of neurons synchronize the movement throughout the body [47]. Supercellular myonemes (contractile actin bundles) provide muscle like functionality. The bundles can span 6-8 individual cells and are involved in body contraction. *Hydra* can sense and adapt its body length via microtubules [48], although the exact mechanism and regulation of this process is not understood.
Hydra reproduces sexually and asexually and is able to switch between the reproduction

modi. Sexual reproduction takes place with the help of ovaries and testes growing on the body column. Asexual reproduction occurs through budding, the emergence of new, smaller animals that grow out of the lower part of the body column, develop from the apical to the basal end and detach after forming a foot. The animals can stretch immediately to the length of adult animals [48] and reach the cell mass of an adult within a week, if fed. This reproduction is possible due to a dynamic equilibrium between loss and production of tissue. Stem cells proliferate constantly. The excess tissue is discarded either via the mouth opening or during budding. A constant low motility of cells is observed [49]. *Hydra* does not age, however, the individual differentiated cells do. Senescence of the animal is induced following sexual reproduction [50].
The most striking capability of *hydra* is the regenerative ability. Lost body part are regrown and aggregates and small tissue pieces of approximately 20.000 cells regenerate into whole new animals. This process is described in section 2.3.1.

2.3.1 Regeneration and axis formation in *Hydra*

Aggregates of single cells [21, 51, 52] and small (around 200 μm in diameter) fragments cut from the body column of *hydra* can regenerate into whole animals [49]. The process of regeneration of small *Hydra* tissue pieces (200 μm) before starts with the formation of hollow spheres and healing of the tissue. These spheres undergo osmotically driven slow inflations that last between 1 and 7 hours. The inflations end with a rupture of the bilayer and a following fast deflation during which some cells are disgorged [14]. The purpose of this expelling is yet unknown. Three regeneration phases have been identified: The first phase is characterized by large, slow inflations and fast deflations. The *hydra* is mostly spherical, during this phase, no axis can be recognized. The breaking of symmetry happens at the transition between the first and the second regeneration phase [22]. The second phase is characterized by smaller inflations and a body axis elongation. The third phase involves the development of the tentacles and the foot of the regenerated *hydra*. During the whole regeneration, no cell- division or -migration was reported.
The regeneration is temperature dependent, there is a temperature optimum at 26 °C. Temperatures above the optimum cause death of the regenerates, temperatures below slow down the regeneration. The effect is strain dependent [53]. The *hydrae* used in this work have their optimum at 21 °C. It has been hypothesized that during this regeneration positional information is lost and a *de novo* formation of the oral-aboral axis and the head organizer is required [23]. Breaking of symmetry is supposed to induce the development of a head organizer which is producing morphogens to establish and maintain the adult

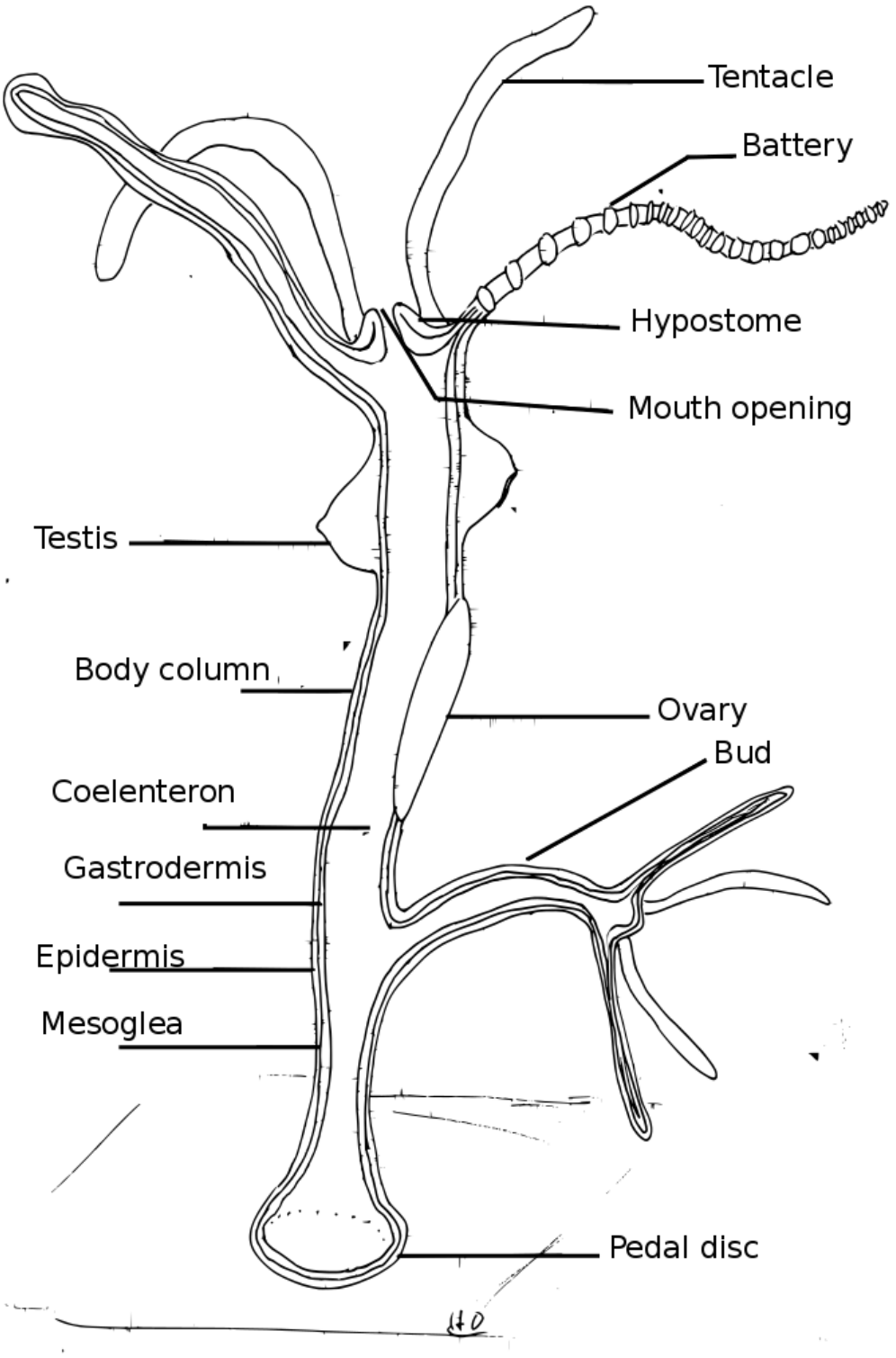

FIGURE 2.1: Schematic representation of the *Hydra* body plan. *Hydra* is a hollow cylinder that consists of a cell bilayer. The inner cavity is called the *coelenteron*. The body can be subdivided into three parts: In the lower third, the foot with the pedal disk produces a sticky substance and attaches to the substrate. Above the foot, buds are branching from the body. In the center of the body column, testes and ovaries can develop under unfavorable conditions like famine. The upper third includes the head with the hypostome, the mouth opening and the tentacles with battery cells.

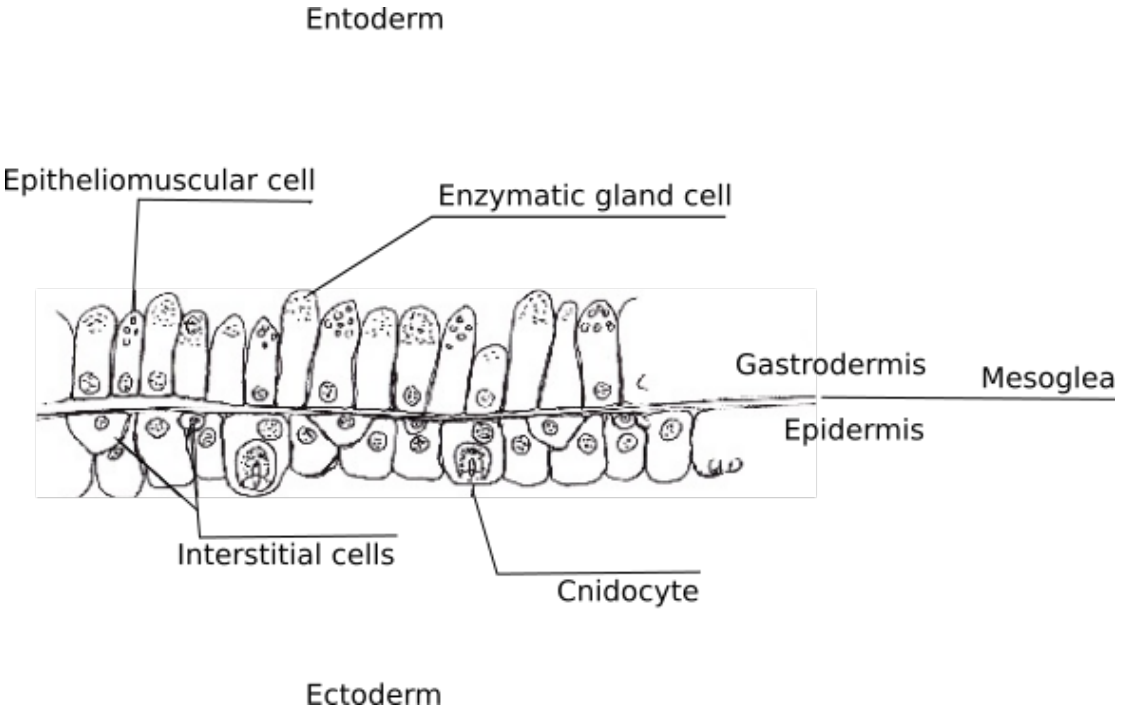

FIGURE 2.2: Epithelial bilayer of *hydra*. The entoderm and ectoderm are connected by the mesoglea, an acellular structure composed of water, collagens and heparan sulphate proteoglycans. The inner epithel or endoderm is called gastrodermis and is composed of epitheliomuscular cells end enzymatic gland cells. The ectoderm, also called epidermis, is composed of muscle cells, interstitital cells (among those nerve cells), and cnidocytes.

hydra body plan and thus defining the axis [22]. An early characteristic of the potential emergence of a head organizer is the local expression of ks1 mRNA [54].

2.3.2 *Hydra* head organizer

The head organizer is a structure located in the hypostome of adult *hydra*. It constantly maintains the structure of *hydra* body through its steady state tissue dynamics [49]. Several wnt genes (section 2.4), TCF (T Cell factor, a gene activated for the de novo creation and maintenance of the head organizer), elevated levels of β-catenin and ks1 are expressed in the head organizer. Wnt genes have been shown to induce head organizer formation, while β-catenin plays a crucial role in maintenance and activity [55]. The importance of β-catenin during the polarization preceding the mesodermal invagination in zebrafish β-catenin has been demonstrated by Brunet et al.. Artificially induced β-catenin activity can initiate gastrulation independently of wnt [7].

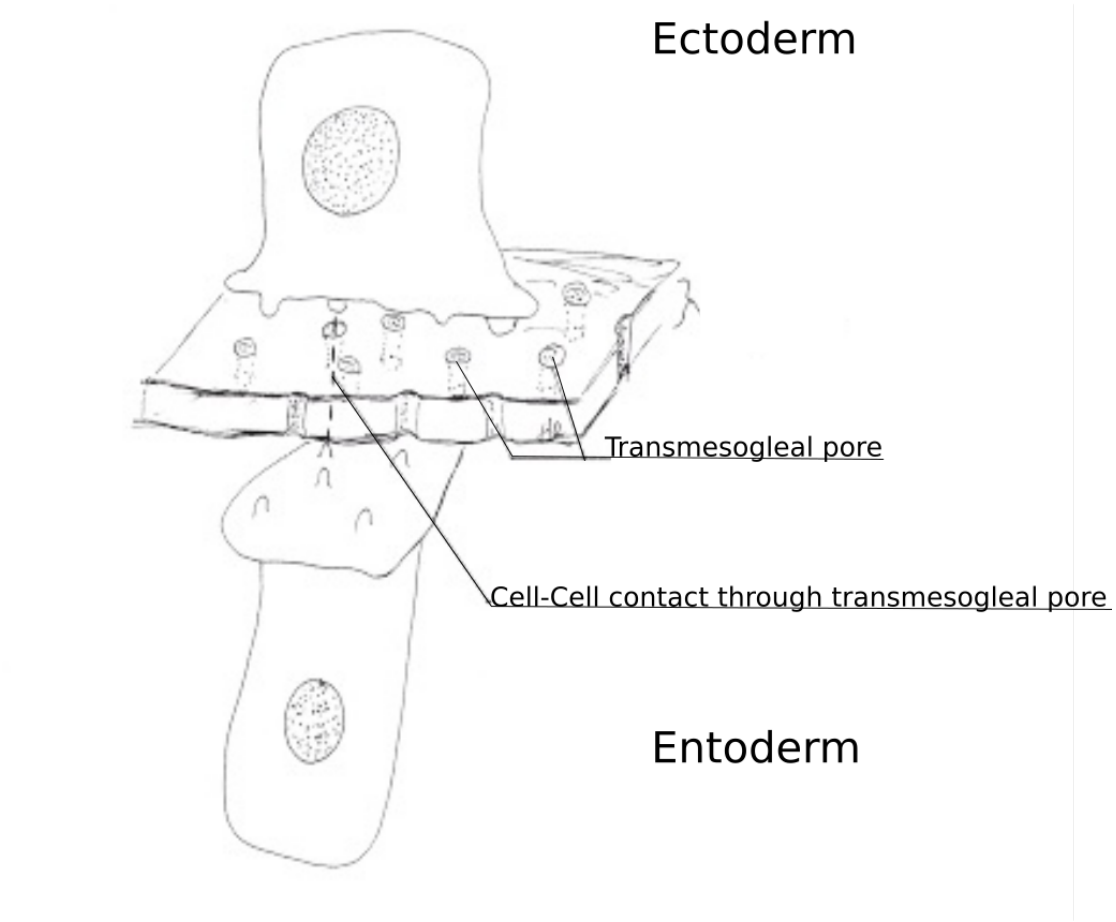

FIGURE 2.3: Detailed view of *hydra* epithelial bilayer. The mesoglea is perforated by transmesoglean holes through which cells of the ectoderm and the entoderm can communicate, exchange food and signals.

2.3.3 Head specific protein 1(Ks1)

Ks1, a *hydra* specific gene first described by [54], is expressed at the base of the tentacles in adult *hydrae*. During regeneration, clusters of ks1 mRNA appear throughout *hydra* regenerates and, at the axis locking moment, exhibit a scale free distribution. Cells with head forming potential need to express ks1 but not all ks1 expressing cells develop into head organizers. Ks1 expression is modulated, among others, by Protein Kinase C (PKC) and is part of the second non-canonical wnt pathway [56], (section 2.4). PKC modulates multiple cellular processes, including the morphology of the F-Actin cytoskeleton [57].

2.3.4 Self-organized criticality in *Hydra* regeneration

A possible explanation for axis formation dynamics in *hydra* is based on self organization in tissue. It solely relies on next neighbor cell-cell interactions. The model proposes a factor X that is produced by every cell with a specific, temperature dependent rate ν. If

a concentration threshold within the individual cell is reached, X is distributed between the neighboring cells, with a certain loss. The concentration of X in the distributing cell is reset to 0 and additional X that it receives from neighboring cells above the threshold, and the production continues. The distribution between the neighbors is much faster than the production of X. The probability of the appearance of an avalanche consisting of X distributing cells and a resulting cluster of Cells with X above the threshold bigger than a specific site follows a power law with a negative exponent. If a cluster of sufficient size appears, the concentration of X stabilizes and the cluster does not participate in the dynamics of the system. The *hydra* sphere is polarized.
This self organization based on a production and decay rate and local distribution of a factor leads to a synchronized behavior of the whole system based on next neighbor interactions. This model reproduces the experimentally observed large clusters of ks1 mRNA (see section 2.3.3) and the observed ks1 mRNA fluctuations, that are scale free during the axis defining moment. In addition, the model predicts the behavior of the regenerating *hydra* in temperature gradients [23], by assuming that ν depends on metabolic rates and is therefore temperature dependent. The exact nature of the factor X remains elusive [22].

2.3.5 Nematocytes

Nematocytes are cells that, upon mechanical stimulation, discharge a harpoon-like venomous structure. They are the unique feature of the *cnidaria*. Nematocytes are used for hunting and defense and are located in the ectoderm of the whole animal with the highest concentration in the tentacles. Every nematocyte contains an organelle called the cnidocyst which is comprised of a bulbous capsule with a hollow tube structure coiled around it. On the outside, a hair like structure (cnidocyl) works as a trigger for the discharge. The discharge causes the tube-like structure to be ejected and to penetrate the target organism. The toxic content of the cnidocyst is then injected through the hollow tube [26]. Within the cnidocysts, intermediate filaments have been identified, showing that these are evolutionary as old as these simple metazoans [58].

2.4 Wnt signaling pathways

WNT is an evolutionary conserved protein family that plays a critical role in embryonic development. Wnt genes are defined by the similarity to the mouse wnt-1 protein and the wingless protein in *Drosophila* [59]. Homologues are found in organisms ranging from mammals to *hydra* [18]. Mutants lacking specific wnt-proteins fail to develop mesoderm and to initiate gastrulation [10]. Inhibited axis formation in (artificially or naturally) developmentally impaired embryos can be rescued by injection of several wnt-mRNAs. A duplicated body axis in *Xenopus* wildtypes can also be induced by wnt-mRNA injection [59, 60].

Wnt ligands have three major roles in organisms: Change of cell fate (canonical wnt pathway), change of cell polarity and embryonic induction (the induction of new embryonic tissue). Wnts are secreted proteins and their ligands are membrane bound [61]. There is one canonical and several noncanonical wnt pathways.

The canonical wnt pathway changes cell fate. In absence of wnt signals, the frizzled receptor binds to dishevveled, allowing a complex of proteins to destroy cytosolic β-catenin. Binding of wnt to the dishevelled/frizzled complex inhibits the β-catenin degradation. β-catenin is subsequently transported into the nucleus and activates TCF (T Cell factor). TCF activations causes cells to change their fate and, in *hydra*, to develop into head organizer cells [15, 17]. In zebrafish and *drosophila* nuclear translocation of β-catenin activates mesoderm specification, a crucial step during gastrulation [7, 62].

The non-canonical planar cell polarity wnt (wnt-pcp) pathway interacts with JNK (c-jun N terminal Kinase) to regulate convergent extension movements in embryonic development [62–64]. JNK also controls microtubule reorganization in cell polarization events [65], a wnt induced JNK mediated reorganization of microtubules has been observed [66]. A major restructuring step of the cellular polarization is the microtubule-mediated asymmetrical transport of wnt-8 mRNA, requiring an asymmetric cytoskeleton reorganization beforehand which is induced by the so called Dorsal Determinant [10, 12]. Additionally, JNK is activated by actin stress fiber mediated polarization events of the cell (section 2.5.2). Conserved wnt pathways play a role in cellular polarization and the subsequent change in tissue shape is similar to gastrulation in vertebrates [10]. Sepich et al. found that the wnt-pcp pathway controls the positioning of microtubule organizing centers within the cell, thus playing a role in cell polarization [67].

The wnt/frizzled/dishevelled complex also activates the Rho-ROCK pathway, a major regulator of the cytoskeleton. The Rho-ROCK Pathway controls acto-myosin contractions in cells (see section 2.5.2). In addition, it mediates the spatial and temporal integration of wnt. ROCK is also involved in the de novo formation of stress fibers.

The Rac-Rho complex, another member of this pathway, mediates the nuclear accumulation of β-catenin. Thus it interacts with the canonical wnt pathway [68]. ROCK also mediates the binding of profilin to actin, which in turn can result in restructuring of the cytoskeleton and gastrulation [64, 69]. This provides a link between cytoskeleton reorganization and cell or tissue polarization.
In addition, the wnt/frizzled/dishevveled complex controls PKC, a protein involved in microtubule dynamics (section 2.5.3) and also in *hydra* specific ks1 (see section 2.3.3). Another non-canonical wnt pathways involves local stabilization of microtubules via dishevveled [70]. The wnt β-catenin induced formation of the body axes has been observed in multiple vertebrates [71] and invertebrates [7, 15, 27, 62]. In *Hydra*, inhibiting the wnt signaling pathway prevents head organizer formation (section 2.3.1), [16].
Recently, an integrated pathway that connects the canonical and the non-canonical pathways has been proposed [72] and observed for one specific wnt (wnt5a) [73]. A review about the role of the wnt pathway (in *Hydra* as well as other organisms like zebrafish (*Danio rerio*)[12] and *Xenopus laevis* [74]) embryonic axis formation has been published by Broun et al. [18].

2.5 Cytoskeleton

The cytoskeleton is a dynamic protein scaffold found in most eukaryotic cells. Its main structural components are actin filaments, microtubules and intermediate filaments. They form a connected network connected between each other, to other cellular structures and the extracellular matrix by a large collection of accessory proteins. Cellular morphology and properties as migration, polarization and attachment to the substrate are determined by the cytoskeleton. Within the cells, nutrient and organelle transport, cell division and the perception of mechanical stimuli is mediated by the cytoskeleton. [26]

2.5.1 Intermediate filaments

Intermediate filaments are rope like structure with a diameter of ≈10 nm. The intermediate filament protein family is structurally very diverse. The common structural unit of the intermediate filament proteins is a ≈340 Amino acid region which is structurally similar in all filament types. The common building block is the coiled coil, a parallel α-helix dimer. Intermediate filaments are non-polar and were generally believed not to be involved in cell polarity [75]. However, recent studies indicate that members of a specific family (Septins) which form non-polar polymers that resemble intermediate filaments are important for cell polarity in a number of cell types [76–78].

2.5.2 Actin

Actin filaments are cable-like structures with a diameter of 6 nm. They consist of a family of over a dozen protein classes. In this work, Filamentous Actin (F-Actin), one of the most abundant and structurally important actins, is investigated. Actin filaments are a left handed helix of actin monomers [79]. The filaments are polarized. They have a fast(+)- and a slow(-)- growing end. Actin generates mechanical forces in the cell and can exert mechanical forces on the surrounding. One possibility is by polymerization and depolymerization, frequently observed in cell motility. Another possibility for actin to generate forces in cells is the assembly with myosin, an action associated motor protein, and connecting proteins into contractible stress fibers. Actin contractility is under the control of the Rho-ROCK pathway [80].

2.5.2.1 Stress fibers

Stress fibers are bundles of actomyosin that can be compared to the actomyosin arrays of muscle cells. They are the main mediators of cell contraction. Stress fiber bundles are formed by 10-30 actin filaments. Their structure exhibits a periodic banding of alpha actinin, F-actin and myosin. New stress fibers are formed *de novo* or by cutting of and elongating existing filaments. A nucleation-promoting protein is Formin [81]. The formation of stress fibers is modulated by Rho GTPase signaling cascades [82], which is in turn part of the wnt pathway [68](see section 2.4). Inhibiting elements of the Rho GTPase signaling cascade with y-27632 (section 2.7) leads to a disassembly of stress fibers [83, 84] and has been observed in this work as well.
Most stress fibers originate from focal adhesions, large macromolecular assemblies that provide a connection between the cytoskeleton and the extracellular matrix of the cell. Another stress fiber connecting structure are adherens junctions which connect the actin cytoskeleton of neighboring cells in tissue. An important component bound in these junctions is β-catenin, which functions in cell adhesion and as transcription factor. The choice between these two roles depends on wnt induced conformational changes [85] (section 2.4). There are three main stress fiber structures. Ventral stress fibers are attached to focal adhesions at both ends. Dorsal stress fibers, which start from one focal adhesion and point away from the extracellular matrix. Transverse arcs, bundles that form on the dorsal side of migrating cells, appear behind the protrusive part of the cell. The ventral stress fibers play the mayor role in contraction of the cell, the exact roles of the other two configurations is not yet understood [86]. Stress fibers are important in migration and cell shape changes during embryogenesis [87].
In *hydra*, myonemes, large supercellular F-actin structures spanning 6-8 cells can be observed that act as muscles and play a role in folding of healing *hydra* tissue during regeneration. Their contraction occurs in less than a second, relaxation is slower and takes several seconds [49, 88, 89].

2.5.3 Microtubules

Microtubules have a pipe-like structure with an outer diameter of 25 nm and an inner diameter of 16 nm. The tubulin family contains five protein classes. Here, only the α and β-tubulin are considered.
The subunits are organized in heterodimers, which form protofilaments that associate laterally to form a sheet that folds into a cylindrical tube that is called microtubule. Due to the asymmetry of the heterodimer subunits, microtubules are polar. Microtubule associated motor proteins as Dynein and Kinesin allow directional transport of vesicles,

biomacromolecules and organelles in cells. Microtubules can be either static, as in flagellae, or dynamic, as in the cytosol of cells, and undergo constant cycles of growth and shrinkage. They exhibit periodic, synchronized oscillations of their length. The observed in vitro periodicities are about 10 min, depending on the exact conditions and on the temperature [38]. In vivo, growth rates are about 30 nm/sec over times of approximately 4 minutes [90]. The dynamics of this process can be altered by microtubule stabilizing- and destabilizing agents. Assembly of microtubules depends on Guanosintriphosphate (GTP), that is converted into Guanosindiphosphate (GDP), thus, the process requires energy. The oscillations depend on a constant conversion of GDP back into GTP. After every assembly, the GTP concentrations decrease quickly below the threshold necessary for tubulin assembly. When the GTP in the solution is depleted, microtubules start to disassemble into Oligo-GDP Tubulin, oligomers of tubulin that bind GDP. Only when this GDP is set free and available in the system it can be conversed back to GTP. The constant, slower conversion of GDP back to GTP restores the necessary threshold levels and allows another pulse of assembly. The difference between the time of the tubulin assembly (depletion of GTP, and increase of GDP) and the lag time until the GTP is set free leads to spatially and temporally synchronized oscillations. The conversion between GTP to GDP and back is mediated by Rho GTPases, which can act as biological timers [91].

Microtubules can act cooperatively. Multiple microtubules exhibit a fluctuating behavior in their growth and shrinking patterns which is different from a single microtubule. In addition, it is easier to add a subunit to a growing microtubule than to a shrinking one, thus adding a nonlinear sub-reaction to the system. The oscillations have been observed in vivo and in vitro. The oscillation behavior of microtubules has been suggested as a possible mechanism behind a biological timer [38]. [92] described rhythmical microtubule dependent oscillations of the cell margin in chicken embryonic fibroblasts. The average microtubule assembly rate in cells is 30 nm/sec, disassembly rate is 500 nm/sec [90]. The behavior depends on the shape of the reaction space and on the oscillation dynamics as described above [38, 93]. Microtubules are, among others, under the control of at least two non-canonical wnt pathways (section 2.4). Dishevelled can locally stabilize microtubules, thus contributing to cellular cytoskeleton asymmetry (section 2.5.4). In addition, phosphorylated β-catenin initiates microtubule regrowth at the centrosome [94] and a Dynein-β-catenin complex tethers microtubules to adherens junctions [95], thus plays a role in tissue polarization.

2.5.4 Role of cytoskeleton in cell and tissue polarization

In cells, polarity is defined by two fundamental properties. First, the asymmetric accumulation of mobile components between opposite poles of the cell, as in the fertilized oocyte. Second, the asymmetric organization of inherently polar cytoskeletal filaments, particularly actin and microtubules, as in all structurally polarized cells as epithelial cells. The translation of the polarity of cytoskeletal structures into polarized functions is realized via motor protein mediated directional transport along the structures, as in polar secretion of vesicle content in synapses [96]. Cell polarization is needed for maintenance or change of cell, as during macrophage permeation of tissue [97]. The ability of cells to react to anisotropic mechanical stimuli, for example different muscle cell reactions to being pulled orthogonally or parallel to their main axis, depends on asymmetry as well. Contrary to historical beliefs, the cytoskeleton is not under the passive instruction of pre-existing spatial cues, but drives its own symmetry breaking process [96].
Actin and myosin can rapidly and locally reorganize in response to polarity signals. These can be mechanical signals as pulling or pushing [98], biochemical signals as in elongation of tissue during development or next neighbor cell-cell interactions as in the development and reorganization of cell junctions.
Two main aspects in the polarization of cells are the *de novo* establishing of a polarity, called symmetry breaking, and the maintenance of polarity. For the formation of polarized cytoskeletal arrays, cytoskeletal building blocks as tubulin and actin must assemble into organized structures.
In the case of the assembly of polarized actin, the activation of nucleation factors as actin-related protein-2/3 (Arp2/3) complex or formin-family proteins (see section 2.7) at defined locations is a key factor. Formin or Arp2/3 promoted actin nucleation occurs most strongly at sites with Rho GTPase activation (see section 2.4 for the connection between wnt and the Rho-ROCK pathways). The nucleation of actin during polymerization is mostly located close to the cell membrane. Actin mediated symmetry breaking can occur due to anistotropic mechanical stimulus.
Microtubule nucleation occurs near the cell center at the centrosome or other microtubule organizing centers (MTOCs). This nucleation is distal to membrane derived signals that stimulate cell polarity. However, deformation of the cell still affects microtubule organization [99]. Microtubule-induced cell polarity is described in neurons [96, 100]. A more common role of microtubules in other cell types is the reinforcement of the initial polarity that has been established by the actin cytoskeleton, especially in larger cells or cells that require stable polarity, like in T-cells. In adherent migrating cells, two sources of microtubule induced asymmetry exist: Centrosome orientation and selective stabilization. Selective stabilization is a process where microtubules are stabilized by post translational modifications [101] and the Rho-GTPase [102, 103].

2.5.5 Microtubules play an important role during cellular symmetry breaking

Microtubules play a major role in symmetry breaking of individual cells upon mechanical stimulus. Malek et al demonstrated that in individual cells upon shear stress, the symmetry breaking of the cells that is evident on the actin and microtubule level can only occur if microtubule polymerization is possible [104] . The mechanical polarization of individual cells, mediated by actin stress fibers, is strongly dependent on an existing microtubule cytoskeleton polarization [105]. Shape changes in individual cells can be caused by microtubule reorganization [106]. Therefore, microtubules can be seen as a mechanotransducer that translates a mechanical stimulus into polarization. Actin stress fibers follow this microtubule rearrangement. However, in some cases actin can create an intrinsic mechanical stimulus and induce microtubule polymerization, which in turn is stabilized by actin, making these two cytoskeleton components strongly interdependent [96].

2.6 Cell- and tissue mechanotransduction

Mechanotransduction is the mechanism which allows cells to convert mechanical signals into biochemical responses. The stimulus or signal can be externally applied or intrinsically generated[107]. The attachment to an extracellular matrix plays a crucial role in mechanosensing of tissue [108]. Mediators of mechanotransduction are

- cell-Cell adhesions, as adherens junctions (see section 2.5.2) or gap junctions,
- membranes with stretch sensitive ion channels, caveolae (indentations of the membrane) or surface receptors,
- the extracellular matrix and the cellular reaction to changes of its rigidity, cell-extracellular matrix adhesions like focal adhesions (see section 2.5.2),
- the nucleus with ion channels and
- the cytoskeleton with all its components (section 2.5).

Organisms use structural hierarchies composed of interconnected networks that span from the nanoscale to the macroscale in order to focus stresses on specific mechanotransduction mediators. The presence of isometric tension (prestress) ensures that the various mechanochemical transduction mechanisms proceed simultaneously and produce a concerted response [25]. The perception of a mechanical signal can cause a change in gene expression, as in differentiation of stem cells in response to a changed rigidity of extracellular matrix [109]. Further, a reorganization of the cytoskeleton and cell polarity [110] as in wound healing and tissue patterning [111] is mediated by mechanotransduction.

2.6.1 Mechanics in gastrulation

Traditionally embryonic development was understood as a process controlled by spatio-temporally coordinated changes in gene expression patterning [107]. The mechanical origin of the rearrangements during embryogenesis have been investigated as early as 1983 [30]. Only recently a global model incorporating both molecular and mechanical processes has been proposed [28, 107].
During gastrulation (see section 2.1), a single layer of identical cells starts to fold on itself, a process during which the germ layers are produced. Cells are deformed and borders, hinges and folds are created [29]. Gastrulation is a fundamentally biomechanical process [28]. [7] proposed mechanical cues as the evolutionary conserved mechanism to induce gastrulation and mesoderm differentiation in zebrafish.

2.7 Cytoskeleton altering drugs

There are several drugs that can be used to alter the cytoskeleton by interacting with tubulin, motorproteins or connecting proteins (see 2.5). Drugs can either stabilize or destabilize cytoskeletal components. Destabilization can happen either by actively destroying crosslinkers or by inhibiting polymerization or the formation of new crosslinks. Drugs used in this work are presented in detail here. For the application protocol in this work see 3.2.

- Nocodazole
  interferes with the polymerization of microtubules. The drug arrests cells in the G2 or M phase and inhibits spindle apparatus formation. In *hydra*, Nocodazole is non lethal and inhibits the cell-proliferation independent elongation of the *hydra* polyp [48]. This makes it an ideal candidate to investigate whether the asymmetry in the *hydra* sphere is based on stretching of a group of cells. Takaku et al. proposed a mechanism for *hydra* to detect the metrical distance between its poles based on the microtubule network, an effect which is inhibited by Nocodazole [48].

- Paclitaxel
  is a chemotherapy drug that interferes with the normal breakdown of microtubules by changing the conformation lattice and arresting the cell cycle. The conformational change is stronger if microtubules polymerize in the presence of Paclitaxel. Drug effect lasts for days after application [112, 113]. In addition, applied on the timescale of hours, Paclitaxel has been demonstrated to completely inhibit catecholamin release and to provoke an increase in cytosolic Ca^{++} [114]. Catecholamines are neural regulators. Cytosolic Ca^{++} concentrations affect the function of a multitude of pathways like the Phospholipase C Pathway. In addition, changes in the cytosolic Ca^{++} concentrations alter the membrane potential of cells. For this work, the influence of Ca^{++} concentrations on contraction of cells is of interest.

- Y27632
  selectively inhibits p 160 rho-associated protein kinase [115]. This kinase is also known as rho-associated, coiled-coil-containing protein kinase 1 and is further referenced as ROCK1. ROCK 1 is a regulator of the actomyosin cytoskeleton which promotes contractile force generation and therefore plays a role in cell motility [116]. OCK1 also plays a role in smooth muscle contraction and actin cytoskeleton organization, stress fiber and focal adhesion formation. Its inhibition by Y-27632 leads to dissolving of the stress fibers [84].

- SMIFH2
  is a selective inhibitor of formin homology 2 (FH2) domains involved in stress fiber assembly. SMIFH2 inhibits *de novo* formation of stress fibers[117] but does not affect actin polymerization.

- Phalloidin
  binds and stabilizes filamentous (F-) actin and inhibits actin depolymerization. It can be bound to rhodamin and used as an fluorescent probe.

- Cytochalasin B
  prevents polymerization of actin filaments. It inhibits both the actin polymerization and the interaction of actin filaments in solution. The polymerization rate is reduced by inhibition of actin monomer addition to the fast growing end of the filament [118].

2.8 Biological oscillators

To understand a biological oscillator, three parameters are necessary: First, the biological variables that are essential to the oscillator. Second, how the interaction between the variables is arranged and third, whether these interactions can lead to oscillations [119]. An essential elements of a simple biological oscillators is an inhibitory feedback loop which includes one or more oscillating variables. Furthermore a delay source in this feedback loop is needed which allows an oscillation variable to overshoot a steady state value before the feedback inhibition is fully effective.
Oscillations in biology can modulate the response to stimuli over time. The same stimulus, received at a different point during the oscillation, can have a different effect. In addition, oscillations can lead to a synchronization of processes in the animal called entrainment. The oscillation stimulates and modulates subsequent effects and development [120]. One example described in the previous sections is the Rho-GTPase induced microtubule polymerization based oscillator described in section 2.5. Kruse et al. proposed the emergence of intrinsic mechanical oscillations occurring in vitro and in developing organisms based on the cytoskeleton and its motor molecules[121]. The cytoskeletal origin is independent of their length- and time- scale. The oscillations generated by the motor proteins can be tracked by and causally linked to rearrangements of the cytoskeleton [122]. Such oscillations were observed for actomyosin systems as well as for kinesins or dyneins interacting with microtubules [92, 121].

Chapter 3

Materials and methods

3.1 Laboratory animals and experimental settings

All experiments with *hydra*, unless stated otherwise, were performed in Volvic mineral water (Danone Waters Deutschland GmbH). *Hydrae* are very sensitive to plastic, direct contact needs to be avoided. Contact with glass surfaces and short contact to plastic Petri dishes is mostly tolerated if no close contact, pressure or confinement is applied.

3.1.1 *Hydra* strains

The wildtype strain *hydra vulgaris* and the transgenic strains *hydra magnipapillata* ks1 GFP, *hydra vulgaris* 12ASAktin+GFP Ecto- and *hydra vulgaris* 12ASAktin+GFP entodermal are used. For most experiments the transgenic *hydra magnipapillata* ks1-GFP are used, the wildtype strain serves as a control to confirm that the findings are not due to the genetic modifications. *hydra vulgaris* ks1 GFP contains green fluorescent protein coupled to the cytosolic protein ks1 (see section 2.3.3).
Both 12ASAktin+GFP strains contain actin promoter driven GFP with 12 Actin Amino acids between the promoter and the GFP. Thus the Actin expression and the GFP expression are simultaneously driven. These strains were used for the actin imaging.
The excitation wavelengths of both GFP strains are 395 and 475 nm, the emission wavelength is 509 nm.
All transgenic strains are stable. For more information about *hydra spec* see section 2.3.

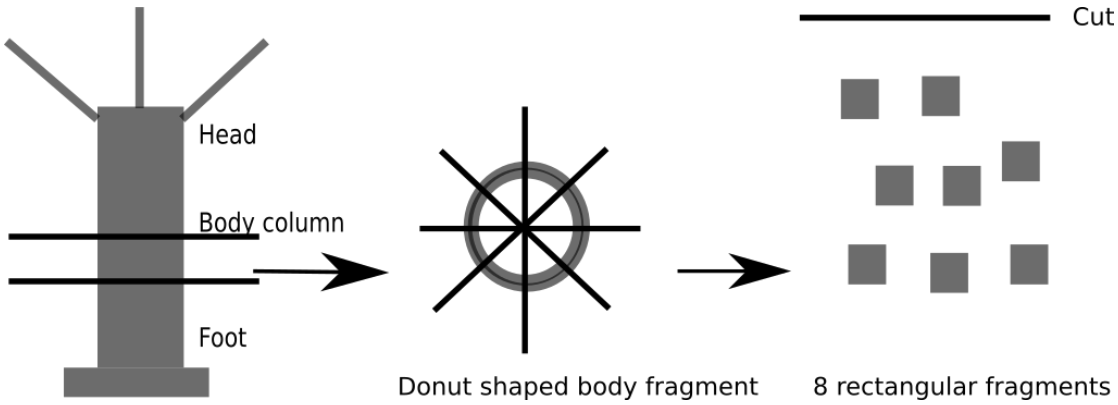

FIGURE 3.1: Schematic of the *hydra* cutting steps. First, a toroid piece with the height of approximately 0.3 mm from the center of the body column is cut. This toroid is cut another 4 times, resulting in 8 rectangular pieces, who then can heal into spheres, as described in section 2.3.1.

3.1.2 *Hydra* culturing

Animals are cultured in glass bowls using Volvic mineral water (Danone Waters Deutschland GmbH) and fed with artemia (approximately 10 artemia per *hydra*) purchased and cultured from aquaristics supply. The saline artemia were washed with deionized water prior to feeding. 30 min after feeding the remaining artemia are removed. 8 and 24 hours after feeding the *hydra* containers are cleaned to remove excrement. In suitable intervals all animals are transferred to clean bowls.

3.1.3 *Hydra* cutting

Hydra are cut under a Stemi Microscope using disposable scalpels. The lids of plastic Petri dishes are used as cutting boards. Foot and head are removed first. If ovaries and testes are present, those areas are not used for experiments. A toroid-like cut from the body axis is subdivided with 4 cuts into 16 square pieces. From these regenerates with a diameter between 150- and 300 μm form. The figure 3.1shows an overview of this process.

3.1.4 Experimental environment for *hydra* during imaging

Confinement of the *hydra* regenerates needs to be carefully done since under most circumstances they have a tendency to either escape or dissolve and die. The best regeneration rates are achieved if the *hydra* is freely floating. Two techniques, depending on the experimental requirements, have been used:

Agarose wells:

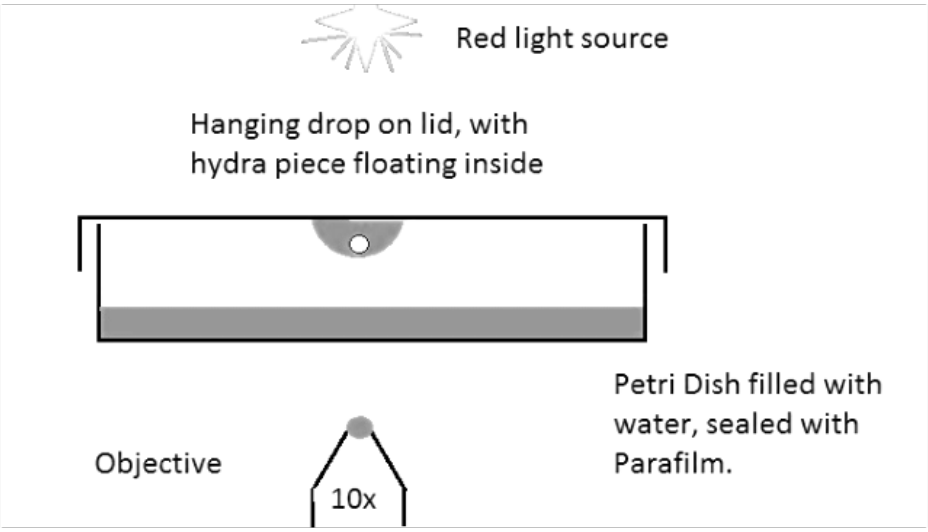

FIGURE 3.2: Schematic of the *hydra* in hanging drop experiment. The Petri dish is filled with water and sealed with laboratory film (not shown) to avoid evaporation. On the lid of the dish a drop of 20 μl is placed with the *hydra* regenerate inside. The dish is placed in a microscope and illuminated with red light.

To keep *hydra* in focus 0.5% agarose in Volvic is prepared with 1 mm wells that are either cut out with a micropipette or imprinted using a homemade gel comb made from a fine-toothed plastic hair comb with blunted tips. The *hydra* sink to the bottom of the well which is usually in a glass container, either the temperature chamber (see section 3.1.6.2) or a petri dish. The size and the position of the holes can be individually adapted. Other possibilities are wells made from PDMS, although the regeneration success rate decreases with most materials other than agarose.

Hanging Drop Experiments:

To avoid imaging artifacts and limit the contact of the *hydra* to the container the hanging drop technique was used. The freshly cut *hydra* pieces are placed in drops of 20 μl on the inside of the lid of a 2.5 cm radius plastic petri dish. The dish is filled with 4 ml of water, the lid is closed and sealed with strips of Parafilm M. The *hydra* pieces sink to the bottom of the drop and due to its shape can only move within an area that is easily covered by the microscope camera.

3.1.5 Flow chamber

The flow chamber was made from a glass pipette. One side was closed with a piece of a cell culture straining mesh attached using UV glue. The other side remained open. The side with the mesh was attached to a pump, the open side to a reservoir Erlenmeyer flask with a hole inside. The chamber was installed at a slope to avoid the escape of the

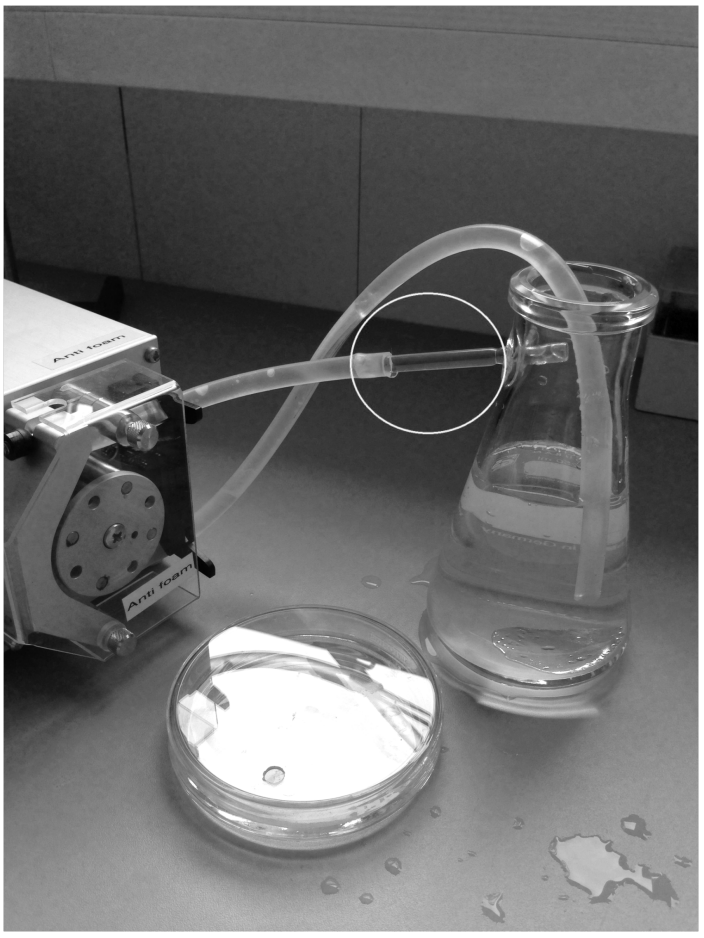

FIGURE 3.3: The chamber used to simulate convection turbulence. A peristaltic pump is connected to a reservoir and a cylindrical chamber, secured with two meshes, indicated by a white circle. The regenerates are kept between the meshes and constantly moved around by the water flow. On the bottom a glass Petri dish with a hole in the lid used for the pipette experiments (3.1.6.1) is shown.

hydra into the reservoir. The pump was pumping the medium from the reservoir and pushing it through the mesh into the chamber. The *hydra* regenerates were constantly moved. The flow chamber is depicted in figure 3.3.

3.1.6 Manipulations of *hydra*

3.1.6.1 Micropipette aspiration

Micropipettes are fabricated using a Sutter Instruments pipette puller. Glass capillaries with an outer diameter of 1 mm and an inner diameter of 0.5 mm are used. After the

pulling the pipettes are trimmed to achieve blunt ends with an outer diameter of 200 μm. For the *hydra* to tolerate the contact the tips need to be smoothed on the outside and the inside of the opening and the diameter needed to be as small as possible. A Leica microforge is used for the processing. The capillaries are connected to a homemade low pressure system using a syringe installed on a screw thread and, to control the pressure, a U shaped capillary with markings. Thus the pressure applied to the *hydra* sphere can be standardized and compared between the experiments without the need of absolute values of pressure.
The setup is mounted on an Olympus IX7 Microscope.
To account for the plastic sensitivity of *hydra* and to avoid evaporation, the capillary experiments are performed in glass Petri dishes with holes in the lid for access of the micropipette. The *hydra* regenerates are allowed to rest and heal for 30 minutes after cutting. The capillary tip is moved to close proximity of the *hydra* and kept in focus using a Xeno Works Micromanipulator from Sutter instruments. After contact the pressure within the capillary is quickly decreased to avoid the escape of the *hydra*. After closing of the seal between the *hydra* and the opening, the pressure is decreased until the marking on the U-shaped capillary is reached and the *hydra* is confined. If necessary, adjustment in the positioning of the *hydra* can be made using the micromanipulator to move it into focus.

3.1.6.2 Temperature gradient

The temperature chamber consists of two Sapphire Alumina ceramic temperature elements and two CP10,127,05,L1,W4.5, CP Series Peltier solid state thermoelectric coolers which are independently controlled by a RHM 4000 temperature controller. PT 1000 temperature sensors are positioned within each sapphire ceramic plate. The distance between the two temperature elements is 2 mm, the whole construction is glued to a glass plate and the Peltier elements are covered with cooling fins. In the gap between the two temperature elements agarose wells are inserted which contain the regenerating *hydra* sphere, thus keeping it centered between the elements. The gap is filled with *hydra* buffer and covered with a glass lid, see figure 3.4. The temperature chamber is mounted on a moving stage to follow multiple regenerations and a microscope below takes the pictures. The control of the temperature in the Alumina elements, the control and synchronization of the stage and the microscope camera is realized using Labview software.

A 0.32 mm 1 cm x 1 cm PT100 temperature sensor has been inserted into the chamber (see figure 3.4). The temperature across the chamber (in the direction of the gradient) and along the temperature elements has been measured . There have been approximately

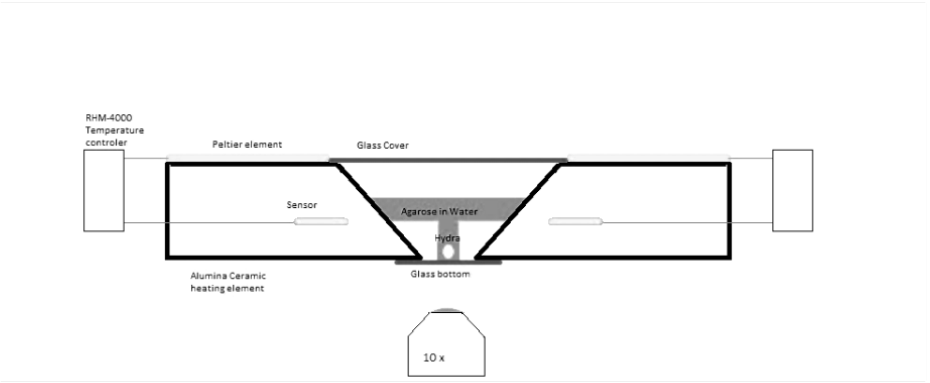

FIGURE 3.4: Schematic of the chamber used for the temperature gradient experiments. The regenerate is indicated in orange. The black heating elements have a distance of 2 mm within the chamber and are heated with Peltier elements (pink). The temperature is monitored by a PT 1000 Sensor (Red) and controlled by a RHM-4000 temperature controller. Within the chamber the *hydra* is enclosed by agarose gel without touching the walls of the enclosure. The setup is installed on a stage that allows to monitor multiple regenerates at once with the microscope.

700 measuring points per sweep along the chamber (3 cm) and 9-10 measuring points across the chamber. The shape of the gradient across the chamber was investigated, so the error due to the width of the sensor along the chamber, giving an average of the temperature over the width of 1 cm, was acceptable. The gradient is read out with a Labjack and Labview Software. The sensor was moved within the chamber using a stage.

3.1.6.3 Bead experiments

Microbeads are used to track the *hydra* movement during regeneration and to allow to investigate a correlation between the rupture points and the axis. An Olympus Ix7 Microscope in phase contrast is used with a HighPower-LED-Modul Rot 1 W 51.2 lm 10 ° 2 V ledxon 9008103. An Olympus 10 x phase contrast objective is used. The Beads are 0.5 μm silicium dioxide beads purchased from Sigma-Aldrich. 1 μl Bead suspension is diluted in 1 ml Volvic.

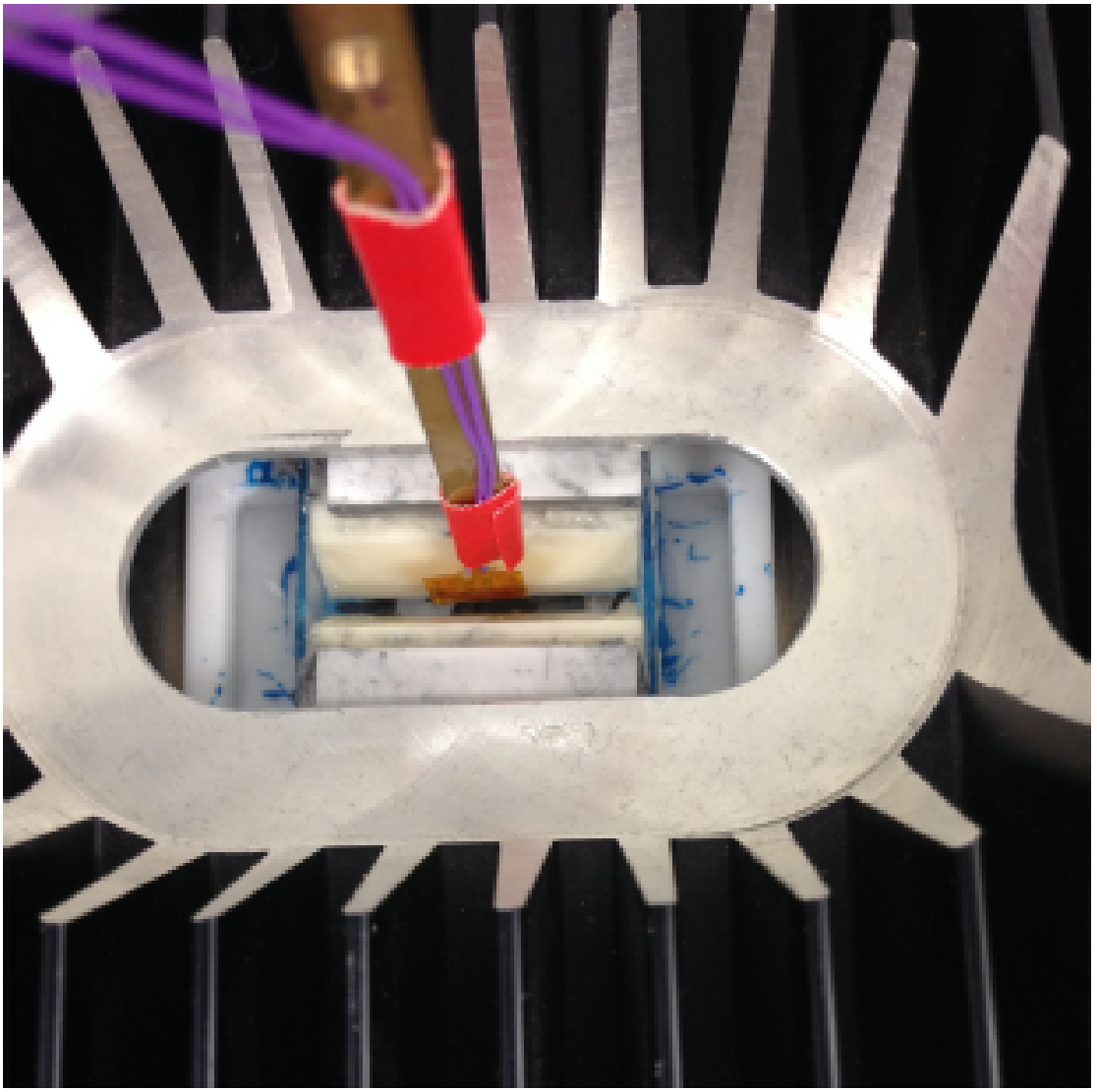

FIGURE 3.5: The temperature sensor used to measure the temperature gradient in the chamber (figure 3.4. The (orange) sensor is a pt-1000 with the thickness of 0.28 mm x 5 mm x 5 mm that allows to measure with a high resolution in one direction. The sensor is fixed and the chamber is moved in two directions.

3.2 Drugs

Several cytoskeleton altering drugs have been used. For a precise description of the effect of the drugs see section 2.7.

- **Y27632**: The working solution was 10 nM. The stock solution was 100 μM in DMSO, stored at -20°C.
- **Nocodazole**: Nocodazole from Sigma Aldrich was stored in $6 \cdot 10^{-6}$ Mol/l in DMSO, the working concentration was 10^{-3} Mol/l.
- **Paclitaxel**: Paclitaxel was used in a 10^{-6}Mol/l working solution and stored as a 10^{-3} M solution in DMSO at -20°C.
- **SMIFH2**: he Stock was stored at -20°C in DMSO, Working solution was 25 μM.
- **Phalloidin**: Phalloidin was used at a 20 μM concentration.

3.3 Microscopy and staining

3.3.1 Antibody and Rhodamine labeling of cytoskeletal structures

Prior to working with transgenic *hydra* the actin structures were labeled with rhodamin/phalloidin, a fluorescent probe specific for F-actin in fixed cells. The excitation/emission wavelenghts are 540/565 nm respectively. Phalloidin inhibits actin depolymerization. Also, staining with Green fluorescent protein labeled human F-actin antibodies that showed to be compatible with *hydra* actin, was performed using the same protocol.
Staining protocol:

1. Rinse in Standard PBS (Phosphate buffered saline, both with and without Magnesium and Calcium were sucessfully used).
2. Relax in 2% Urethane
3. Wash in PBS, 3 x 5 min
4. Fix in Paraformaldehyde 4% 10 min
5. Wash in PBS, 3 x 5 min
6. Permeabilize in Triton X 300 0,1% in Distilled Water 10 min
7. Wash in PBS 3 x 5 min
8. Stain in Phalloidin (40 μ l auf 1 ml), 45 min
9. Wash in PBS 3 x 5 min
10. Treat with Hoechst 33258, or, if long term fixation is desired, with Moeviol/Hoechst Solution, both with Hoechst working concentrations of 1 μg/ml.

The antibody used against Vimentin was Vimentin Antibody (V9): sc-6260 from Santa Cruz Biotechnology. The actin antibody was an anti human F-actin antibody.

3.3.2 Confocal microscopy

Confocal microscopy was performed on a TI-Eclipse inverted microscope from Nikon
Spinning head : Yokogawa head CSU-W1 from Andor, pinhole 50 μm
Laser: Nikon combiner LU-NV. 488 and 561 nm, 70 mW; 405 nm with 20mW and 647

nm with 125 mW
Camera : ORCA Flash 4.0 V2 CMOS camera from Hamamatsu. 4 million pixel
Objective : 20 x CFI-Plan Apo NA 0.75, working distance 1,0 mm with a 20 x objective to allow for the large working distance required by the living animals.

3.3.3 Brightfield and phase contrast microscopy

Brightfield and phase contrast microscopy were performed on a modified Olympus IX7 with a HighPower-LED-Modul Rot 1 W 51.2 lm 10 ° 2 V ledxon 9008103, an objective adapter to allow for the increased working distance in the hanging drop regenerations and a custom made phase blend to work with the objective.

3.4 Regeneration pattern analysis

3.4.1 Processing of the regeneration image stacks

Brightfield Microscopy yields Image stacks of different grey values. To automatically calculate the projected plane of the *hydra*, binary pictures need to be generated. The Open Source Fiji/ImageJ Software was used for all Imaging analysis. The interpretation of the regenerations in agarose Wells requires some preparation steps, the hanging drop experiment analysis at step 4.

1. The Image sequence is loaded into a virtual stack, processed into 8 bit pictures and saved as a .tiff file.

2. Unwanted light gradients and darker gray areas need to be removed from the picture. For this the a posteriori Shading correction plugin 514 V 3 (open source) is used. The shading model is used as mask to correct all the pictures in the stack. If the shading changes during the experiment a macro can be used to automatically make the shading model and the subsequent correction for every single picture of the stack, although this was rarely necessary.

3. The agarose Well needs to be removed from the picture in order to allow clean binary pictures of the *hydra* sphere. The Region of interest (within the agarose well, outside of all the *hydra* positions during the experiment is chosen, inverted and the outside cleared).

4. From here on the Image processing is the same for all experiments. If necessary the contrast of the stack can be enhanced using either the "'Contrast"' option or the thresholding tool, both yielding the same result.

5. For the subsequent steps Batch Processing is needed for the virtual stack. The following commands are used: run("8-bit"); setOption("BlackBackground", false); run("Make Binary"); run("Fill Holes"); and the resulting Binary files are saved into a new folder. If the *hydra* is bright on dark background the "BlackBackground" Option needs to be true to achieve black particles on a white background. The "'Fill Holes"' option is necessary to compensate for brighter areas at the center of the sphere or in the rim regions caused by the thinning of the sphere during movement or the cellular structures visible in the rim.

6. Analyze particles: Fiji/ImageJ automatically analyzes the Area of the sphere, the Major and the Minor axis, the angle of the major axis with respect to the x axis of the picture, the circularity $4\pi \cdot area/perimeter^2$ of the picture.

7. Special case: If the pictures are in Phase contrast the Variance filter allows to change them into binary pictures.

3.4.2 Analysis of the oscillation patterns

The subsequent interpretation of the Fiji Files is performed using Origin Pro 8.6 Data Analysis Software. The regenerating *hydra* is approximated as a rotational ellipsoid. In the hanging drop pictures *hydra* tends to oscillate with the major axis perpendicular to the optical axis of the microscope, so the area and the measured axes can be directly used to calculate the volume. Most of the time the regenerating *hydra* has a pronounced major axis so the calculation of the volume is better suited to observe the physiological changes.

1. The data files produced by Fiji/ImageJ are imported into Origin. To allow for a comparison between experiments the Volume is normalized to 1. The normalized volume over time is plotted.

2. The angle between the major axis and the x axis of the image is plotted over time and compared to the volume over time.

3.4.3 Interpretation of the normalized oscillation data for the Fast Fourier Transform analysis

The inflations were linearly detrended and a spectral analysis using Fast Fourier Transform (FFT) was performed after [123].
The Amplitude over Frequency data was analyzed using the impulse analysis, using a threshold of 20% and the absolute and local maxima to define a signal. Hidden peaks were extracted using the second derivative.
The received impulses were directly compared to see whether there are some common frequencies during different experiments. The impulses were multiplied with the duration of the oscillation to allow for comparison between different oscillations and experiments. To compare the development of the frequency contributions over the regeneration time the amplitude was also normalized to 1.

3.4.4 Analysis of shape fluctutations

To analyze the shape fluctuations, the same processing steps as described in 3.4 were performed. Resulting binary pictures were analyzed and the angle was calculated by

the particle analysis tool. The angle is measured between the main axis of the particle and the lower frame of the image. The difference between two subsequent angles was calculated, resulting in the "angle difference". Angles between 0· and 180· result in very high angle differences that do not reflect the reality. To remove this artifact, a threshold was chosen and, for angles 10· around 0 or 180 the smaller possible difference was chosen using the following matlab code:

```
function Angle=Winkel(angle)


for i=1:(length(angle)-1)
a=angle(i);
b=angle(i+1);
if (a ≥ 175&&b ≤ 5)|(a ≥ 175&&b ≤<= 5);
A=max(a,b)-min(a,b);
B=180-max(a,b)+min(a,b);
Angle(1,i)=min(A,B);
else
Angle(1,i)=max(a,b)-min(a,b);
end
end
```

To see how the angle behaves, the time the *hydra* spends in a state of high angle difference or low angle difference state was counted. The threshold to define what high or low difference means was chosen based on *hydra* behavior with a fixed angle. The probability of the hydra to stay in one of the states longer than a given amount of time was plotted. The following code in matlab was used: function test=zweiteZeile(data)

```
n=0;
A=zeros(1,length(data));
L=length(data);
k=1;
erg=5*ones(1,L);
if data(1)10
A(1)=1;
else A(1)=0;
end;
for i=2:L
if data(i)¿0.2
A(i)=1;
```

```
else A(i)=0;
end;
if A(i)==A(i-1)
n=n+1;
else erg(k)=n;
k=k+1;
n=1;
end;
end;
c=max(erg);
b=zeros(3,c);
erg=erg(erg =5);
for i=1:c
b(1,i)=i;
b(2,i)=length(erg(erg==i));
end;
for i=1:c
b(3,i)=sum(b(2,i:end));
end;
cl=b(2,:)¿0;
fi=find(cl);
test=b(:,fi);


subplot(2,2,1)
plot(data)
subplot(2,2,2)
plot(log(b(1,:)),log(b(3,:)),'.');
```

Chapter 4

Results

.

4.1 Very small temperature gradients are sufficient to affect axis orientation of regenerating *hydra*

4.1.1 Specification of the gradient

Prior experimental work by Soriano et al. demonstrated an orientation of the body axis of regenerating *hydrae* in the direction of a temperature gradient (see section 2.3.4)[23]. In the experiments and the proposed model, a linear gradient was assumed. The exact temperature difference was calculated, but not measured [22].
Temperature gradients were generated in a chamber constructed of glass and sapphire ceramic heating elements, as described in the supplementary of [23]. The gap between the heating elements was 2 mm. For temperature control, a feedback system involving a temperature sensor and controller was installed. For the exact shape and construction of the temperature chamber see section 3.1.6.2, figure 3.4. The temperature gradient was measured using a flat PT-100 Sensor and simulations were performed to optimize the gradient regarding steepness, linearity and stability.
The temperature gradient experiments were performed by Dr. Aravind Pasula. In some of the experiments the orientation of the *hydra* exhibited an unexplained 30° tilt of unknown origin.
Partial differential equation simulations using Matlab (PDE Tool) predicted a strong dependence of the gradient on the shape of the chamber. In addition, a strong dependence of the external temperature was observed. The simulations indicated that only if the temperature settings are perfectly symmetrical around the room temperature, high temperature differences can be achieved. In addition, simulations with Energy2D, an interactive heat transfer simulation tool that considers convection, were performed and predicted that a tilt in the gradient could be caused by insufficient lateral temperature insulation of the chamber.
The shape and the actual temperature values of the gradient have been measured using a custom made PT 1000 temperature sensor that was moved using a stepper motor driven stage. The sensor dimensions are 0.2 mm x 0.5 cm x 0.5 cm, allowing to achieve a high spatial resolution (approximately 700 data points for 2 mm) of the measurement in the direction of the gradient. The absolute temperature and the shape of the gradient in the temperature gradient chamber have been measured and determined. Experiments were performed with and without lateral thermal insulation of the temperature chamber using polystyrene. Experiments with symmetrical and asymmetrical temperature settings were performed.
Contrary to the simulations with the Matlab PDE Tool, higher and more homogenous gradients were achieved using an asymmetrical temperature setting shifted towards the

cold side. Adjusting the hotter side further away from the room temperature resulted in a very irregular gradient or a complete gradient breakdown. Symmetrical adjustment of the same temperature difference caused up to a 50 % drop of the gradient (see table 4.1).
Adding lateral polystyrene insulation to the chamber significantly increased the area with a homogenous gradient and removed the 30° tilt in the center of the chamber (see figure 4.1 for before and figure 4.2 for after the improved insulation).
The absolute gradient values were much lower than expected (see table 4.1). The highest possible gradient with this setting exerted a temperature difference of 0.6 °C on the *hydra*. This gradient caused a high mortality in the regenerates and can be considered the maximal viable gradient. See figure 4.3 for the qualitative results of 0.13, 0.19 and 0.6 °C gradients.

The tilt in the data due to the inhomogeneity in the temperature gradient was solved

Δ T expected (°C)	Δ T measured (°C)
0.6 (with insulation)	0.3
0.9 (with insulation)	0.315
1 (as used in previous experiments, without insulation)	0.195-0.225, depending on the position
1.2 (asymmetrically adjusted, with insulation)	0.6
1.4 (symmetrically adjusted, with insulation)	0.345

TABLE 4.1: Comparison of the expected and the measured gradients.

by using polystyrene as an insulation of the chamber (see 4.2).

4.1.1.1 Summary and Discussion

The experimental setting strongly depends on the environment, responding to even small changes, such as changing the type of the insulation. Small fluctuations in room temperature can also strongly change the gradient up to 50 % in the course of the experiment. To achieve a reproducible quantitative result, the room temperature as well as the insulation need to be tightly controlled. Alternatively, the gradient needs to be verified prior to each experiment.
The 30° tilt demonstrates that the axis orientation is influenced by the temperature, not the chamber itself.
The results demonstrate that gradients as low as 0.13°C influence axis formation. This

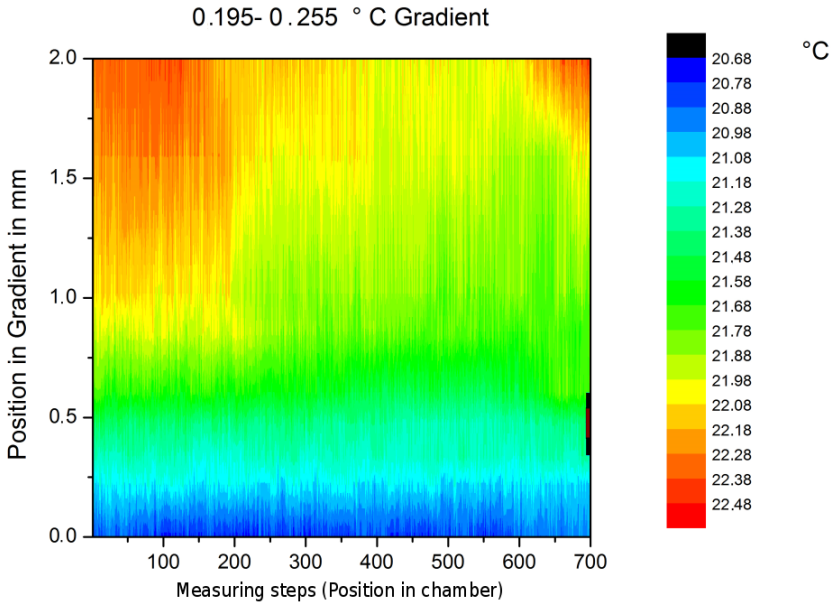

FIGURE 4.1: Left: a schematic depiction of the temperature chamber, T1 and T2 are the thermoelements, *hydrae* are indicated in white. Right: Measurement of the gradient exhibits an inhomogeneity that causes the tilt in the axis orientation. This effect was seen in various intensities depending on the gradient boundary temperatures. In this case, gradient over the *hydra* regenerate (200 μm diameter) was calculated to span 1 °C, but, in fact, amounted to 0.195-0.255 °C, depending on the position.

conforms with the prediction of [22] and the model of self-organized criticality (see section 2.2.1 in fundamentals). In a self organized system on the point of criticality, a small stimulus is sufficient to induce a change in the system. Thus, the result that even smaller than assumed temperature gradients induce axis formation supports the model of self-organized criticality.

Technically steeper gradients are possible by improving the insulation and adjusting the symmetry of the chamber. At one point the gradient breaks down and convection takes over. However, in an optimized setting, this takes place at temperature differences that are not viable for the regenerates. The cause of death in high gradients is unknown, an inability to break symmetry due to asynchronous behavior of *hydra* cells on the cold and hot side is possible. In addition, *hydrae* are very sensitive to mechanical stimuli. One of the first control experiments was performed to investigate the question whether irregular flow within the chamber caused by convection is the cause of death in the experiments.

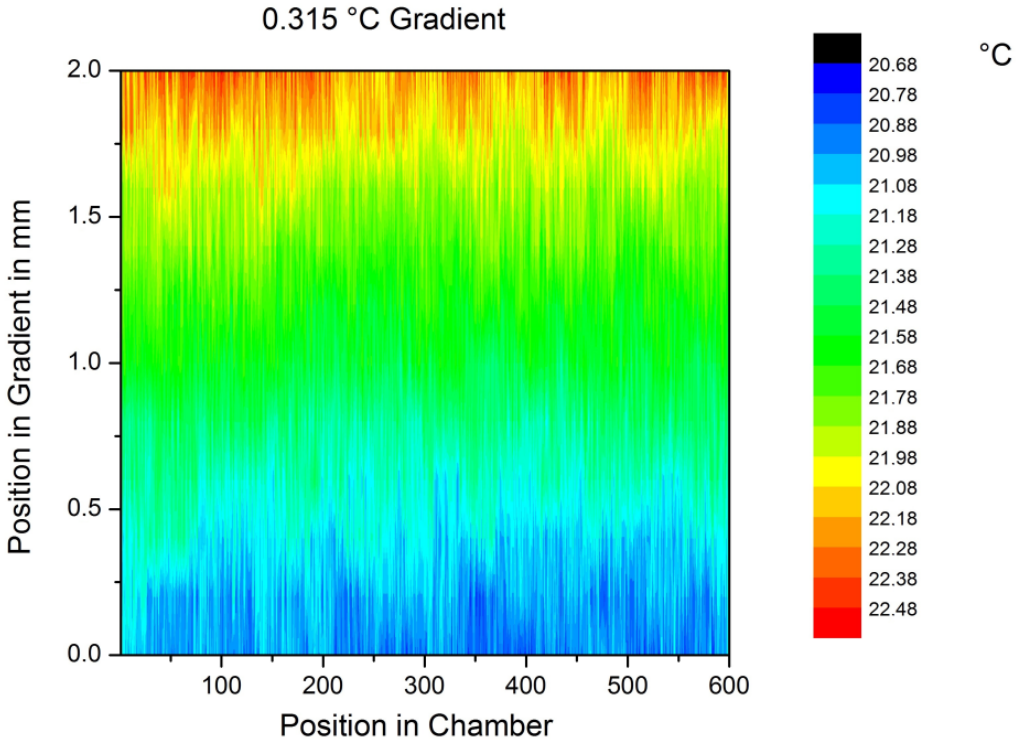

FIGURE 4.2: The temperature gradient after adjustment of the insulation and temperature regulation parameters. Left: Schematic depiction of the temperature chamber, T1 and T2 are the thermoelements, *hydrae* are indicated in white. Right: The actual measured temperature gradient differs strongly from the assumed gradient of 1 °C. The insulation and temperature setting adaptation removes most inhomogeneities.

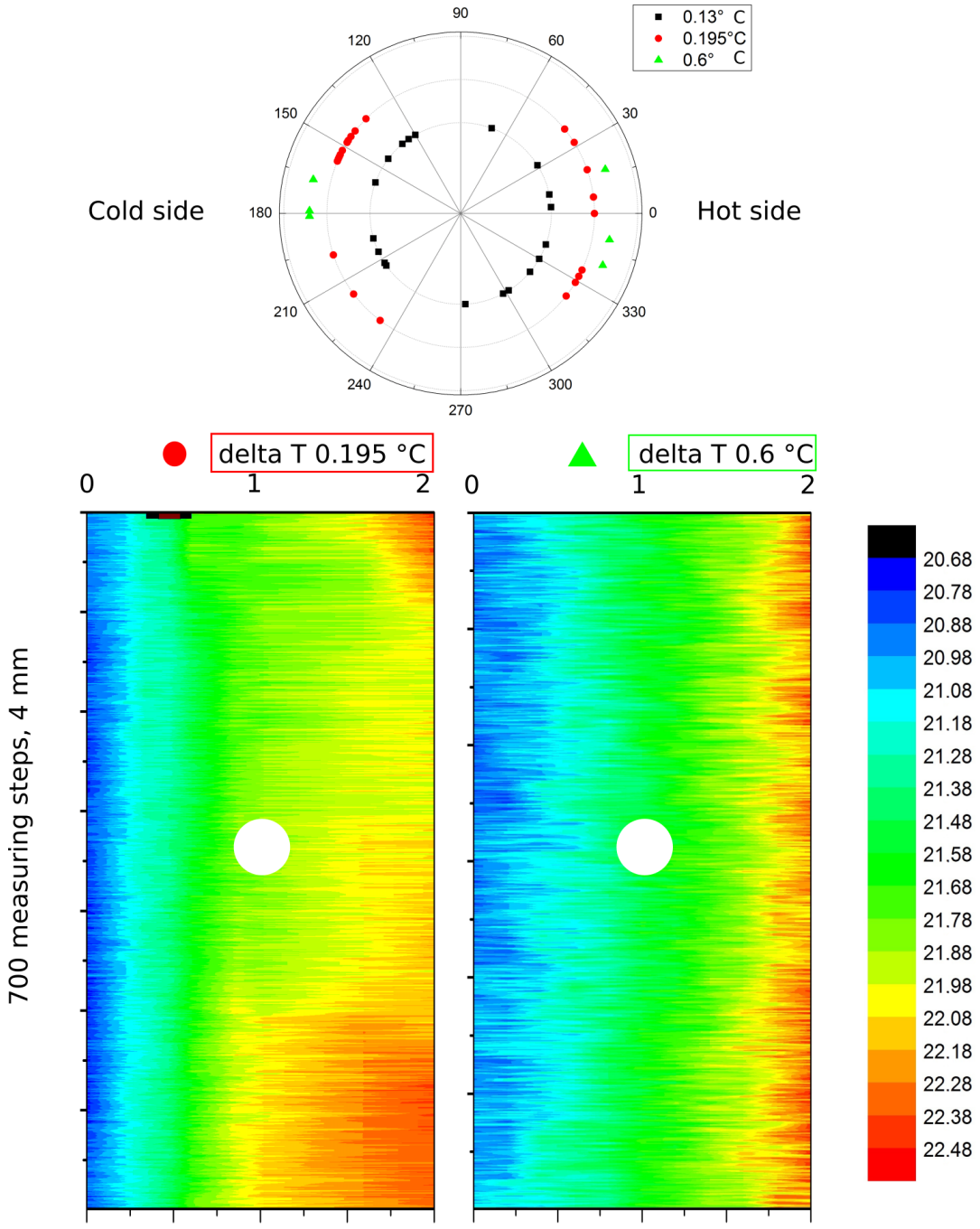

FIGURE 4.3: Experimental data with a depiction of the applied gradients. The upper panel demonstrates the distribution of the head formation in three gradients. Effective gradients for the regenerates are calculated. The 0.13 °C gradient induces no preference for an orientation. The 0.6°C gradient exhibits a bimodal distribution with no preference of the head orientation. The amount of experiments is low because of the lethality of this gradient. The 0.195 °C gradient exhibits a bimodal distribution, with a 30° tilt on the cold side. Lower panels demonstrate the measured gradients, the regenerates are indicated as white circles. The lower left panel shows the temperature in the chamber. On the cold side, the gradient is perpendicular to the chamber. On the warm side, irregularities can be observed and the gradient is distorted in several areas. This could explain the 30° tilt in the results.

4.1.2 Influence of irregular flow due to convection on the regeneration success

Convection as a possible cause of death in steeper gradients (as described in section 4.1.1) was investigated. Convection could expose the regenerates to a constantly changing mechanical stimulus by touching the bottom or the walls of the chamber. As shown in sections 4.2 and 4.3, the regenerates are very sensitive to mechanical manipulations. A flow chamber was built to expose regenerating *hydra* to constant movement in the medium, thus simulating irregular flow and constantly changing mechanical stimulus (see figure 3.3 in section 3.1.5).
In total, 4 Experiments have been performed using between 10 and 20 regenerates each. The success rate of the regeneration was close to 100 %, 2 *Hydra* regenerates were lost during the process. This corresponds to a normal regeneration success rate.

4.1.2.1 Summary and Discussion

The mechanical stimulus caused by irregular flow does not prevent regeneration of the *hydra*, indicating that movement due to convection in higher gradients does not play a role in the mortality.
The gradients used in the experiments are within the viable and regeneration-friendly temperature range for *hydrae* [53]. Therefore the metabolic asynchronism in the sphere is probably the cause of axis orientation and of death in steep gradients.

4.1.3 Discussion and Conclusion

The actual temperature gradients used in the quantitative measurements are almost 50 % lower than the assumptions based on the calculation of the gradients. Setting a 1 °C (1 °C assumed, 0.2 °C in reality) gradient based on the calculations gave and actual gradient that was lower than the lowest assumed gradient (0.6 °C assumed, 0.3 °C in reality). The quantitative experiments demonstrate that the regenerates are sensitive to small temperature differences. The setting of the temperature gradient cannot be calculated based on a linear temperature gradient without convection. Experimental measurement and control of the gradient is necessary. Simulations that are taking convection into account are a useful tool to predict the shape of the gradient. The temperature gradient is easily distorted by a change in lateral insulation. A possibility to further improve the gradient would be to add insulation on the top and bottom of the chamber without blocking or distorting the path of light of the microscope. Very thin double layered glass could be a possible solution. Simulations of different chamber geometries (without taking the convection into account) predicted that blunt points in the cross section of the thermoelements could also allow to establish higher gradients. However, since the highest possible gradient in this chamber is not viable for the regenerates anymore, higher gradients are not useful for hydra experiments. Investigation of expression patterns demonstrates that the head is induced prior to the foot [17]. In the gradient with a 30° tilt on the hot side the foot is oriented in the direction of the tilt. This points to an indirect, perhaps head-suppressing effect of the hot side of the gradient, which agrees with the orientation towards the cold side of the head demonstrated by [22]. Another explanation of the effect could be that in a situation with competing gradients there are ideal gradients or temperatures that influence the head formation stronger than either higher or lower gradients.

4.2 *Hydra* regeneration from small tissue pieces follows specific regeneration patterns

Small tissue pieces are cut from the center of the body column. They heal and turn into spheres of approximately 300 μm in diameter (for more details on size see section 4.2.5). After cutting and healing, *hydra* regenerates undergo sawtooth-like oscillations. Soriano et al described a specific oscillation pattern that is linked to symmetry breaking. Three phases were described, first large slow oscillations followed by faster oscillations after symmetry breaking. The transition is distinct and sudden. The second phase, as described corresponds to the elongation of the regenerate . The third phase describes is distinguished by the emergence of the head and the foot [124].
In this work the oscillation patterns were investigated more closely and new tools were introduced. At the first glance, most *hydra* regeneration follows this basic pattern similar to the one described by Soriano et al. [124]. However, there are individual deviations with respect to regeneration time, number of oscillations and other factors that are described in the following section. In total, three regeneration phases before head and foot emerge could be identified, thus, 4 in total (see section 4.2.1).
The circularity during regeneration was investigated. Mechanical symmetry breaking is characterized by an irreversible elongation of the regenerate. The process of the circularity highlights the regeneration process further (see section 4.2.2).
To pinpoint the exact time of symmetry breaking, a marker for mechanical symmetry breaking, the directionality, or angle, was established. This marker allows to confirm whether a symmetry breaking process takes place in regenerations with deviating patterns (see section 4.2.3). Regenerations were recorded with 1 frame per second and turned into binary pictures. Fiji Imaging Software was used to analyze Volume over time, Circularity and directionality/angle. An overview of the investigated parameters is shown in figure 4.4.

4.2.1 Volume over time

Volume of the regenerates during every recorded point in time was calculated by performing a particle analysis of the binary pictures (see section 3.4). The two main axes (a= major axis, b= minor axis) were measured. As shown in figure 4.5, the *hydra* is fitted by an ellipsoid and the volume in every individual image is calculated using

$$V = \frac{4}{3}\pi \cdot a \cdot b^2 \tag{4.1}$$

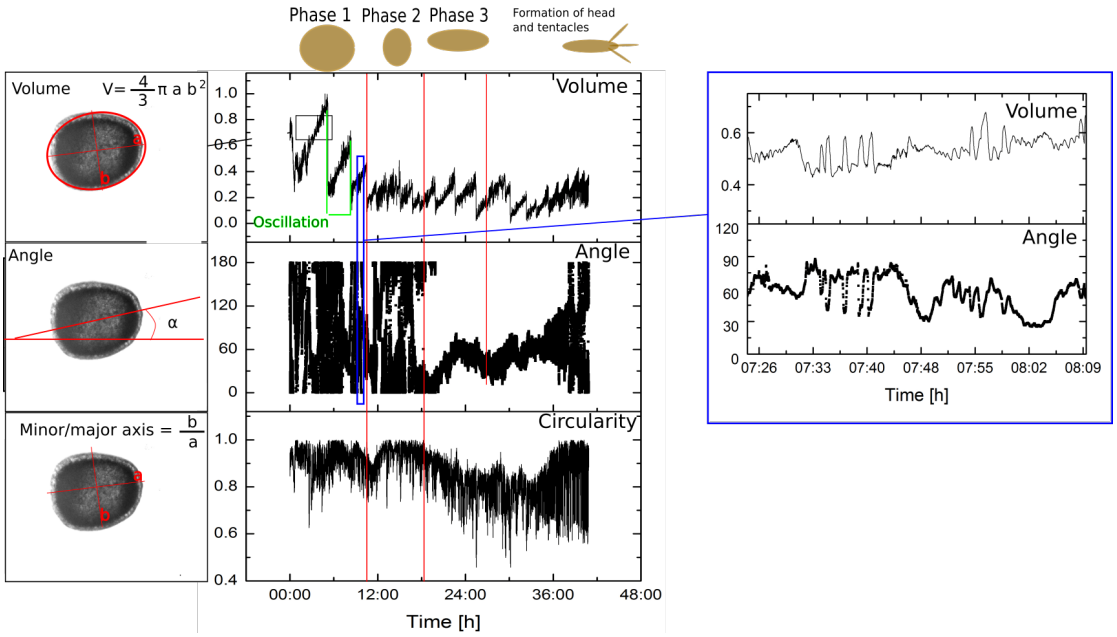

FIGURE 4.4: An overview of the investigated parameters. Temporal resolution is 1 data point per second. The regenerate is indicated as a brown circle/ellipsoid. Volume as a function of time demonstrates the course of the osmotically driven oscillations. One oscillation is indicated in green. During the inflations, rhythmical trembling is observed. The angle of the main axis, with respect to the image frame, is plotted over time. The blue frame shows the correlation between the trembling and the angle during regeneration. Circularity C shows the proportion between the minor and the major axis. 1 means the axes are equally long, smaller values indicate a more oblong shape. Four phases can be distinguished regarding the regeneration and are indicated by the schematic regenerates on top, brown. Phase 1 is defined by an (on average) spherical regenerate that undergoes large oscillations and has an unstable angle. Oscillation period correlates with regenerate size. In Phase 2, the regenerate is smaller, still spherical on average. The oscillations are irregular and shorter, the angle is undefined. Phase 3 exhibits regular oscillations, a stabilization of the angle and an elongation of the regenerate. Phase 4 marks the appearance of the tentacles and foot.

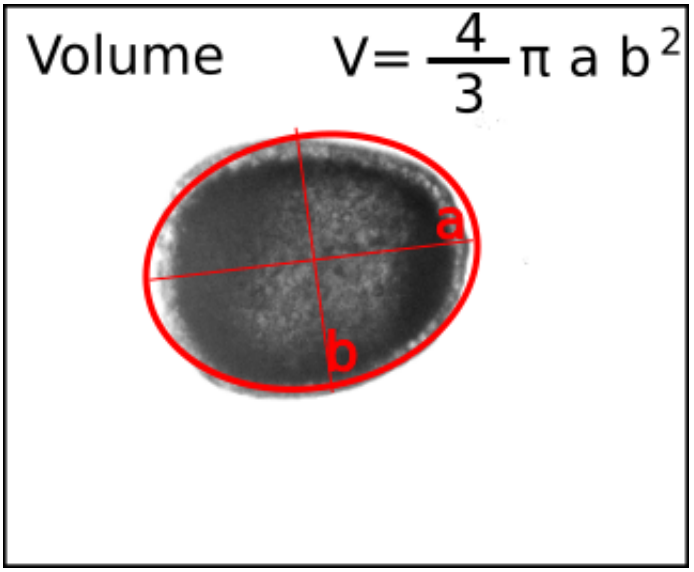

FIGURE 4.5: The volume of the regenerate is calculated by fitting of an ellipse and calculating of the volume from the two main axes of the ellipse.

In reality, the regenerate exhibits bulges and takes up irregular shapes, investigated in section 4.5.1. Since these bulges are very small compared to the overall *hydra* size they were neglected in order to obtain an analysis of the global behavior.
The parameter of normalized volume over time allowed to gain a more detailed insight into the oscillating behavior. For the biological background of the inflations see section 2.3.
Most regenerations exhibit sawtooth like oscillations in volume (See supplementary for more regeneration patterns). The volume change happens in slow, between 10 min and 7 hours long, inflations and quick deflations, determined to last between 1 and 20 seconds. During the first oscillation the regenerate reaches its maximum size. The slope of the inflations was calculated using a linear fit of the individual inflations and is $2.3 \cdot 10^{-5}$ % of the normalized volume per second (standard deviation of $9 \cdot 10^{-6}$) in all regenerations. This indicates that the duration of the oscillations corresponds to the size of the regenerate, since larger regenerates need a longer time to be inflated until they burst. The deviation in the slope is due to the irregular course of the regeneration and the resulting discrepancies while performing the linear fit. After 2-3 oscillations, the oscillation amplitude drops. In most cases, a phase with irregular oscillations, which do not necessarily look like a sawtooth, appears. After this irregular phase a third phase appears where the *hydra* resumes regular sawtooth-like oscillations until the head and foot are formed. Deviations from this pattern were the following: either less, irregular or no large oscillations. A more or less pronounced irregular second phase could be observed, in addition, not every regeneration exhibited this phase. An example of the volume during regeneration is shown in figure 4.6.
An example for a deviating regeneration is shown in figure 4.7.
The exact shape and pattern of the oscillations did not depend on the initial size of the *hydra*. The size of the spheroids ranged from 0.19 mm to 0.3 mm (fully deflated) at the beginning of the regeneration. Before the elongation, the size of the regenerates remained stable independently of the initial size of the freshly cut fragments. This indicates an internal size correction mechanism, a phenomenon that is examined and discussed in more detail in section 4.2.5.
During the large inflations, rhythmical patterns of smaller inflations and deflations that I termed "trembling" (see figure 4.4) were observed and further investigated in section 4.5.5.

4.2.1.1 Summary and Discussion:

Most regenerations exhibit sawtooth-like changes in volume, as described by [124]. The oscillation patterns show, despite large discrepancies, some commonalities between the

regenerations. Large oscillations and fast deflations, the possibility to distinguish several phases and trembling are always present. The differences are characterized by the time until the oscillation pattern changes and in deviations of the pattern itself. The exact point when the symmetry is mechanically broken or whether a symmetry breaking happens at all cannot be decided from the oscillations alone. To pinpoint and describe the symmetry breaking event, further parameters need to be investigated.

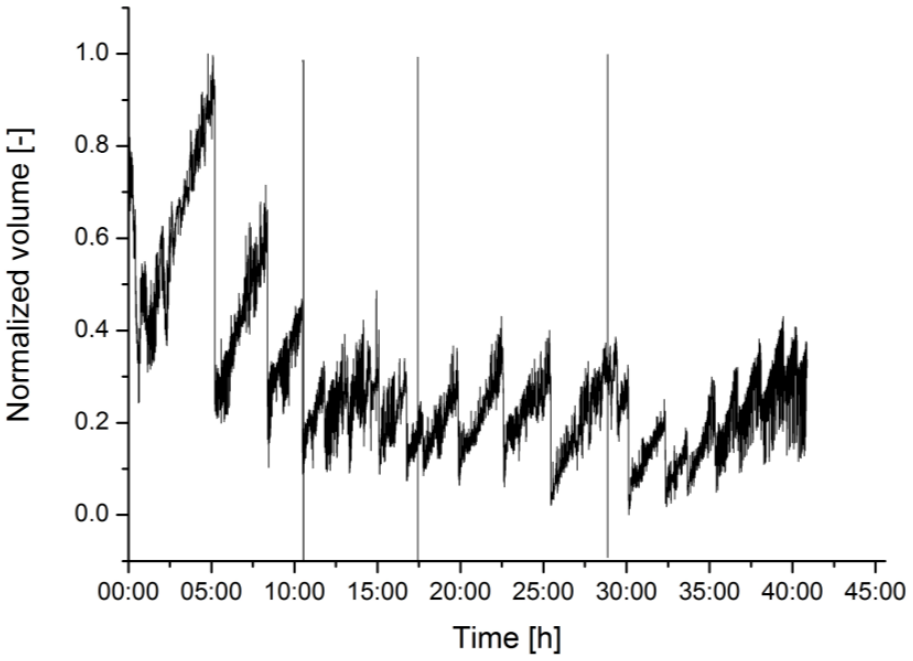

FIGURE 4.6: An example of a regeneration. During the first three oscillations the amplitude decreases. This is caused by discarding of tissue during the deflations. After 10 hours (first line), irregular oscillations start. Regular sawtooth-like oscillations are resumed after 17.5 hours (indicated by the second line). After 28 hours the behavior of the regenerate changes again. The head with tentacles becomes visible at this stage, indicated by the third line.

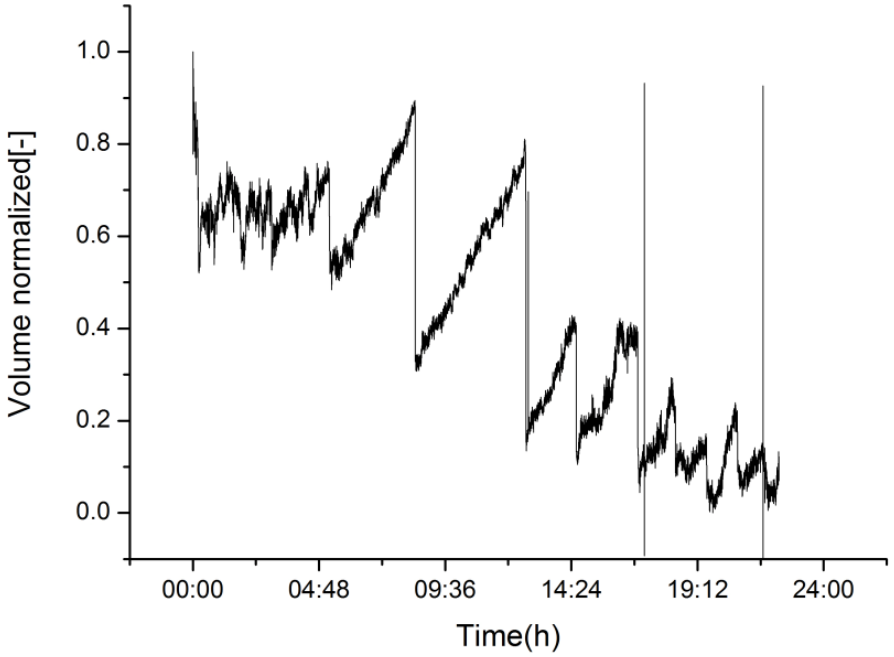

FIGURE 4.7: Volume as a function of time for an atypical (but successful) regeneration. There is a lag time of almost 5 hours with small, irregular oscillations. After two large oscillations, two smaller ones appear, the second irregular. The first line indicates the point in time of the elongation of the sphere, the second line the appearance of tentacles. This regeneration took place within 19 hours.

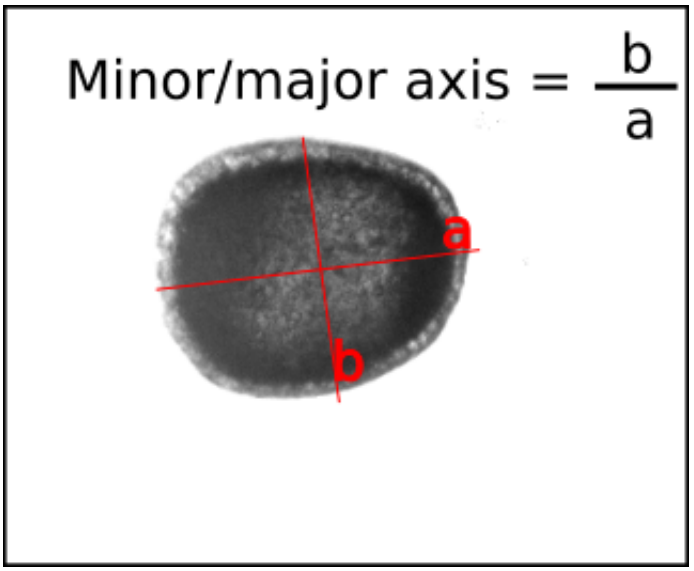

FIGURE 4.8: The Circularity of Minor/Major axis ratio is obtained by fitting an ellipse to the regenerate at every measured point in time. The ratio of the minor to the major axis of the ellipse corresponds to the circularity, with a value converging to 0 corresponding to a line and a value of 1 corresponding to a perfect circle.

4.2.2 Circularity or the ratio between the minor to the major axis is a visible manifestation of mechanical asymmetry

The visible manifestation of a mechanical symmetry breaking is the transition between a symmetrical spherical object to an ellipsoid object with an irreversibly fixed axis.
The Circularity C has been investigated and correlated with the oscillations. Circularity is calculated from the ratio of the minor to the major axis of an ellipse fitted to the regenerate at every measured point in time, see fig. 4.8). A Circularity 0 corresponds to a line, 1 to a perfect circle.

The *hydra* regenerates are not perfectly spherical. They oscillate in ellipsoid shapes even before the elongation. The circularity changes quickly during the regeneration. It varies mostly around 0.8 and never exceeds 0.95 during the first phase. During the oscillations in the first 2 regeneration phases the circularity decreases and increases again, demonstrating that the inflations and deflations do not follow an isotropic spheroid shape, but are ellipsoid with an unstable main axis direction. There does not seem to be a correlation between elongation and oscillations (see figure 4.10), except that fully inflated regenerates are in general more circular than more deflated ones.
A phase where the average circularity remains constant is followed by a phase where the circularity decreases and an irreversible elongation of the ellipsoid takes place. The start of the final elongation coincides with the change in oscillation pattern. The oscillations change from either phase 2 to 3, if present, or from phase 1 to 2, if the undefined

phase is skipped (see figure 4.10). The circularity drops repeatedly prior to irreversible elongation. This indicates that the the *hydra* undergoes short reversible periods of elongation before symmetry is broken. This demonstrates that there is a reversible asymmetry (see 4.9) even before the regenerate elongates.

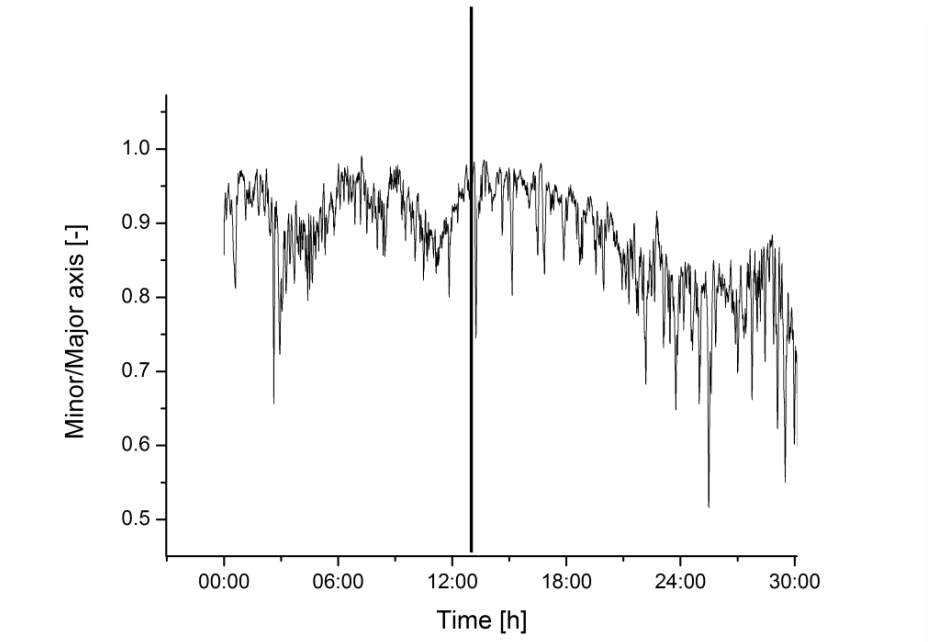

FIGURE 4.9: The progress of the Circularity as a function of time. At the beginning of the regeneration, there are reversible phases of higher or lower circularity. Irreversible elongation of the regenerate starts after several hours (beginning indicated by line). Tentacles were visible after 27 hours.

4.2.2.1 Summary and Discussion:

As described by [23], circularity is a suitable parameter that can be used as an indicator of mechanical asymmetry. Before irreversible decrease in circularity, regenerates experience short peaks of asymmetry and never reach perfect circularity. The shape seems to fluctuate between different shapes before stabilizing, investigated in section 4.5.1. Contrary to the initial thesis that the symmetry breaking is defined by the emergence of an axis, so far it seems that symmetry breaking is the process of irreversibly stabilizing one of many axes that emerge over time. This indicates that symmetry breaking manifests as a mechanical process. The regenerate seems to slowly change between an isotropic and anisotropic state, a phenomenon which is investigated more closely in section 4.5.3.

4.2.3 The process of the main angle direction implies a directionality, which can be taken a marker for mechanical asymmetry and symmetry breaking

To further investigate and quantify the fluctuations of the regenerate, a different parameter to define the mechanical symmetry of the regenerate needs to be established. As shown in section 4.2.2, the regenerates exhibit shape fluctuations. Conveniently the experimental conditions in the hanging drop force the *hydra* to oscillate perpendicularly to the path of light. Even if it is elongating within the direction of the path of light, the regenerate quickly reorients due to gravity.
During the regeneration, *hydra* orientation can be specified by the angle between the major axis and a line parallel to the bottom frame of the image, see figure 4.11.

Since the regenerate is never a perfect sphere, orientation is well defined at any point in time. For the exact analysis see section 3.4 and subsection 3.4.4.
Within the experimental setup, no preferred directionality that could be induced by external factors, was observed.
In addition to the absolute angle, the angle difference between two subsequent point in times was investigated. The angle difference is a measure of the stability of a direction of the main axis. A high difference indicates a quick change of angle, a low difference indicates a slow angle change. To set the threshold and define what "high" or "low" means, the angle differences of *hydra* with a defined axis were investigated. These changes yield the minimum threshold to distinguish turning from the whole regenerate from a shape change. The exact procedure of the analysis is described in section 3.4.4.
The change in angle behavior between scattered and stable correlates with an elongation of the sphere (figures 4.10 and 4.12). Correlation between directionality and circularity is, on average, 0.832, standard deviation of 0.19. This shows that the elongation corresponds to a change in directionality.
All regenerations exhibit two different phases. The main axis orientation during the first phase is scattered between 0° and 180°, with short intervals of stability in between. The stability intervals correspond to periods with a lower circularity.
The final transition into the irreversible stability period does not appear different from the other transitions. The transition between the fluctuations is always very abrupt (see figure 4.11). With regard to the angle difference, the same behavior can be observed. The results exhibit fluctuations in main axis orientation between a stable angle (low difference) and changing angle (high difference), see figure 4.4. These fluctuations have been closer investigated in section 4.5.3. The transition between the fluctuating and the stable phase correspond with a change in oscillation behavior and the circularity, as shown in 4.10.

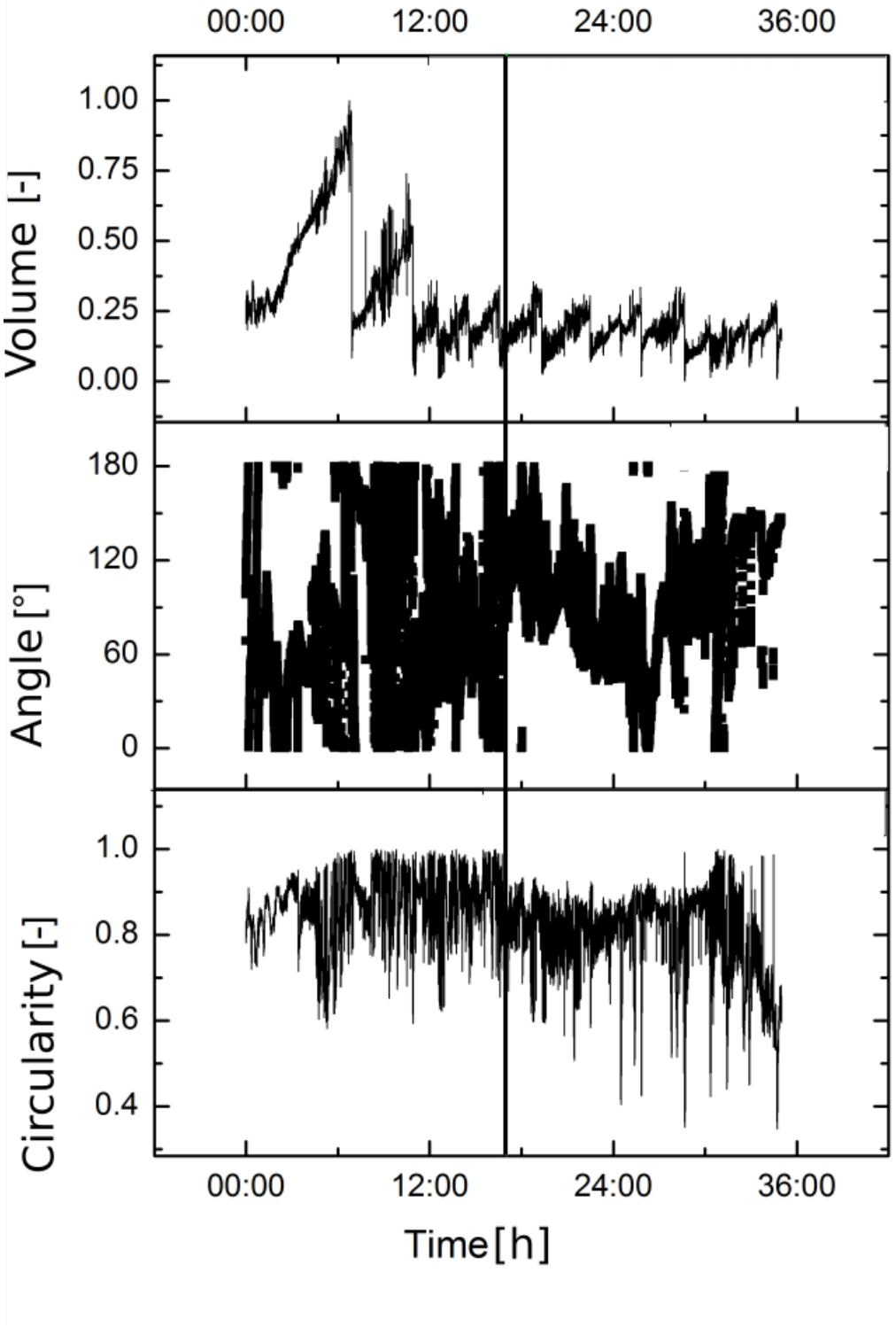

FIGURE 4.10: The Volume, Angle and Circularity of one regeneration are plotted over time. Correlation between the change in oscillation pattern, the stabilization of the directionality and the decrease of the Circularity are visible and indicated by a line. The change in oscillation pattern corresponds to a change in the angle fluctuation behavior, as described in figure 4.4 and section 4.2.3.

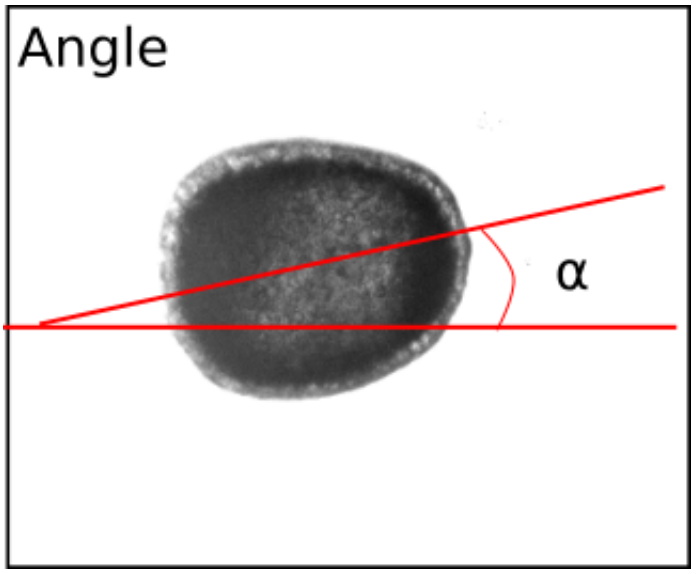

FIGURE 4.11: The angle is calculated at every given measurement by comparing the angle of the main axis of the regenerate to the picture frame. The series of these values that describes the angle in the course of the experiment is the directionality.

4.2.3.1 Summary and Discussion:

The stability of the axis orientation with respect to the image frame is a suitable tool to determine the exact point in time of mechanical symmetry breaking. The abrupt transition between the stable and unstable phase indicates a global mechanical synchronization of the regenerate. The slowly changing circularity corresponds to the shape fluctuations, indicating that phases with a low change in axis orientation induce an elongation. The stability of the main axis direction over time has not yet been described in literature and is therefore more closely investigated. The shape fluctuations are discussed more closely in section 4.5.1.

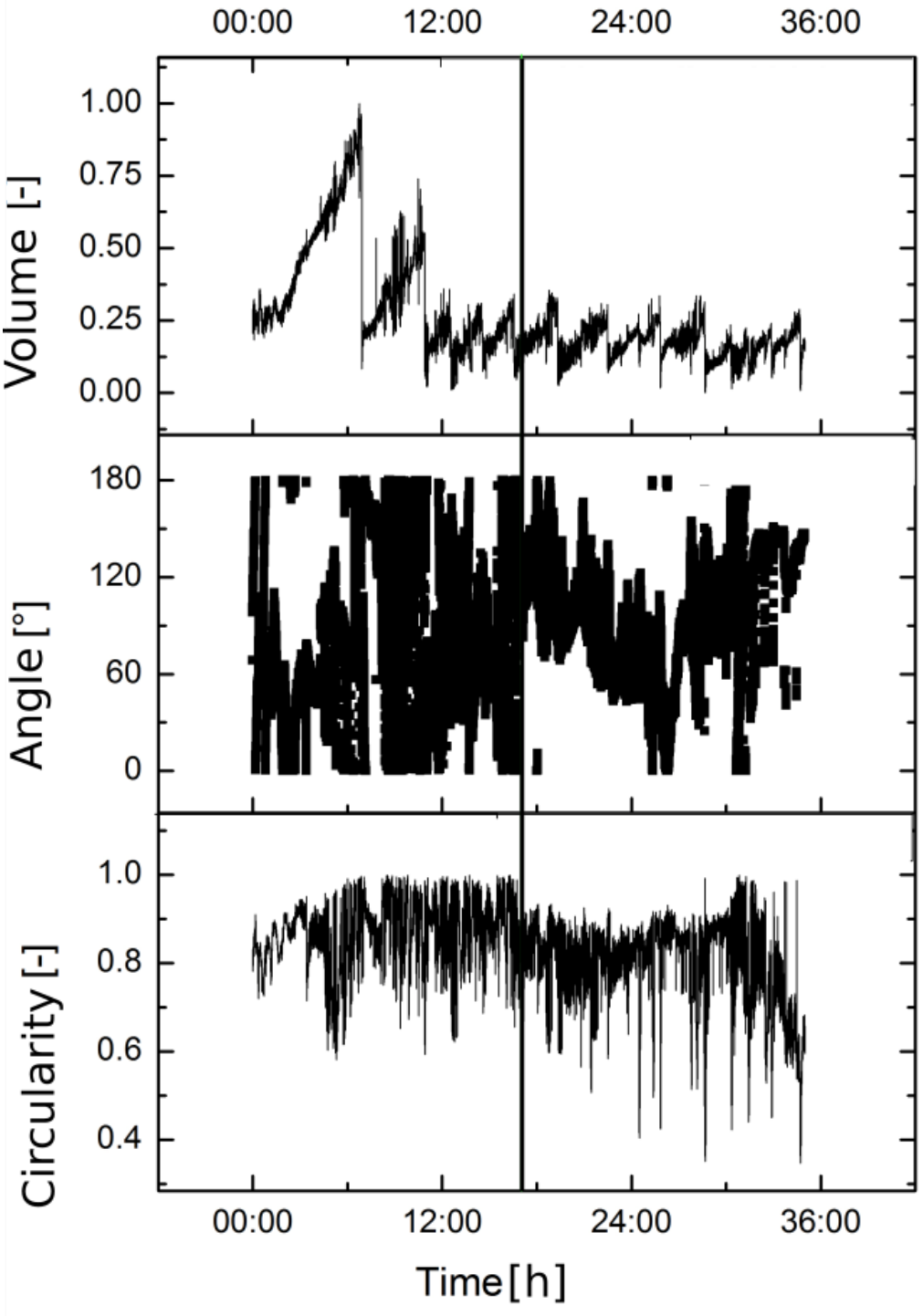

FIGURE 4.12: The time course of volume, angle and circularity during the regeneration of a *hydra* fragment. The first, large oscillations and the following irregular oscillations coincide with a fluctuating angle. With the beginning of the regular oscillations, the angle stabilizes and the *hydra* has a preferred direction.

4.2.4 Examples of deviating regenerations

Regeneration in agarose wells (contrary to regenerations in hanging drops) caused most regenerations to display a mechanical asymmetry from the beginning (see figure 4.15). 2 regenerations in 8 exhibited a clear transition between mechanical symmetry and asymmetry. Symmetry breaking could possible be induced by the mechanical stimulus of the agarose well, however, the reason why a temperature gradient seems to be able to override this stimulus is unknown. Some regenerations lack the second phase with irregular oscillations. A defined axis direction can either be present from the beginning or not (figures 4.13 and 4.15). In some cases, oscillations are not present (4.14 and 4.16), the latter being an example without a pronounced change in directionality. All regenerations exhibit trembling, discussed in section 4.5.5. To illustrate the diversity of the regeneration patterns and their commonalities, examples are shown in figures 4.12-4.16.

4.2.4.1 Summary and Discussion

The volume oscillations exhibited by the regenerates follow very individual patterns. However, symmetry breaking does not always seem to correlate with oscillation patterns. Soriano et al [23] presented only one type of regeneration pattern. However, the regenerations took place in agarose wells, not in hanging drops. It is possible that the lack of mechanical disruption in the hanging drops allowed some fragments who would not have survived in an agarose well, to regenerate. A possible background of the oscillation patterns and a cause for their individuality is discussed in the next section.

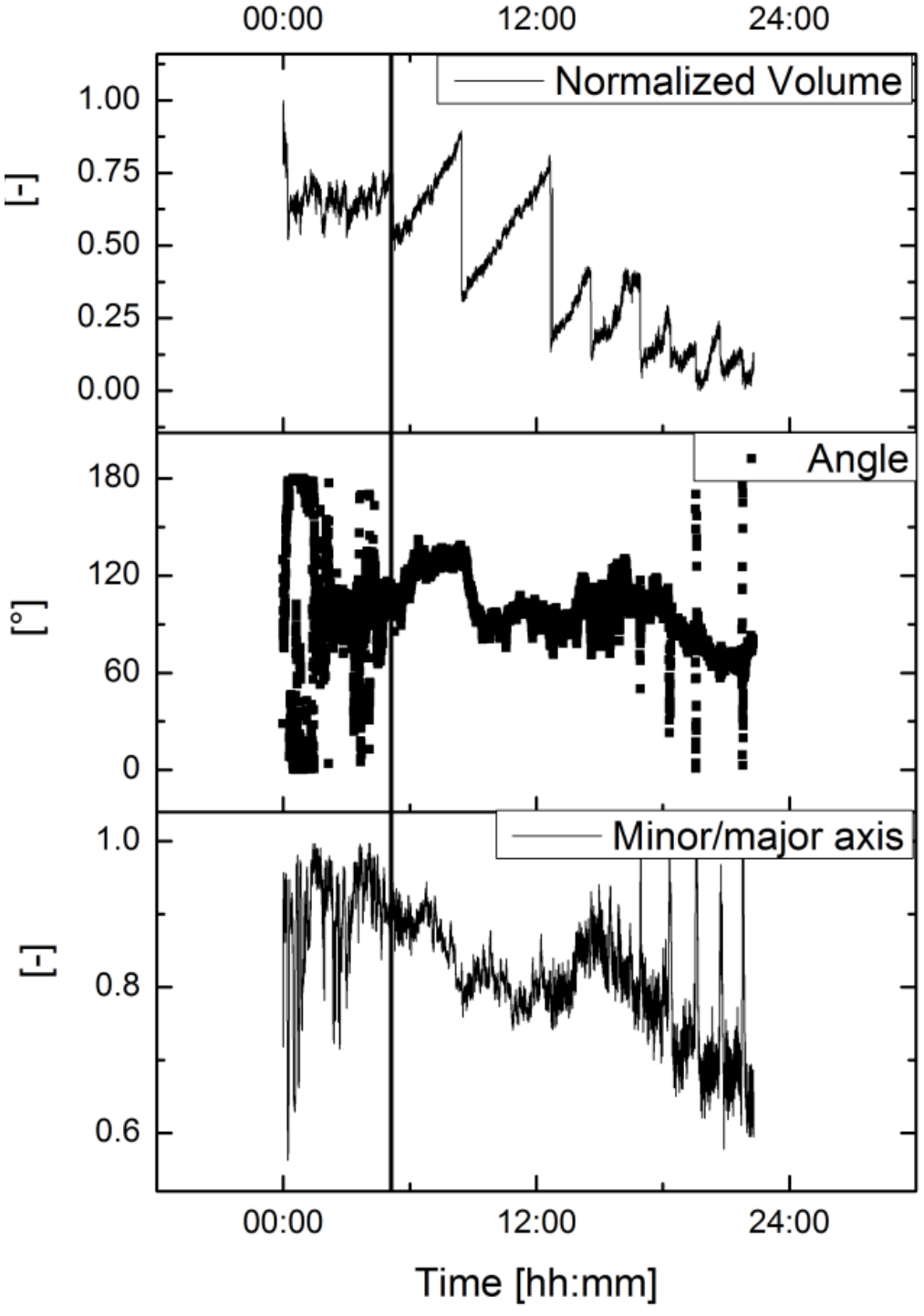

FIGURE 4.13: An example of an uncommon regeneration. The first and second oscillation phases seem to be exchanged. First, a phase with small irregular oscillations, at the end of which the directionality stabilizes, takes place. At the beginning of the large oscillations with decreasing amplitude and duration, the axis is already stabilized and the irreversible elongation takes place. Active behavior with appearance of tentacles starts after 13 hours.

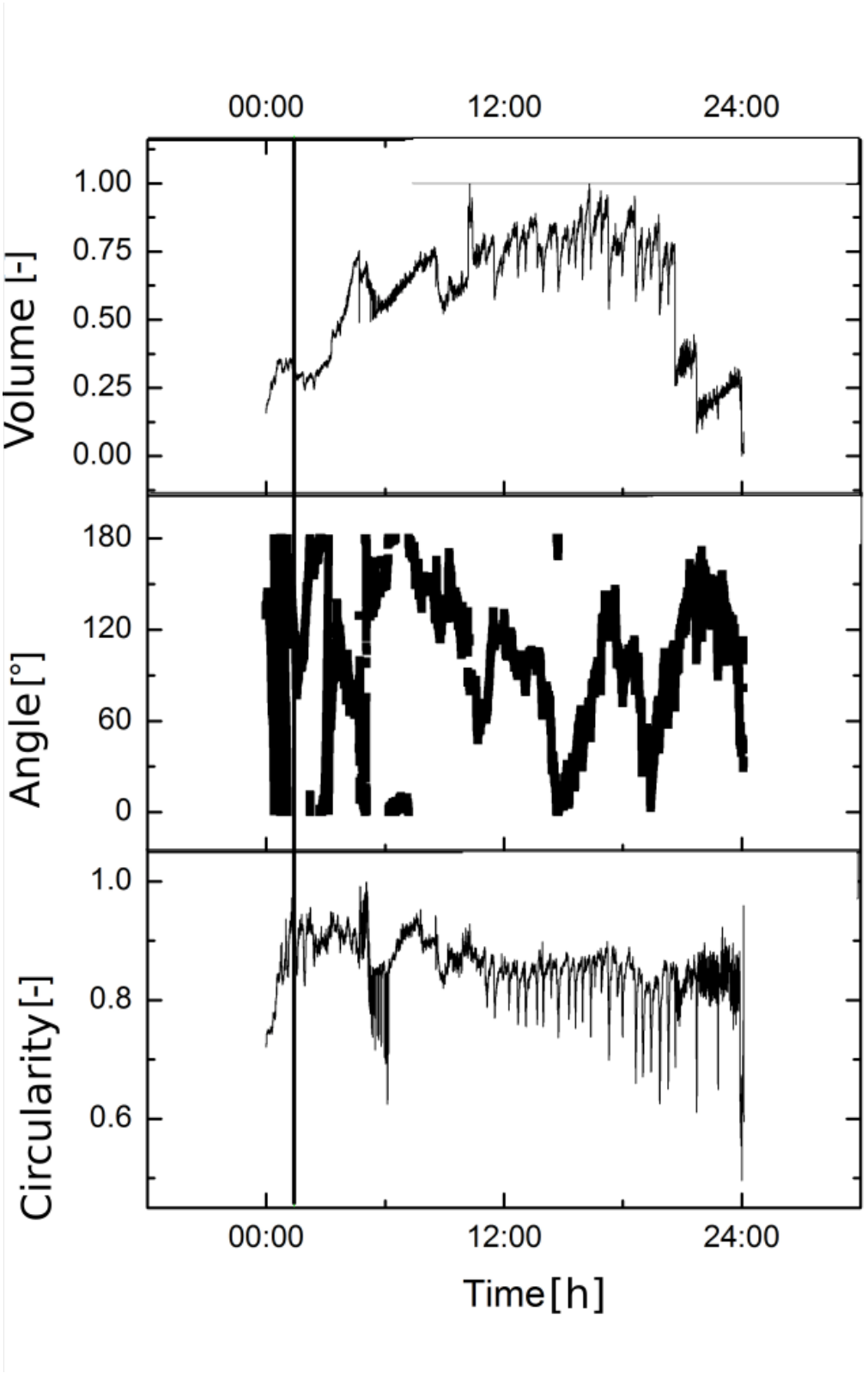

FIGURE 4.14: A regeneration that is an example of a stable angle before the start of the oscillations. A short period of unstable angle is present at the beginning (end of this period indicated in green). The total volume does not change as in other regenerations, the symmetry breaking is either achieved quickly or the asymmetry present from the beginning. However, the latter is unlikely, for reasons discussed in section 4.6

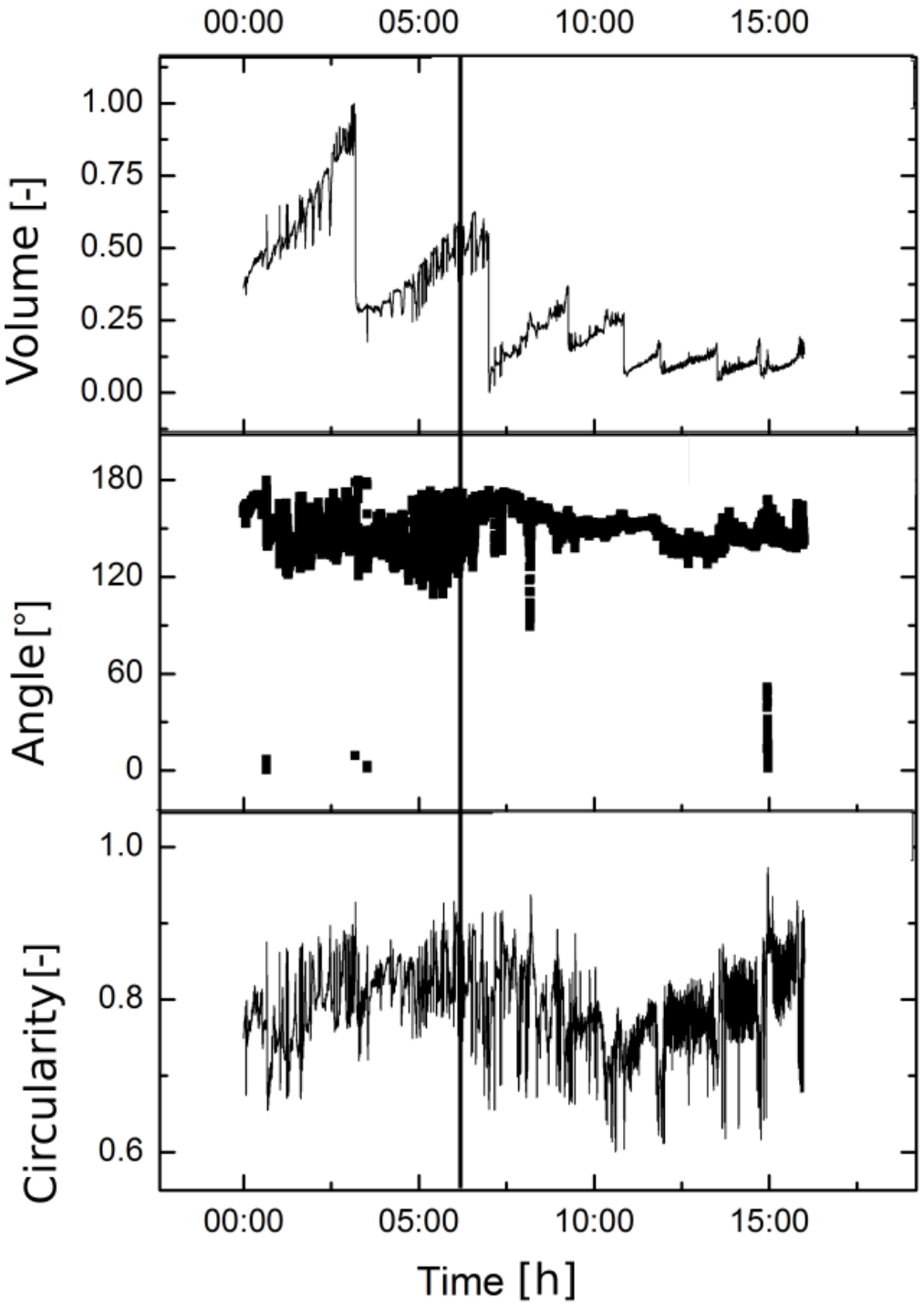

FIGURE 4.15: An example of a regeneration in an agarose well. The angle appears fixed from the beginning. However, clear oscillations and two regeneration phases are visible. The elongation is indicated in green. The regenerate is very small compared to other regenerations. This regeneration demonstrates that agarose wells can change the appearance and possibly the outcome of the regeneration.

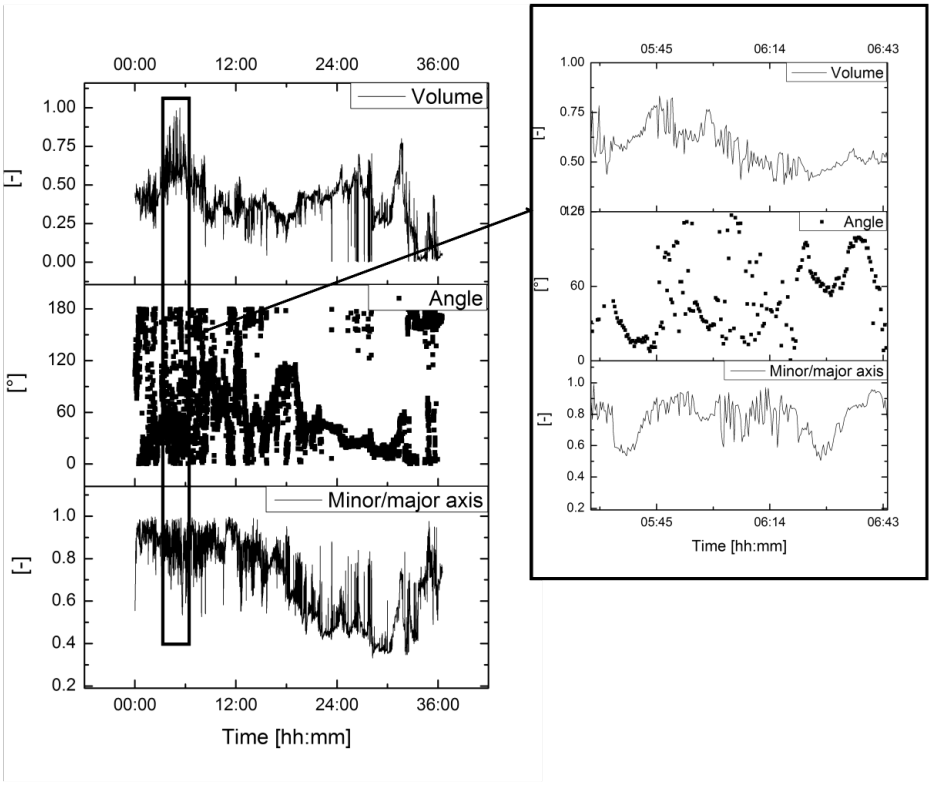

FIGURE 4.16: This regeneration exhibits symmetry breaking without clearly developed oscillations. Symmetry breaking and oscillation patterns do not necessarily correlate. The trembling behavior and shape fluctuations, however, are visible, as magnified in the box.

4.2.5 *Hydra* regenerates self-adjust to their ideal regeneration size during oscillations

As described in section 4.2.1, during the first inflation cycles, regenerates decrease in size by disgorging cells during each deflation. The total disgorged amount of cells differs between individual inflations and experiments. Some regenerates do not disgorge cells at all. This section investigates whether the amount of disgorged cells is random and whether this phenomenon correlates with symmetry breaking.
The size of the *hydra* regenerates at the beginning of the regeneration depends on the size of the cut fragments and is determined by the experimentalist. As described in 4.2, the size of the regenerates stabilizes before symmetry breaking. Initial size was measured at the minimum after the first oscillation. Size was measured again at the point in time after which the regenerate size stabilized, at the minimum of the oscillations after the size reduction. The initial and final size were compared.
The diameter before the adjustment, measured at the peak of the first oscillation, is 0.3

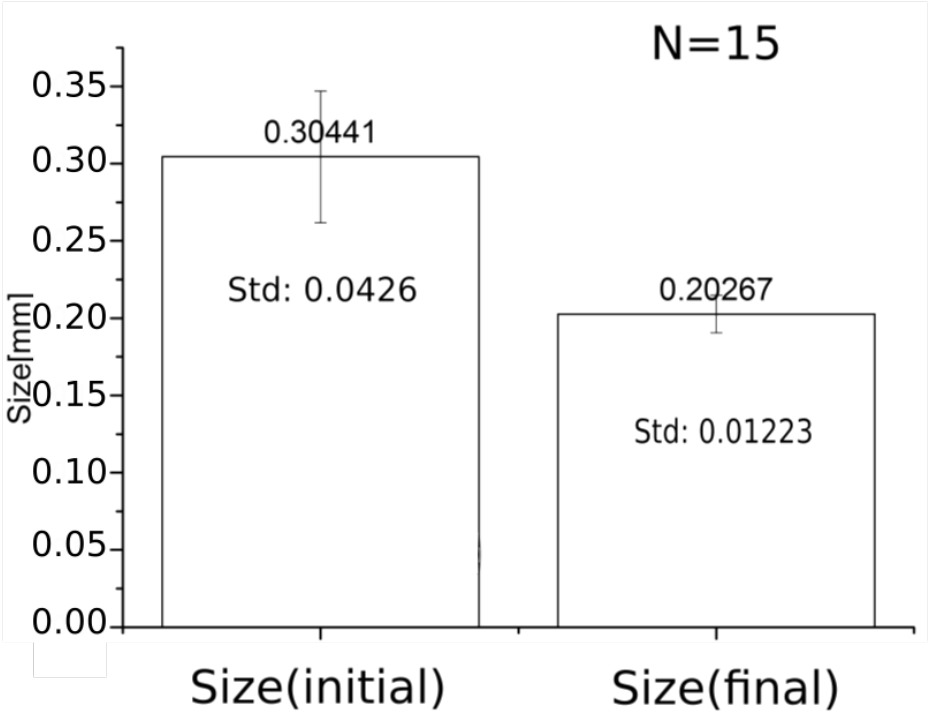

FIGURE 4.17: Comparison of the size of the *hydra* regenerates at the minimum of the first large oscillation and at the minimum of the first oscillation after the finished size change of the regenerate. The standard deviation decreases, suggesting an ideal size for regeneration. N=15. The standard deviations are strikingly low for both cases, indicating that during healing of the regenerate a first size correction could already take place.

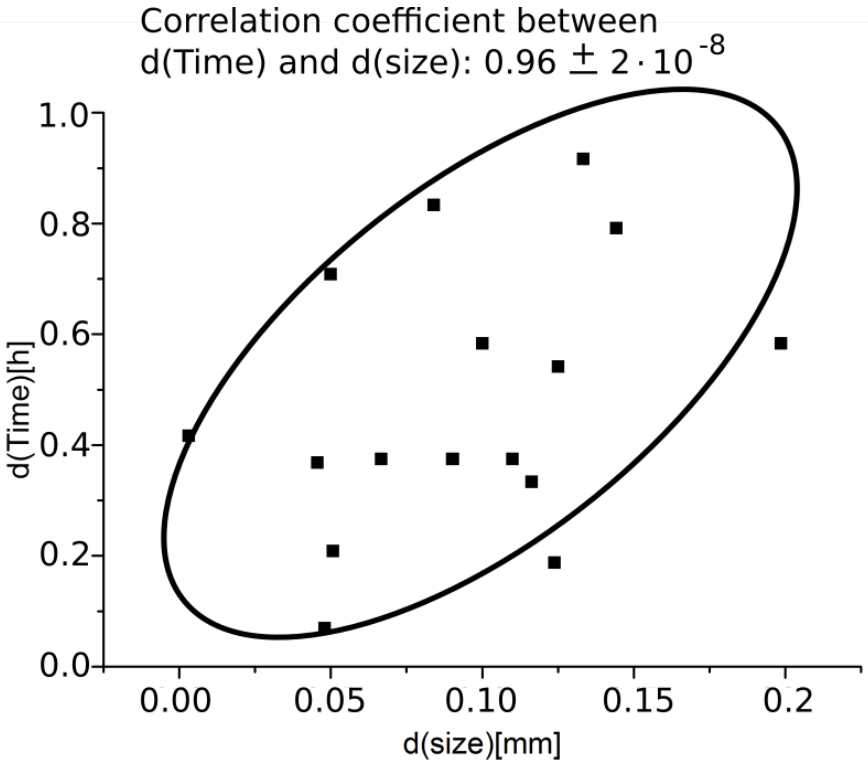

FIGURE 4.18: The time that is needed until the size change is finished seems to roughly depend on the amount of the size change, although a variance is observed.

mm with a mean deviation of 0.04 mm. The diameter after the adjustment is 0.2 mm with a mean deviation of 0.01 (N=15), see figure 4.17. The time until the *hydra* regenerate reaches its final size depends on the amount of the reduction. The time needed for the size correction depends on the size difference of the regenerate, as shown in figure 4.18. There seems to be an ideal regeneration size of 0.2 mm in diameter to which the regenerates always adjust prior to mechanical symmetry breaking (see fig. 4.17). This indicates that the symmetry breaking mechanism is size dependent. The mechanism is strikingly accurate, as demonstrated by the small standard deviation of the corrected size.

The time until symmetry breaking after scaling of the regenerates differs. *Hydra* spheres that undergo a size change between 0.06 and 0.15 mm have a higher regeneration success rate than initially smaller or larger regenerates. Within a size change of 0.06 to 0.15 mm the individual times until symmetry breaking vary substantially, ranging from 3 to 24 hours, and do not correlate with the size change (Spearman correlation coefficient -0.01, significance 0.97.). For the regenerates outside of this range, the time until symmetry breaking is considerably longer (see figure 4.19) and the regeneration success rate lower. Only three out of 10 regenerations outside of the ideal size range were successful, compared to a regeneration success of 100% in regenerates within the ideal size range, if performed in the hanging drop.

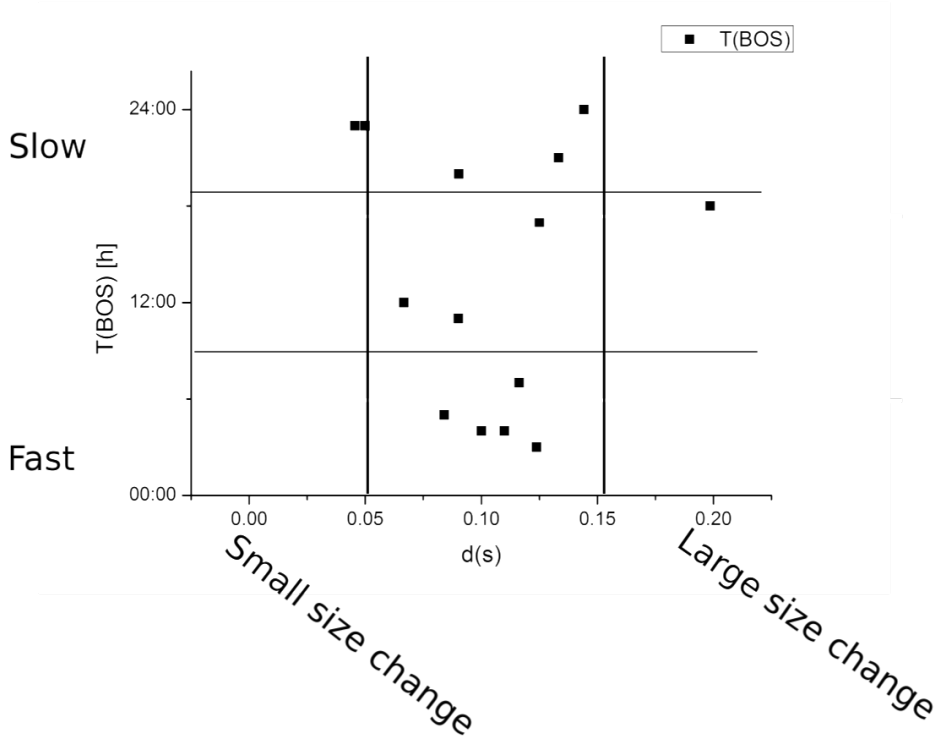

FIGURE 4.19: The time until mechanical asymmetry (T(BOS), normalized) in correlation to the size change (d(s)) of the *hydra* regenerate. There seems to be an ideal size change range between 0.06 and 0.15 mm that allows to reach the BOS faster in some cases, but the parameters do not correlate (Spearman correlation coefficient -0.01, significance 0.97.)

4.2.5.1 Summary, Discussion and Conclusion:

There is a size range where sucessful symmetry breaking and regeneration occur more frequently. The mechanism for size correction and the mechanisms for symmetry breaking are uncorrelated, however, symmetry breaking only occurs within the observed size range. The process of size correction seems to have other benefits besides the adjustment, as *hydra* that exhibit a certain size change regenerate more often and in shorter timespans than *hydra* that do not reduce their size (Fig. 4.19). One possibility is that the *hydra* removes cells that have been damaged during the cutting process. The mechanism that allows the *hydra* to perceive and correct its size is unknown. A strain rate dependent mechanism of size perception is possible. The end of the size correction process correlates with a change in oscillation pattern. The time for size correction depends on the amount of size correction that is necessary. The time between the size correction and the mechanical symmetry breaking varies independently of any observed parameter. Since the mechanical breaking of symmetry always happens after the size correction and

the size is within very narrow limits, one may assume an ideal symmetry breaking size. One may assume that the tissue ruptures always happen at a specific maximum or total strain applied on the tissue[124, 125]. In addition, the slope of the volume progress over time does not change if the size changes. What changes is the time that is needed to undergo one inflation (deflations allways take place within seconds). In smaller regenerates, the same maximum strain occurs in a shorter time, as smaller regenerates do not take as long to fully inflate. Thus, the time in which a specific strain is applied, decreases, and the strain rate increases. This is in agreement with the results of the micropipette stimulus experiments (discussed in section 4.3). There the strain distribution in the regenerate was changed by excluding a part of the regenerate from the oscillations and by pulling on an area. The exact role of the strain rate in symmetry breaking is not clear yet.

An important aspect is that the fluctuations of the angle and the fluctuations of the shape already appear during the size correction process. However, the stabilization of the asymmetry only takes place after the correct size is reached. This could be explained by two separate mechanisms that are responsible for either transient symmetry breaking (size independent) or stabilization of the new asymmetry (size, or strain rate, dependent). The transient symmetry breaking manifests in the fluctuations of the main axis orientation and seems to be microtubule dependent. The stabilization of the new asymmetry could also be cytoskeleton dependent. Especially the stabilization of actin stress fibers is strain rate dependent [126]. Therefore, the stabilization and subsequent elongation of the new asymmetry in the regenerates could be stress fiber mediated. The role of stress fibers and large contractile actin structures during regeneration is investigated in the next section 4.6. The hypothesis of stress fiber dependent stabilization of the new asymmetry is investigated in section (4.7).

4.2.6 Discussion and Conclusion

Every regeneration exhibits an individual pattern regarding the large oscillations. Most (20 of 25) regenerations exhibit clear oscillation patterns with three phases. First, regular large oscillations, where the regenerate adjusts to an ideal regeneration size, occur. After that, a phase with irregular large oscillations with varying duration occurs. The beginning of a third phase with shorter, regular sawtooth like large oscillations coincides with mechanical symmetry breaking. After the third phase, *hydrae* develop a head and a foot and start to move actively. In other regenerations, the irregular phase is more or less pronounced or completely missing.
One function of the large oscillations seems to be the size correction.
The orientation of the main axis with respect to the image frame of the regenerating ellipsoid over time can be used as an indicator of mechanical symmetry breaking. The stabilization of the angle always coincides with the beginning of the elongation of the sphere. The close correlation between angle- and shape fluctuations indicates that regenerates alternate between a state with transient asymmetry and asymmetry, until asymmetry stabilizes.

Only two regenerations did not exhibit a sign of mechanical symmetry breaking (figure 4.16, no large oscillations, and 4.15, with large oscillations). In conclusion, most regenerates of the appropriate size seem to loose their symmetry. The maximal size of regenerates that allows a symmetry loss is investigated in section 4.6.
The patterns of the volume oscillations over time are helpful, but not sufficient to describe the symmetry breaking process in *hydra* regenerates. Every regeneration exhibits an individual pattern, but all share common traits. Mechanical stimulus from agarose wells seems to influence the fluctuations of the main axis orientation(Example see figure 4.15). Therefore the effect of a mechanical stimulus on axis determination is investigated in more detail in the next section 4.3.

4.3 Mechanical stimulus by Micropipette aspiration determines direction of body axis

Hydra regenerates exhibit a remarkable sensitivity to mechanical stimuli. Confinement leads to death or escape. This suggests a mechano-sensitivity or adhesion of regenerates which, in combination with the mechanical changes during regeneration (see section 4.2), may play a role in the determination of the body axis.
Micropipette aspiration was used to investigate the effect of local mechanical stimulus on the regenerating *hydra* sphere. After a healing phase of 30 minutes, regenerates were fixed to the pipette by aspiration (see section 3.1.6.1 and 4.20). The regenerates only touched the pipette, not the bottom of the glass dish. The depth of the aspirated tissue in the pipette was 60 μm, roughly one quarter of the diameter of the sphere, leading to an elongation of the sphere perpendicular to the pipette (see figure 4.20). Only regenerates, who were held by the micropipette for the whole regeneration process (defined by the appearance of a head and foot), were analyzed.
Deviations in the aspiration pressure, the micropipette tip shape or diameter lead to either escape or death of the regenerates. Oscillations occurred and different regeneration phases could be distinguished. The tissue within the pipette contained no lumen and is excluded from osmotic inflations. The time until symmetry breaking and occurrence of tentacles corresponded to the control experiments.
The regeneration success was 60% (dead and escaped regenerates were counted as not successful). The angle of the axis in the focal plane was plotted (figure 4.20). Some *hydra* were oriented in the path of light (n=3), the others in different directions, but always in a circular area around the pipette tip (see figure 4.20). Interestingly no surviving *hydra* regenerated with the tentacles facing down, pointing to a sensitivity to gravity, as introduced by Hiroshi Shimitzu [127].

4.3.1 Discussion and conclusion:

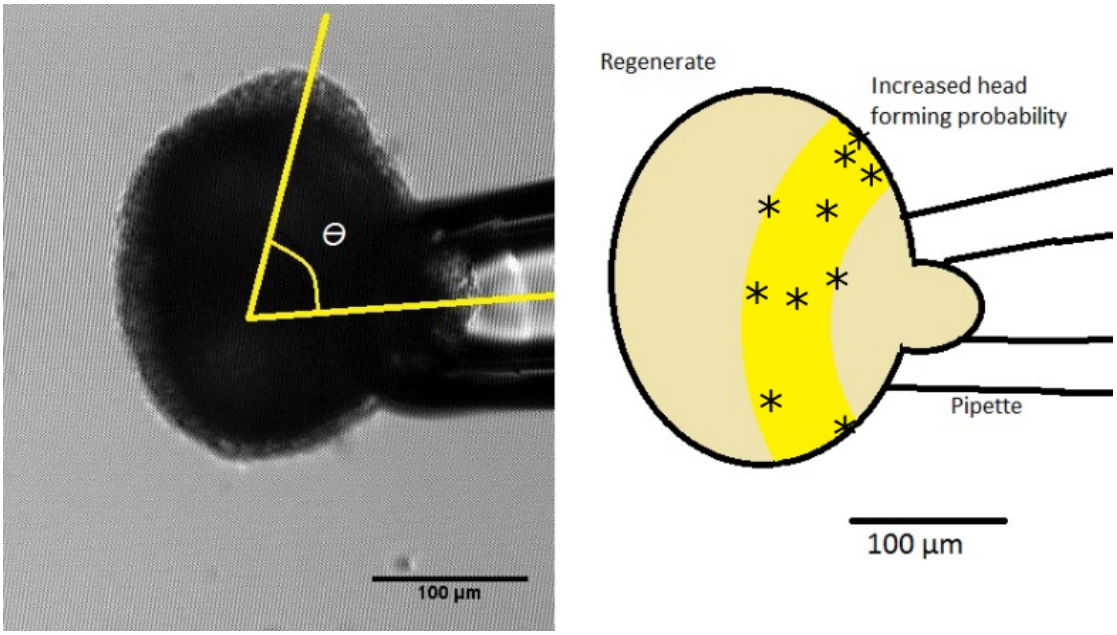

FIGURE 4.20: On the left, a *hydra* regenerate fixated with micropipette aspiration immediately after healing. The *hydra* regenerated in the plane oriented 40-70 ° to the pipette. Tissue was aspired 60 μm into the pipette, this part contained no lumen. On the right side, a schematic representation of the fixed *hydra* is shown, Head orientations are indicated as asterisks, the area of possible head appearance is lighter grey. No heads outside of this area were observed.

4.4 Location of rupture spots during first regeneration phase does not correlate with the later mouth opening

During regenerations *hydra* spheres inflate until a tissue rupture causes deflation. During deflation, excess cells and tissue are disgorged. It is possible that these ruptures are caused by a weak spot that is determining the head orientation from the beginning. Thus, no symmetry breaking process would take place.
To investigate whether these rupture spots predetermine the location of the later mouth opening and to distinguish turning and location of the later mouth opening, movement of the *hydra* and the locations of the ruptures were tracked and correlated with the new body axis and mouth opening. The regenerates move and turn during the regeneration, making it difficult to track the specific rupture spots on their surface. For experiment, the *hydra* was embedded in silica micro-beads, which allowed to track its movements during regeneration and pinpoint and follow the exact position of the rupture points despite its activity. Best tracking results were obtained in Silica Beads of 0.5 μm, the experiment also worked with larger or smaller beads, as long as the observation was performed in phase contrast. An exemplary picture is shown in figure 4.21, exact bead type and protocol are described in section 3.1.6.3. Turning and rupture of the *hydra* left traces in the beads, allowing to track the rupture points during regeneration.
The first rupture point is assigned as 0°. The last data point is the direction of the mouth opening and the tentacles. For the comparison of different experiments, the mean of the angle values during the first and the second regeneration phase and their standard deviations were calculated, see figure 4.22.

There was no correlation between the rupture points during the first phase of the regeneration and the axis. However, during the second phase, the rupture points corresponded to the later mouth opening, as shown in figure 4.22.

4.4.1 Discussion and conclusion:

The rupture points occurring in the first phase with unstable directionality do not determine the mouth opening. During the phase with stable directionality, the correlation is stronger, suggesting a structural reorganization of the sphere after the symmetry breaking. Deviations fall within the scope of the turning of the regenerate and correspond to the variation of directionality after symmetry breaking, as described in section 4.2. The changes in the mechanical properties of the regenerate point to a mechanical symmetry breaking and confirm the loss of symmetry.

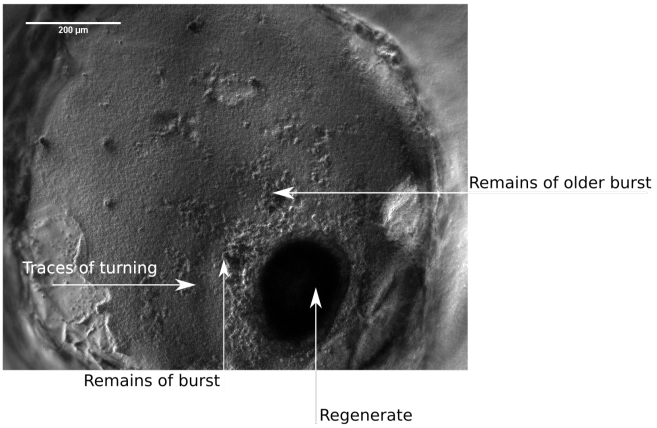

FIGURE 4.21: A regenerate surrounded by silica beads in phase contrast. The well is made of agarose (1,2%), the fine structure on the bottom of the well are the beads. The coarser structures surrounding the *hydra* regenerate are discarded cells. Those stick partially to the *hydra* surface and leave traces in the beads. This allows to track the turning of the *hydra*. The lighter areas in the beads indicate previously occurred ruptures.

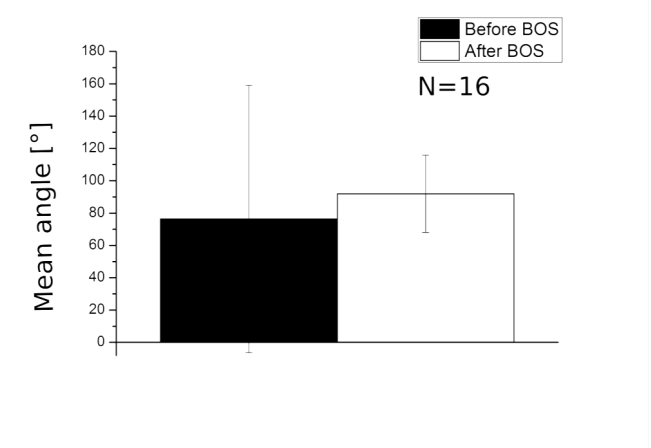

FIGURE 4.22: Comparison of the relative orientation of the rupture spots. Direction of the bursts (mean, and the standard deviation), comparison before and after symmetry breaking (as determined by oscillation patterns). Before BOS, the standard deviation is very high and no correlation between the bursts is observed. After BOS, the standard deviation is low, showing that there is a correlation between the bursts. Turning and movement of the *hydra* have been accounted for, as described in 3.1.6.3.

4.5 Global mechanical behavior of the regenerates exhibits rhythmical behavior and correlates with symmetry breaking

The nature of the mechanical behavior of the regenerates and its role in symmetry breaking is investigated in this chapter. As shown in section 4.2 and figure 4.23, *hydra* regenerates exhibit active mechanical behavior. Their quickly changing shapes are illustrated in section 4.5.1. The inflations exhibit trembling behavior that is reminiscent of a signal, which is investigated in section 4.5.2. In addition, inflations are characterized by alternating phases. Rhythmical trembling, where volume and angle are quickly changing, alternates with phases of angle stability (see figure 4.23, right panel). The dynamics of this process are investigated in section 4.5.3. The correlation between the fluctuating shapes and the trembling behavior is investigated in section 4.5.4. Finally, the role of the active mechanical behavior is investigated in section 4.5.5.

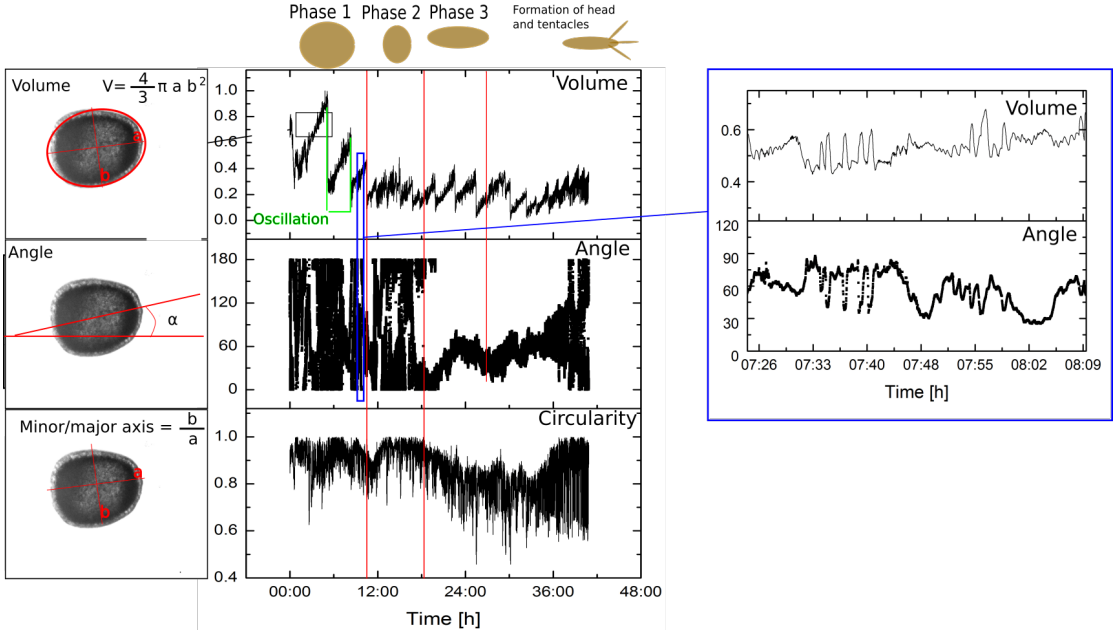

FIGURE 4.23: Overview of the mechanical behavior of *hydra* regenerates. The left panel schematically shows the investigated parameters volume, angle and circularity. Center panel shows an example regeneration. Red lines indicate changes in mechanical behavior. Right panel shows a magnification of the parameters volume and angle to illustrate the rhythmical changes between stable (low amplitude angle fluctuations) and unstable (high amplitude angle fluctuations) state.

4.5.1 Regenerates fluctuate between different shapes

Before mechanical asymmetry, the shape of the regenerates is, on average, spherical (see section 4.2). During each point in time, however, unique shapes can be observed. At each point in time, the regenerates can be either ellipsoid, pear shaped or exhibit up to three bulges in the plane of observation. An overview of observed shapes is given in figure 4.24. The shape changes correlate with high amplitude angle fluctuations and the behavior changes after symmetry breaking. The effect of microtubule manipulating drugs on the shapes is observed (see figures 4.26 and 4.25). Paclitaxel causes the pear shapes to be more pronounced compared to control. Nocodazole treated regenerations seem to lack pronounced pear-shapes and exhibit less bulging.

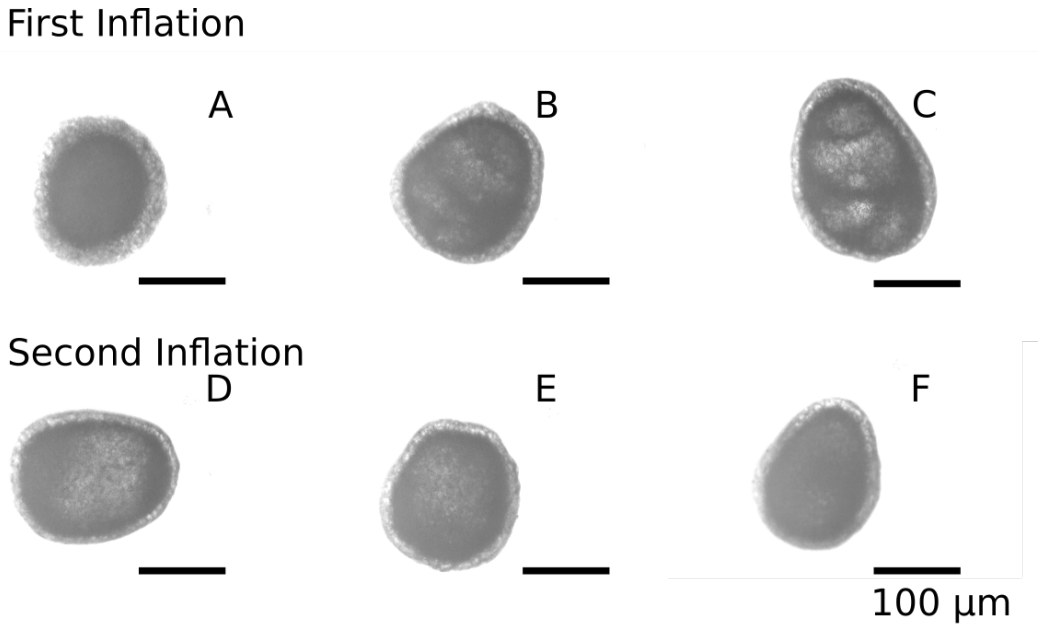

FIGURE 4.24: Examples of different possible shapes the regenerates can generally assume before mechanical asymmetry are shown. A-C during first inflations, D-F during second inflation, all before mechanical asymmetry. (A) Shows the regenerate immediately after healing. (A) Spherical, (B) Beginning pear shape, (C) elongated pear shape (D) rectangular-ellipsoid, (E) angular, (F) Pear shaped.

4.5.1.1 Summary and Discussion:

As described in sections 4.2, 4.5.5 and 4.5.2, *hydra* regeneration is characterized by fluctuations that coincide with symmetry breaking. The regenerates can change from one shape to the other within seconds. The possible or preferred shapes depend on microtubule polymerization. In regenerates with successful symmetry breaking, bulges can be observed with or without drugs. Drug treatment that inhibits symmetry breaking causes less pronounced bulges. Shape fluctuations are reminiscent of vesicle shape fluctuations,

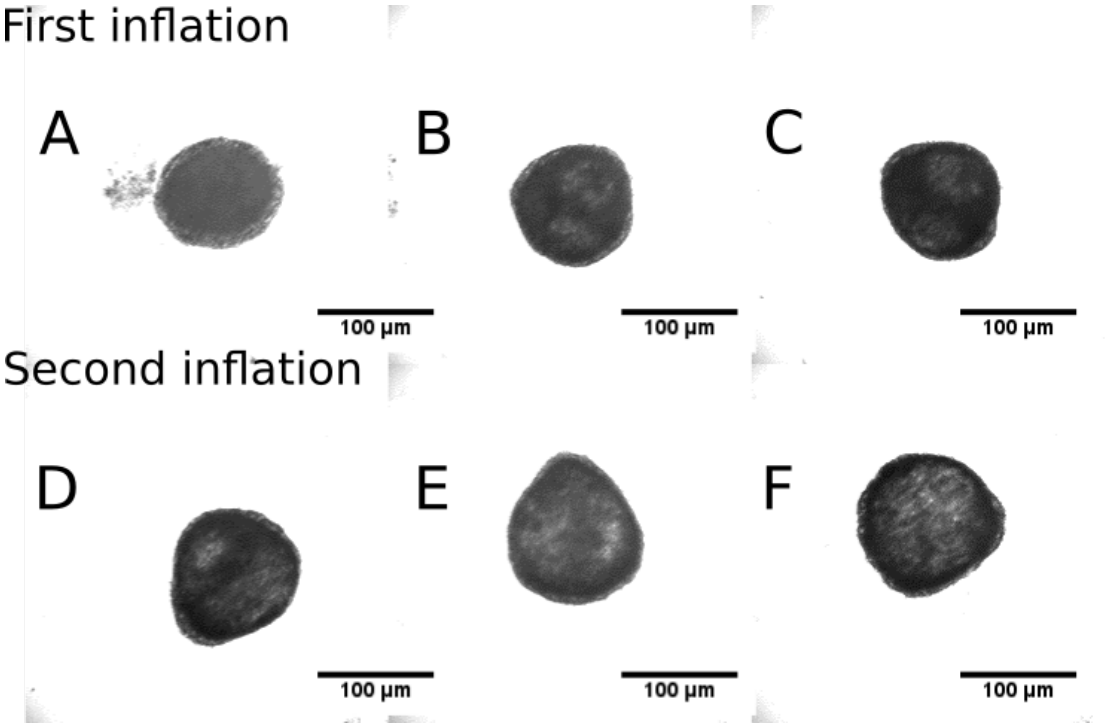

FIGURE 4.25: Example of regeneration treated with paclitaxel. First inflation: (A) Beginning of regeneration, spherical. (B) Spherical with bulges, (C) Two bulges. Second inflation: (D)Pear shaped with two bulges, (E) Pear shaped, (F) Two bulges.

as described by [128]. The bulging, which corresponds to the shape fluctuations, is microtubule polymerization dependent and plays a role in symmetry breaking.

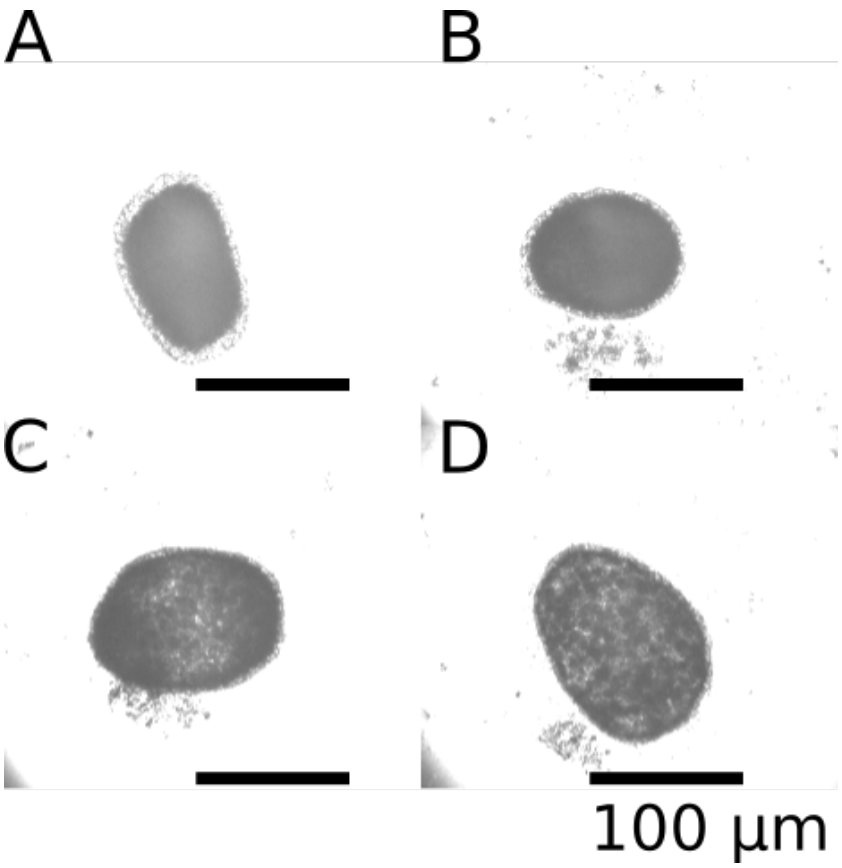

FIGURE 4.26: Examples of regenerate treated with nocodazole. (A) shows regenerate immediately after healing, rectangular ellipsoid. (B) rounded ellipsoid, (C) Ellipsoid with bulges, (D) Angular-pear shaped. In comparison to untreated or Paclitaxel treated regenerations, clear pear-shapes with small bulges are not observed.

4.5.2 Spectral analysis of large inflations reveals 1/f scaling behavior and biological timer

All regenerations exhibit high and low angle fluctuations before regeneration. To the bare eye, these fluctuations occur on the timescale of minutes. They can manifest as positive or negative peaks of the volume with respect to the average linear volume increase during the inflation. The behavior of the fluctuations during the symmetry breaking process has been investigated.

To investigate the characteristics of the trembling, a spectral analysis using Fast Fourier Transform (FFT) was performed on individual, detrended inflation cycles. Fast Fourier Transform allows to unravel a function or a signal into its sinusoid and cosinusoid components, example see Fig: 4.27. The significance of the spectrum depends on the frequency of the input signal. The Nyquist–Shannon sampling theorem establishes a sufficient condition for a sample rate that permits a discrete sequence of samples to capture all the information from a continuous-time signal of finite bandwidth. If a function contains no frequencies higher than N hertz, it is completely determined by individual datapoints spaced 1/(2N) seconds apart. A sufficient sample rate would be anything that is 2·N samples/second.

Here the frequencies were analyzed up to 0.1 hertz. According to the Nyquist-Shannon sampling, analyzing these frequencies requires a sample rate of 1 per 5 seconds. The imaging rate in the experiments was 1 image/second, therefore the data and the analysis satisfy the Nyquist Shannon criterion. Applying FFT to the detrended oscillations allows to investigate whether the course of the inflation is random or whether it follows a rhythmical pattern. A Fast Fourier Transform was performed as described in section 3.4.3. The Amplitude spectrum

$$\sqrt{R^2 + I^2}(\omega)$$

is analyzed.

Inflations where the beginning end end could be clearly identified were analyzed. This excluded some of the irregular inflations observed after size correction (4.2). Fast Fourier Analysis reveals a spectrum that exhibits two main components (see figure 4.28): For low frequencies up to 0.01 Hz, individual signals can be distinguished.

The spectrum, of all large inflations (N=20) exhibits a peak at 0.001 Hz in all inflations that were possible to analyze. This means that *hydra* regenerates undergo oscillation cycles of 16 minutes. This oscillation occurs no matter the state of regeneration or the shape of the oscillation patterns. Control experiments using particles instead of regenerates in the experimental setting did not exhibit this signal, therefore an experimental artifact is unlikely.

Except for the 0.001 Hz peak, the other observed peaks do appear to be at different

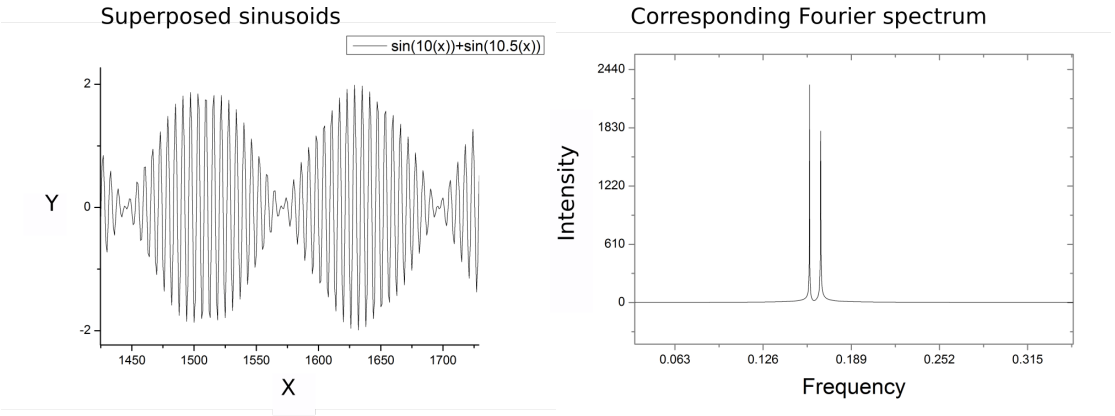

FIGURE 4.27: A Fourier analysis unravels the sinusoid and cosinusoid components of a signal. Left panel shows an example for the superposition of two sinusoid signals. Right panel shows the corresponding Fourier spectrum with a peak for each sinusoid.

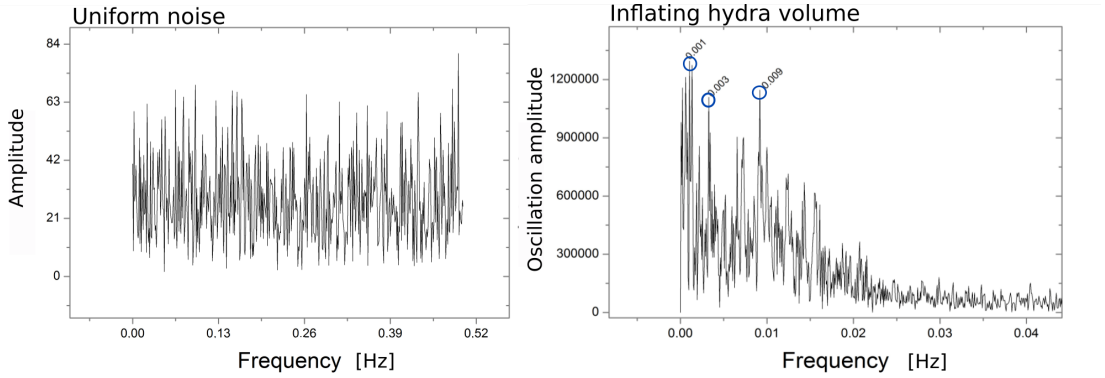

FIGURE 4.28: Comparison of Fourier spectrum of uniform noise (left) with an example of a Fourier spectrum of an oscillation (right). Intensity of the peaks (in uniform noise) or amplitude (in hydra) is plotted as a function of frequency. In uniform noise, the peak distribution is uniform across the frequency range. In *hydra*, spectral analysis of the detrended oscillations exhibits individual strong peaks (pronounced signals indicated by circles) and signal decay for frequencies higher than 0.01 Hz, which is also investigated in this section.

frequencies in each individual regeneration. However, normalizing the frequency with respect to the duration of the inflation, reveals a different picture. The frequency was multiplied by the duration of the inflation. As all experiments were recorded with 1 fps, the frequencies were multiplied by the amount of the datapoints within each inflation. This normalized the signals with respect to the duration of the inflation. This demonstrates that all oscillations exhibit the same periodicities in their mechanical behavior. Every oscillation in the 20 oscillating regenerations in reference to its duration exhibits a peak in their normalized fourier spectrum at 1, 2, 3, 4 and 6. This indicates that the course of every inflation follows a sinusoid (indicated by the peak at 1 in the normalized fourier spectrum) which is superposed by 2, 3, 4 and 6 sinusoid waves.

In other words, the course of all oscillations is not random, but exhibits periodicities which are the same with respect to the duration of the oscillations. As the duration

of an inflation depends linearly on the size, larger spheres undergo a longer inflation than smaller spheres (see section 4.2). The obtained Fourier signals are therefore size-independent.
This indicates that no matter the size, the shape or the course of the inflation from totally relaxed to bursting always follows the same pattern.
The third observation in the Fourier spectra is the 1/f scaling behavior for frequencies above 0.01 Hz. The decay of the intensity in the Fourier spectra above 0.01 Hz can be reproduced by a power law fit using the following equation:

$$I = \frac{1}{B \cdot f^{\alpha}} \tag{4.2}$$

with α between 1.25 and 1.8. The average exponent α is 1.41 $\pm$0.2, N=9. The influence of cytoskeletal drugs on the trembling was investigated. As described in section 4.7, altering microtubule polymerization with drugs can influence the symmetry breaking process. Nocodazole can suppress symmetry breaking, paclitaxel changes the dynamics of the fluctuations described in section 4.2. Therefore, the oscillation spectra of regenerations that were treated with microtubule polymerization altering drugs were investigated as well. Considering this parameter, there was no difference between control and paclitaxel treated regenerations. However, nocodazole treated regenerations exhibited an average exponent of 0.84 $\pm$0.12 (N=9), see figure 4.30. In addition, in control and paclitaxel treated regenerations, two regimes can be observed. Signals can be observed from the smallest frequencies to 0.01 Hz. Between 0.01 and 0.5 Hz, noise with the same exponent as in control is present. The transition between the two frequency ranges is very clear in all oscillations. In nocodazole treated regenerations this transition is not visible, the whole spectrum looks like noise (see figure 4.29). Therefore the presence of polymerized microtubules seems to play a role for the presence of the two regimes. However, the degree of polymerization is not important if it is at or above the natural polymerization level.

4.5.2.1 Summary and Discussion:

The fourier analysis of the inflations of the regenerates allowed three observations: A repeating signal that occurs every 16 minutes, an inflation pattern of superposed sinusoids that is independent of the duration of the regenerates and 1/f scaling behavior.

0.0001 Hz signal The 0.001 Hz signal seems to correspond to an intrinsic trembling frequency of the regenerates. This corresponds to a sinusoid every 16 minutes. The presence of the peak in the spectrum does not change depending on drug treatment or regeneration success. This rhythmical movement of the regenerate could be either the

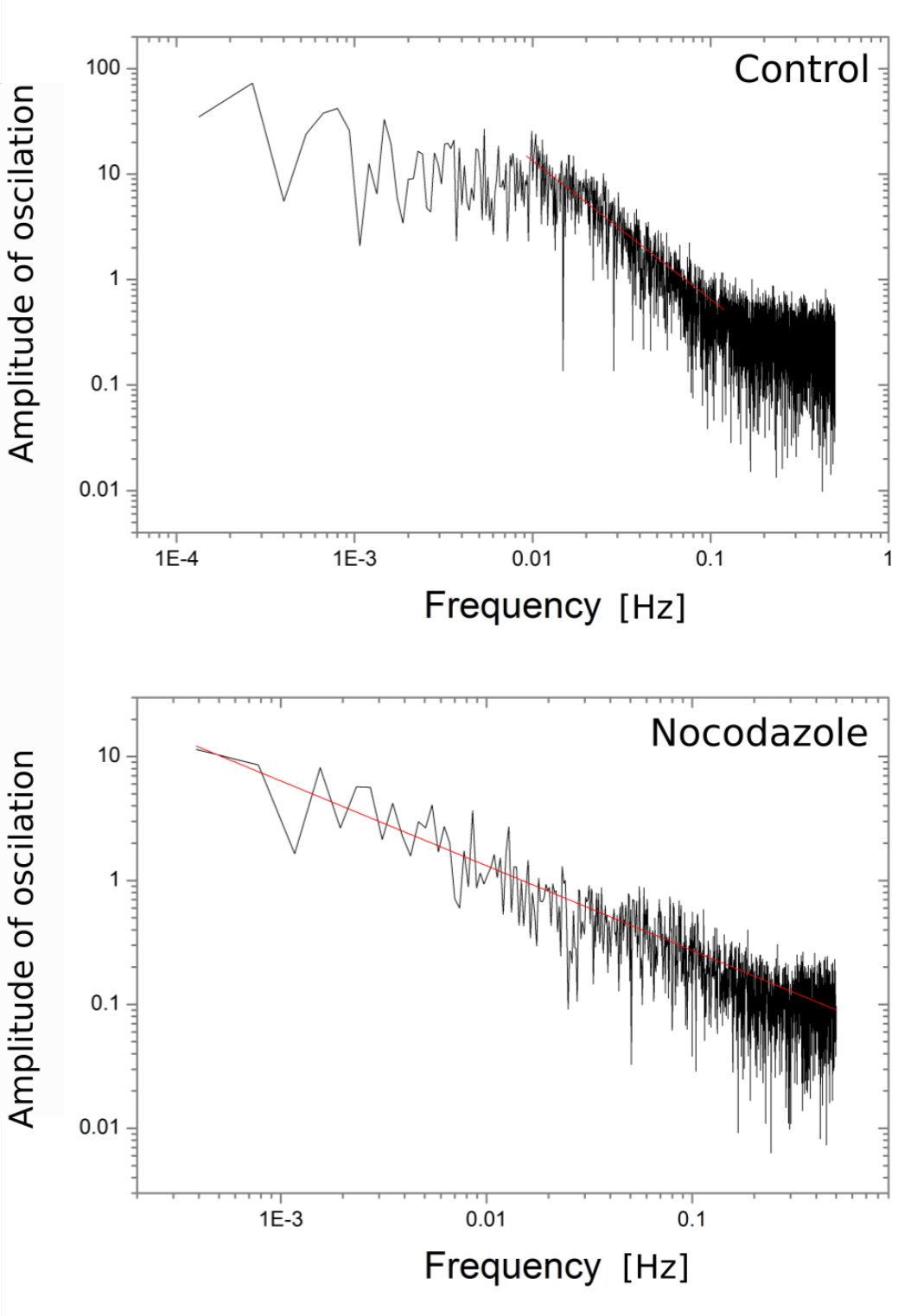

FIGURE 4.29: Double-logarithmic plot of Fourier spectra of control (left) and nocodazole treated(right) regeneration. The average exponent α in control regenerations is 1.43, standard deviation 0.21 (N=8), in nocodazole treated regenerations 0.84 standard deviation 0.12 (n=9), see fig. 4.30. The spectrum of nocodazole treated animals exhibited only noise.

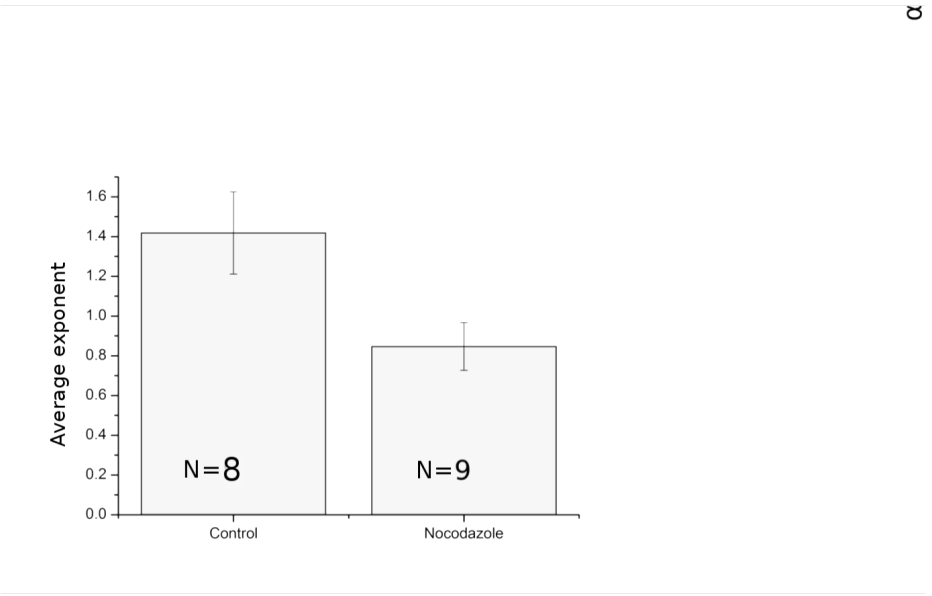

FIGURE 4.30: The average exponent α in the noise of the regeneration trembling is shown. In non-treated regenerations, the average exponent is 1.43, standard deviation 0.21 (N=8). In nocodazole treated regenerations, the exponent is 0.84 on average, standard deviation 0.12 (n=9)

eigenfrequency of the system, induced by the mechanical movements generated by the tissue. However, as eigenfrequencies depend on the material properties, the stiffness, the thickness etc..., a size dependence could be expected.

4.5.3 Shape fluctuation dynamics of regenerates exhibit power law behavior

Regarding the mechanical symmetry, hydra can be either in a state of high amplitude angle fluctuations or low amplitude angle fluctuations (see section 4.2.3). The angle difference (see Fig. 4.31)demonstrates how much the spatial orientation changes within a second and is a measure for axis stability. This parameter also allows one to vizualize the fluctuations of the main axis orientation.

To investigate the dynamics of this behavior the angle difference has been normalized. Comparison of the fluctuating phase with the stable phase suggested a threshold of 0.2, see Fig. 4.31. The threshold clearly separates the two different conditions: Either the main axis is stable and the *hydra* turns and "wobbles" without changing its symmetry, or the main axis changes within seconds and is unstable.
If the angle is close to 0 or 180, artificially high angle differences can occur (for example, the *hydra* turns from 170 ° to 10 °, which is actually a movement of 20 °, but is displayed as a change of 160°. These artifacts have been corrected by the following procedure (see section 3.4.4 for the exact coding): For every data point, if it is close to the boundary of 0 ° or 180 ° either a larger or a smaller step can occur (170° to 10°= 20° or 10° to 170° = 160 °) Of these two possibilities, the smaller ones have been chosen. The allowed distance to the boundary for this correction was based on the average change in angle after symmetry breaking.
The time points the *hydra* spends in one of the states have been counted. The normalized frequency of occurrence of a period of stability longer than a given value is plotted against the duration of the period of stability, see figure 4.32.
The shape fluctuation stability follows a power law.

$$y = B \cdot x^A \tag{4.3}$$

The fit is applicable from very short periods of low amplitude angle fluctuations in the range of less than 10 seconds and ends just before the longest period of low amplitude angle fluctuations after the symmetry breaking. The amount of the periods of specific durations follows a power law with an exponent A of -0.62 ± 0.003 for periods of durations between 1 and 200 seconds. A longer period of low amplitude angle fluctuations occurred only after the symmetry breaking as a stabilized asymmetry. Changing of the microtubule polymerization with paclitaxel (1 μM, applied after cutting) changes the power law exponent, see figure 4.32. Differences in the drug treatment can be caused by

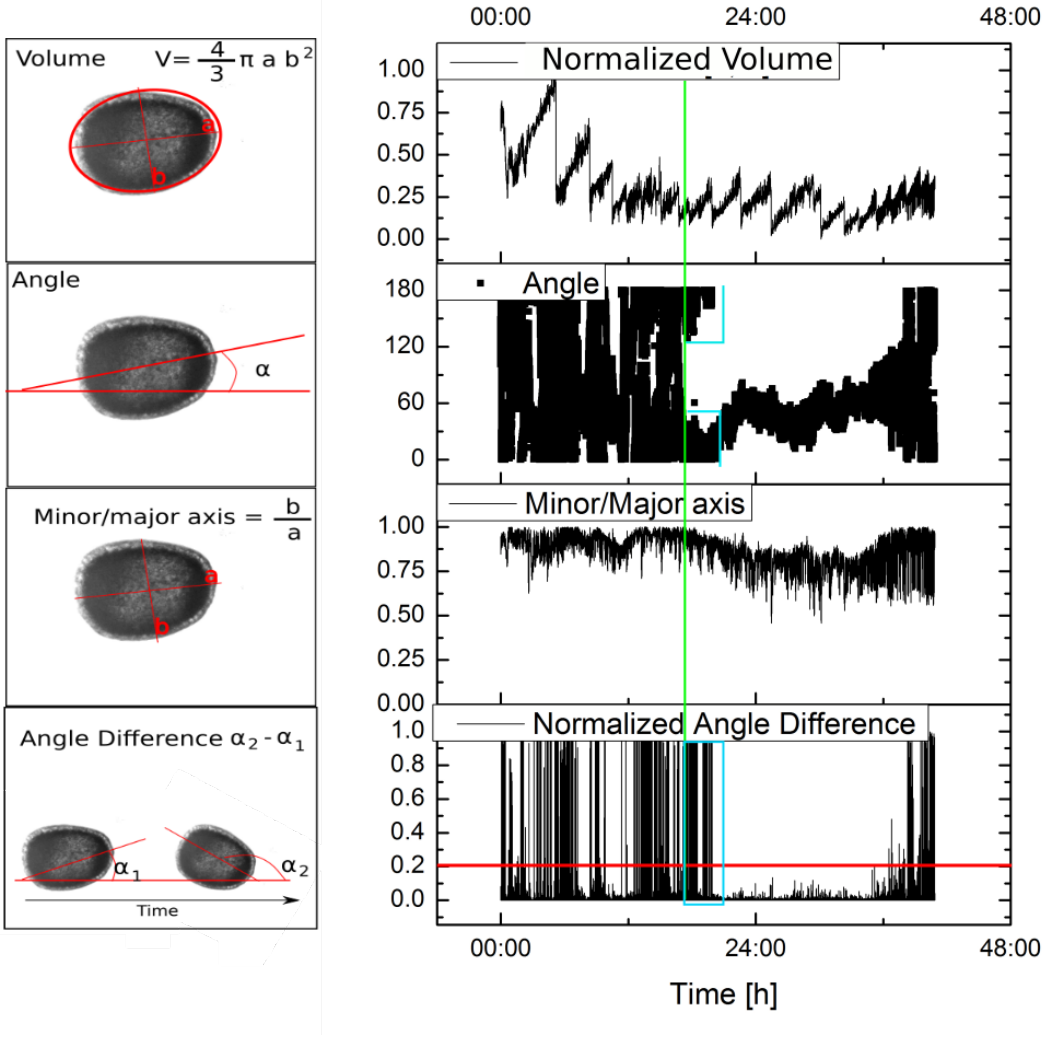

FIGURE 4.31: Example of the angle difference in context with other regeneration parameters and symmetry breaking, green. Volume demonstrates the development of the volume over time. The angle shows the spatial orientation of the *hydra* main axis. Minor/Major axis shows the circularity of the regenerates. The angle difference shows the difference of two subsequent angles of the spatial orientation of the *hydra* main axis. It measures how much the orientation changes within one second. Red indicates the threshold chosen to distinguish unstable from stable angle. Indicated by the cyan boxes is a common artifact from the angle difference calculation: If the angle changes between 180° and 0°, it cannot be distinguished whether it is a very small or a very large change. This is partially corrected by setting a threshold that determines how close the individual data points can be to either 0 or 180 °. The two possible differences are calculated and the smaller one is chosen in the subsequent analysis, visualized by the divided cyan box in the angle.

dosage imprecision caused by transferring the cut regenerates into the drugs with varying amount of liquid, or by initial size differences in the regenerates, or other unknown reasons.

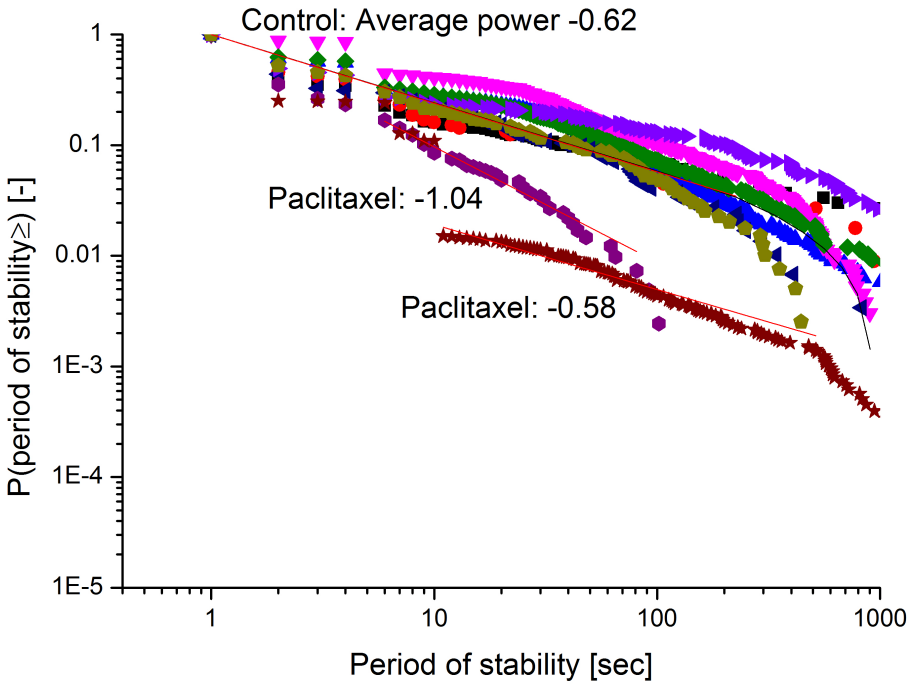

FIGURE 4.32: Time distribution of a period of stability (P(Period of stability≥)) value against the duration of this period, logarithmic plot. The data is averaged and, between 1 and 200, fitted with a power law. The resulting power is -0.62 with an error of 0.003 for control. Treatment with microtubule stabilizing drug paclitaxel changes the power of the dynamic to a lower value, indicating that shorter periods of mechanical asymmetry are sufficient to break the symmetry of the regenerate. The paclitaxel experiments differ, probably due to size dependent or dosage variation effects.

4.5.3.1 Summary and Discussion:

The distrubution of low amplitude angle fluctuations before the final stabilization of the main axis follow a power law. Before the irreversible mechanical asymmetry sharp transitions from stable to unstable state occur.

The sharp transitions indicate a global mechanical synchronization of the regenerate. In addition, the existence of a second mechanism for stabilization of the mechanical symmetry breaking can be postulated, that correlates with the elongation of the sphere, since the final phase of low frequency angle fluctuation does not fit into the power law. Stabilization of the mechanical asymmetry could depend on the time the regenerate spends in this asymmetry, as the elongation correlates with the time spend in the asymmetric state, see section 4.5.4.

Treatment with Rho Kinase inhibitor Y-27632 and Formin inhibitor SMIFH2 does not change fluctuation dynamics. Modification of microtubule polymerization changes the fluctuation behavior, stabilizing microtubules changes the power and the coefficient. Inhibiting microtubule polymerization suppresses shape fluctuations. This points to a microtubule mediated mechanism of shape fluctuations.

Gamba et al [22] demonstrated that a temperature gradient influences axis orientation, an experiment which was confirmed in this thesis in section 4.1.1. Based on fluctuating RNA expression patterns of head formation associated genes a model was proposed that exhibited 1/f scaling behavior and self-similarity.

Mechanical shape fluctuations as a key player in symmetry breaking in *hydra* could explain the results of the temperature gradient experiments as well. The results presented in section 4.5.2 demonstrate the dependence of the fluctuations dynamics on microtubule polymerization dynamics, which are also temperature dependent[90]. In a high temperature gradient, the colder side would fluctuate at a different frequency than the hotter side.

Temperature dependence of axis orientation is in agreement with a microtubule dependent non-equilibrium driven dynamic that plays a role in the symmetry breaking process of *hydra* regenerates.

4.5.4 Correlation between Shape Fluctuations and Trembling patterns

During the grouped peaks investigated in sections 4.5.5 and 4.5.3, differences between subsequently measured angles of the main axis appear, indicating a quickly fluctuating shape. The question whether the trembling either correlates with or causes the shape fluctuations was investigated. The difference between two subsequent angles was calculated and called the angle difference. A cross-correlation (N=17 regenerations) between the Oscillations and the Angle difference revealed that there is a strong correlation between trembling and high frequency angle fluctuations (without the sawtooth inflation/deflation patterns) with a correlation coefficient of 0,9±0.0306, for individual oscillations. In addition, the Circularity also exhibited a high correlation of 0.83±0.19 with the angle. Drops in the circularity ratio correspond to peaks in the trembling pattern (see figure 4.33). If the large oscillations are taken into account by analyzing a complete regeneration, the correlation coefficient drops to 0.8 ±0.08.

4.5.4.1 Summary and Discussion:

The volume course over time and the stability of the directionality exhibit a strong correlation, indicating that these two phenomena are be linked, and they may be caused caused by the same source. The influence of microtubule polymerization and depolymerization on the trembling indicate that microtubules play a crucial role in the process of symmetry breaking.

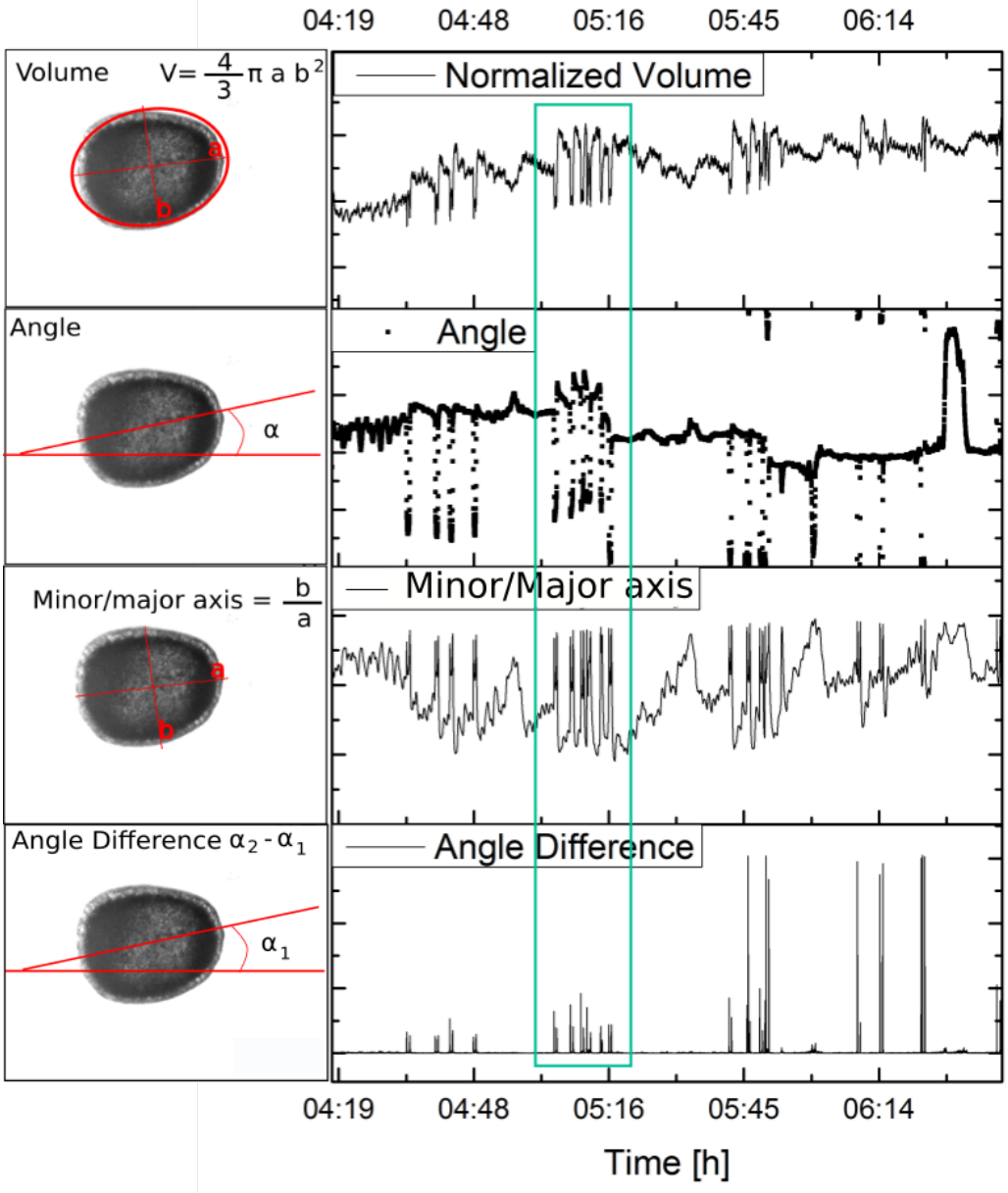

FIGURE 4.33: Normalized Volume, angle, circularity and angle difference of a regeneration exhibit correlated behavior. Rhythmical deflations of the volume correspond to increased minor/major axis ratio. During these rhythmical deflations the angle difference is also increased. The change in angle during these deflations is about 90°. One exemplary group of correlating volume, angle circularity and angle difference is highlighted by the frame.

4.5.5 Rhythmical trembling and fluctuations of the main axis orientation correlate with symmetry breaking

As described in section 4.5.2, *hydra* regenerates tremble rhythmically during large inflations. All successful regenerations exhibit trembling, while characteristics of oscillation patterns can vary. Thus, trembling is a more general mechanism.
To investigate whether this trembling plays a role in the regeneration and the mechanical symmetry breaking, cross-correlation with the shape fluctuations has been performed. In the volume over time plots it appears that the individual inflations follow specific patterns and the fast movement of the *hydra* is rhythmical (figure 4.34).

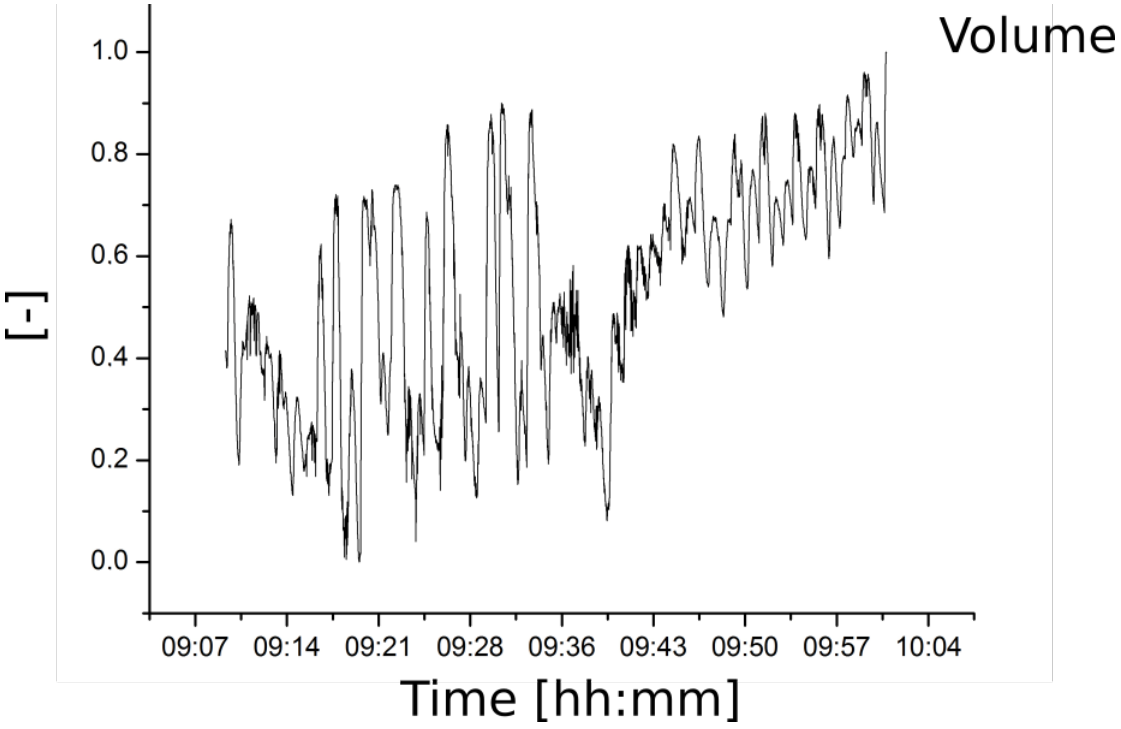

FIGURE 4.34: Example of fast rhythmical twitching of the regenerate during the oscillations before symmetry breaking. The peaks seem to be grouped, here with a distance of 1 min for either in- or deflations. Noise is also present and interfering with the signal. In addition, regenerations can also exhibit peak groups with a distance of 2 to 5 minutes between maxima or minima. Within individual groups, the peaks are equidistant.

Groups of equidistant peaks appear throughout the inflations, exhibiting quick rhythmical twitching of the *hydra* approximately every 2 to 5 minutes. The volume during this twitching sometimes increases, sometimes decreases, both directions appear as groups. Twitching appears as groups of volume increase or decrease with respect to the baseline. Before symmetry breaking, fast trembling appears and coincides with changes in the angle. The angle changes up to 90 ° in 25 seconds, see figure 4.35. After symmetry breaking there are also peaks, but they do not appear in rhythmical groups.
This behavioral change can also be observed during the transition between stable and

unstable phases (section 4.5.3) before symmetry breaking. The transition is very sudden (figure 4.36).

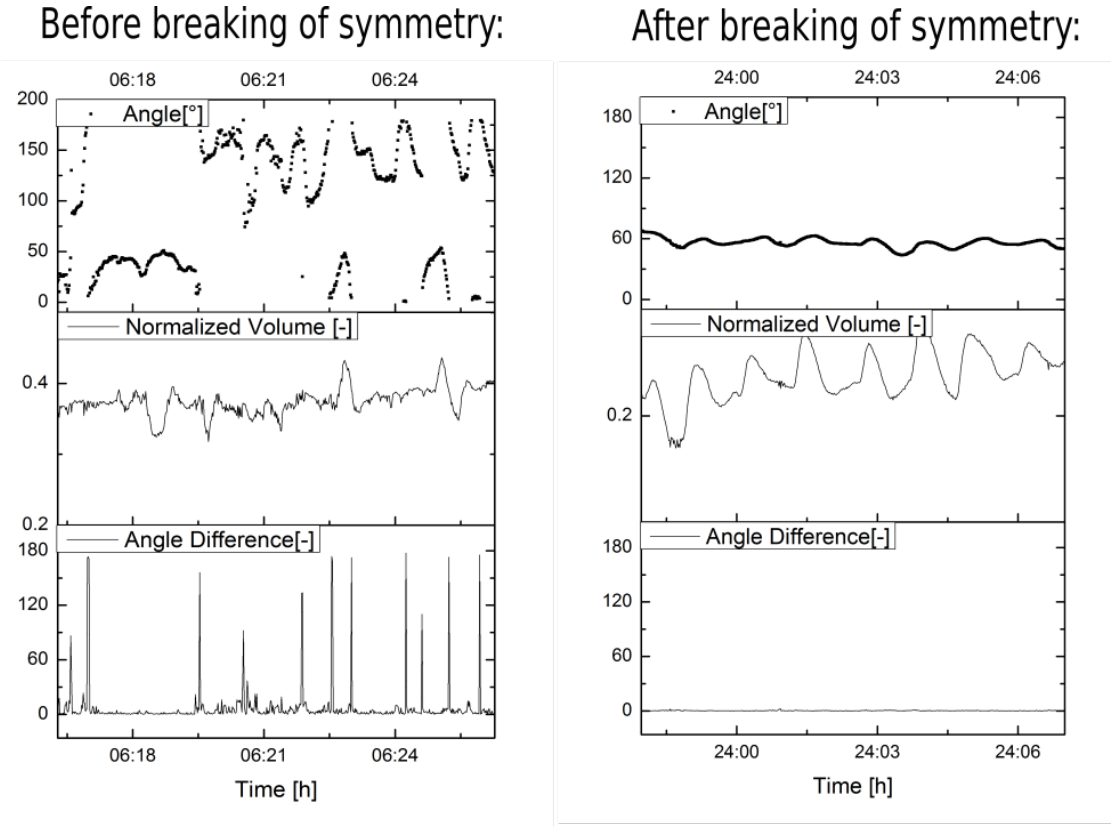

FIGURE 4.35: Detailed view of angle, volume and angle difference. Both panels are equally scaled. Left panel shows behavior of regenerates before symmetry breaking. The fast change in the angle, also seen in angle difference, coincides with the trembling, as shown in volume. After symmetry breaking, the change in angle is much lower and the trembling is replaced by a wave-like Volume change.

4.5.5.1 Summary and Discussion:

The trembling seems to correlate closely with a change in the angle and main axis direction (see 4.37) and therefore the shape fluctuations (chapter 4.5.1). The transitions are very sudden, there are no intermediate states. The regenerate undergoes fluctuations of the main axis orientation that change whether a main axis direction is present or not. he changes in trembling during the periods of stability that occur before the final symmetry breaking are identical to the changes in trembling after final symmetry breaking. This indicates that even before the symmetry breaking a mechanical asymmetry is present, but does not stabilize. Therefore the fluctuations give the regenerate a reversible asymmetry. Between the symmetrical and the asymmetrical state a clear differentiation is possible. The transition occurs withing less than a second. The transition into the final low amplitude fluctuation of the main axis orientation which is defined as the symmetry

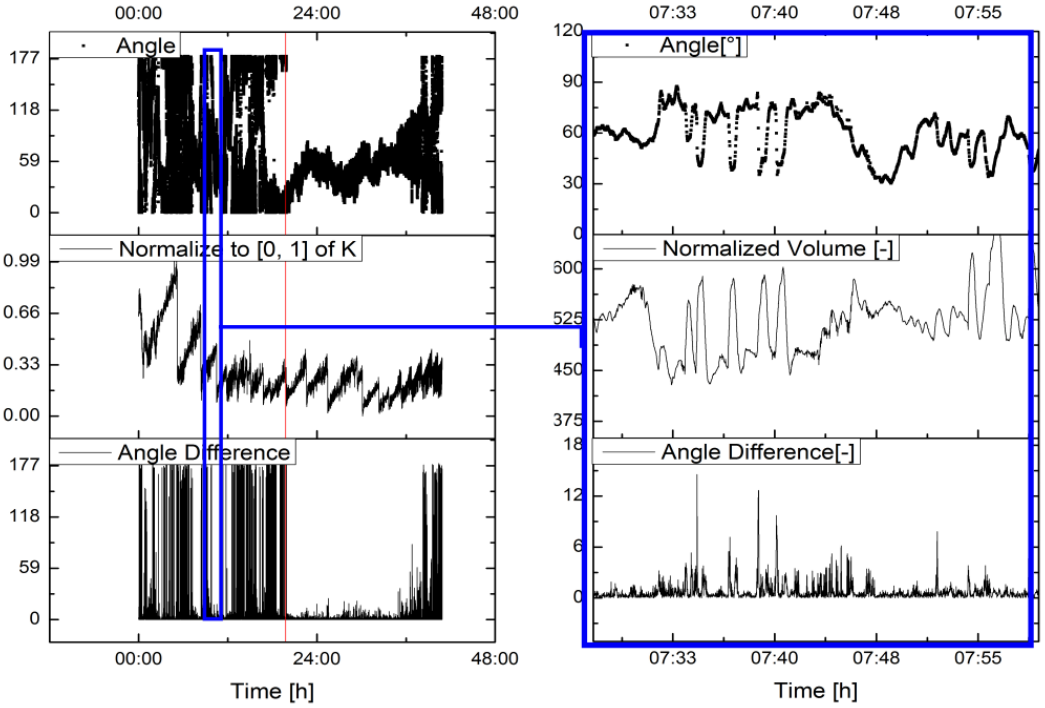

FIGURE 4.36: A complete regeneration (left)and a detailed view at the fluctuation behavior during the first regeneration phase. Both panels show angle (top), volume (center) and the difference between two subsequent angles (bottom). On the right side a time window of 30 minutes shows that the shape fluctuations correlate with a change in angle (indicating a shape change) and that the transition between the two states, stable and unstable, is sudden.

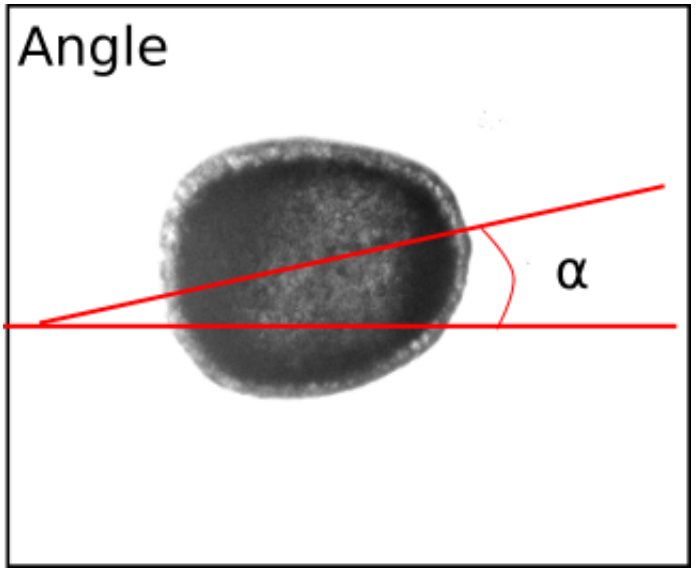

FIGURE 4.37: The angle is the direction of the main axis of the regenerate with respect to the image frame. The course of the angle over time reveals whether the main axis direction stays stable and can reveal whether fluctuations of the main axis orientation are present or not.

breaking (the irreversible asymmetry of the regenerate) is not different from the transition between the high and low amplitude angle fluctuations prior to this moment. For final symmetry breaking an additional mechanism is therefore necessary to stabilize the new asymmetry.
These results lead to the conclusion that the symmetry breaking and the elongation of the regenerate are controlled by two different mechanisms. This is supported by one of the experiments described in 4.7 that exhibits symmetry breaking without subsequent elongation following treatment with a formin inhibitor. This is in agreement with the conclusion of Bode et al [49], who claim that the setup and the maintenance of the head organizer in *hydra* regenerates are controlled by two different mechanisms.

4.5.6 Summary and Conclusion:

Mechanical symmetry breaking is the stabilization of the main axis orientation. Symmetry breaking of *hydra* regenerates is connected to its global mechanical behavior. Fluctuations of main axis orientation occur and demonstrate a microtubule dependent power law dynamic. Both the mechanical behavior and symmetry breaking depend on the microtubule cytoskeleton. This indicates that the mechanism to generate fluctuations of the main axis orientation is microtubule based. The mechanism that stabilizes the shape fluctuations is not known. To elucidate these mechanisms the behavior of the actin cytoskeleton (see section 4.6.1) and the influence of cytoskeletal drugs (see section 4.7) during regeneration are investigated in the next chapters.

4.6 Cytoskeletal components, especially actin, reorganize during regeneration

The active behavior of the regenerating *hydra* and mechanical manifestation of symmetry breaking suggests an involvement of the cytoskeleton. The three main cytoskeletal components are actin, intermediate filaments and microtubules (see section 2.5 in fundamentals). Here, F-actin and vimentin as an example of intermediate filaments during regeneration were investigated with confocal fluorescent imaging. Microtubules were investigated indirectly, described in section 4.7.

4.6.1 Actin

Hydra contains three major actin structures:
Myonemes, supercellular structures spanning $\approx$ 6 cells (see section 2.3);
Stress fibers, contractile actin structures within the cells (see section 2.5) and
cortical actin.
To visualize actin components, confocal imaging of either fixed, rhodamin/phalloidin stained *hydrae* or of transgenic life-act *hydra* (see section 3.1) was performed. The main difference between the two staining methods is that rhodamin/phalloidin stains all actin, while the life-act-gfp construct binds to polymerized cytosolic actin. The phalloidin staining protocol is relatively harsh and requires fixation steps, thus, some actin structures are destroyed during the staining process. Actin was investigated before cutting, 1 hour after cutting, 4 and 9 hours after cutting and after symmetry breaking (18-20 h).

4.6.1.1 Cellular and supercellular actin strucures disappear in small regenerates and reappear after symmetry breaking

Myonemes were investigated using Rhodamin/Phallodin staining. The structure of the myoneme network in the adult animals was investigated (see figure 4.38). Myonemes form two orthogonally arranged layers of actin filaments spanning several cells. The inner layer is oriented in the direction of the body axis, the outer layer perpendicular to it. They disappear 1-2 hours after cutting and reappear after the mechanical symmetry breaking. The structures are visibly re-established after 18 hours, which is after the longest symmetry breaking time, but prior to the appearance of structures like tentacles or foot. The exact point in time of reestablishment differs between regenerates, which

agrees with the differing time until mechanical symmetry breaking described in section 4.2.

Stress fibers can be directly observed in transgenic life-act *hydrae* (see figure 4.39). Y-27632, a drug which inhibits p160ROCK and leads to dissolving of filamentous actin and reduced contractility of acto-myosin, see section 2.7 caused a visible dissolving of the stress fibers within a short time (10-30) minutes.

In control animals, the stress fibers collapse one hour after cutting and appear as shortened and recoiled structures, indicating a tearing process, as opposed to a slow degradation (see figure 4.40).

After symmetry breaking (18-20 hours after cutting), the *hydra* exhibits a higher and diffuse actin signal around the future mouth opening (figure 4.41). This indicates either unstructured actin without the presence of stress fibers, which could be the result of insufficient or nondirectional mechanical stimulus of the cells; or a biochemical suppression of stress fiber formation (see sections 2.5 and 2.4). A strong actin expression could also mask the signal of stress fibers, however, even investigations with high resolution and high contrast did not reveal any structured actin within these cells. Except for the cells surrounding the mouth opening, stress fibers are clearly visible. This indicates that the cytoskeletal and probably the differentiation status of cells around the future mouth opening is different from the rest of the regenerate.

4.6.1.2 Maintenance of cellular actin structures depends on the size of the regenerate and indicates symmetry status

The minimum tissue size for aggregates to regenerate is 300 cells [52]. Larger aggregates and tissue fragments regenerate as well, however, the maximal size where the symmetry is lost and a new symmetry breaking needs to take place is not known yet. The cellular actin structures disappear in the regenerates that undergo symmetry loss and symmetry breaking. The size dependence of the loss of the cellular actin structures was investigated (see section 4.6.1.2). Several regenerates of different sizes were prepared from the center of the body column and incubated for 1 hour. Confocal imaging to investigate the cellular actin structures was performed. Regenerates were investigated via confocal imaging. Regenerates smaller than 400μm in diameter all lost the cellular actin structures (figure 4.43). The *hydra* toroids and large *hydra* fragments above 500μm in diameter maintained the actin structures, as shown in figure 4.42. Fragments above the size of the actin structure loss are very active and constantly changing their size, especially during light exposure, supporting the connection between the contractile actin structures and the ability to actively respond to stimuli by movement. Not only the loss of actin structures,

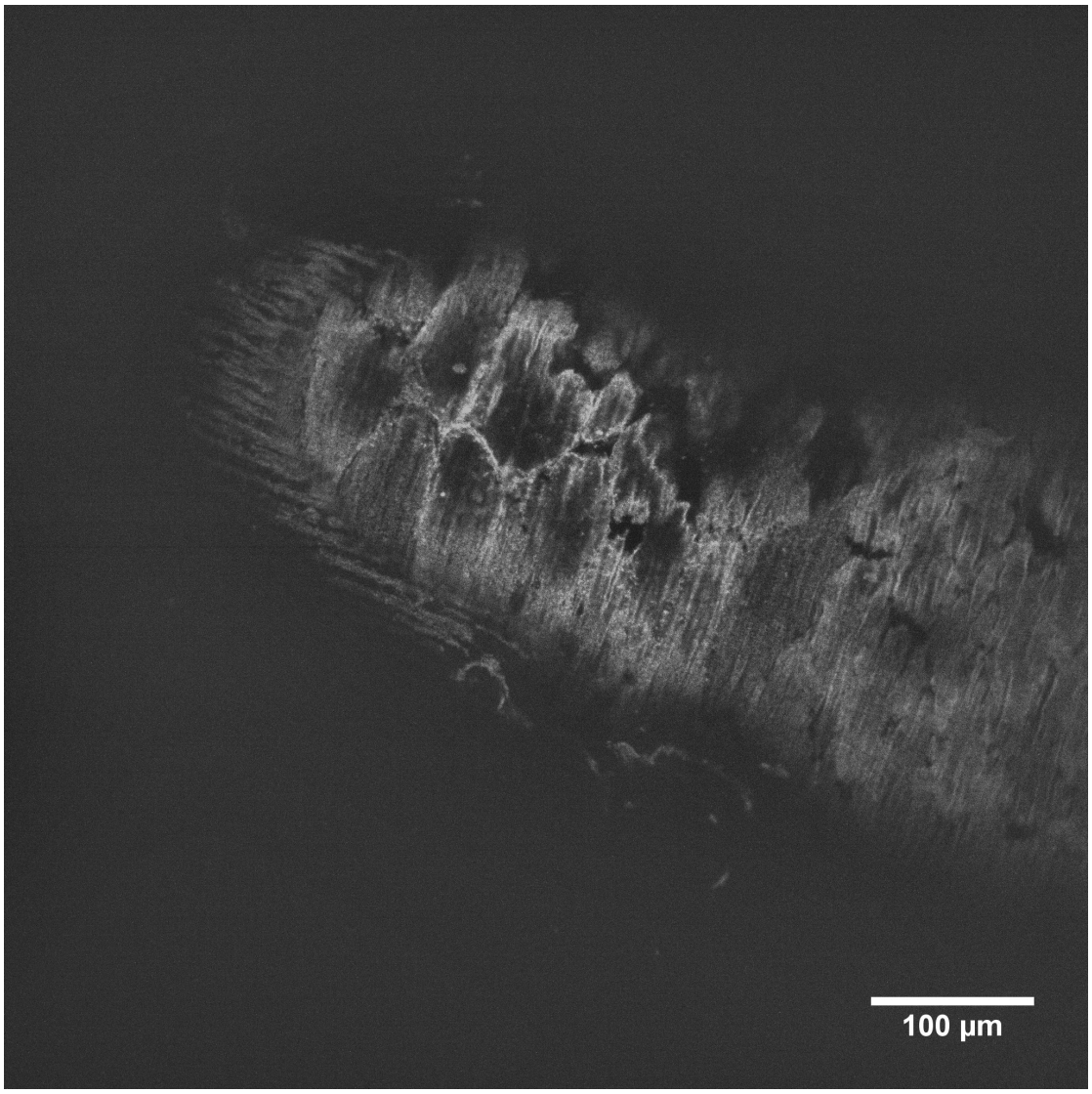

FIGURE 4.38: The myonemes in adult *hydra* tissue, stained with rhodamine-phalloidin. The orthogonally arranged structures can be seen in one focal plane. Surrounding the individual cells, the cortical actin cytoskeleton is labeled. Other intracellular actin structures are destroyed during this staining process.

but also the loss of directional movement in response to an external stimulus can be seen as an indicator of symmetry loss.

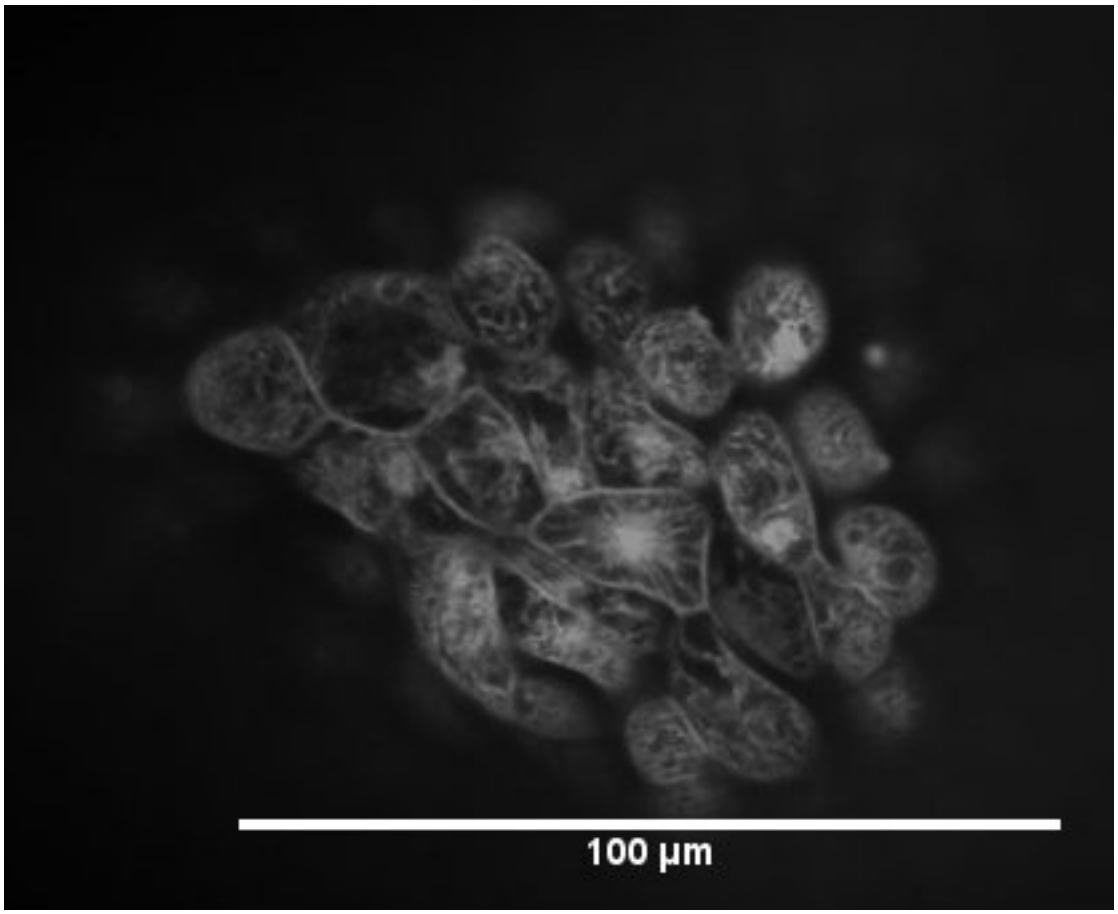

FIGURE 4.39: Stress fibers in ectodermal *hydra* tissue in adult animals. The actin stress fiber network and the cortical actin are visible.

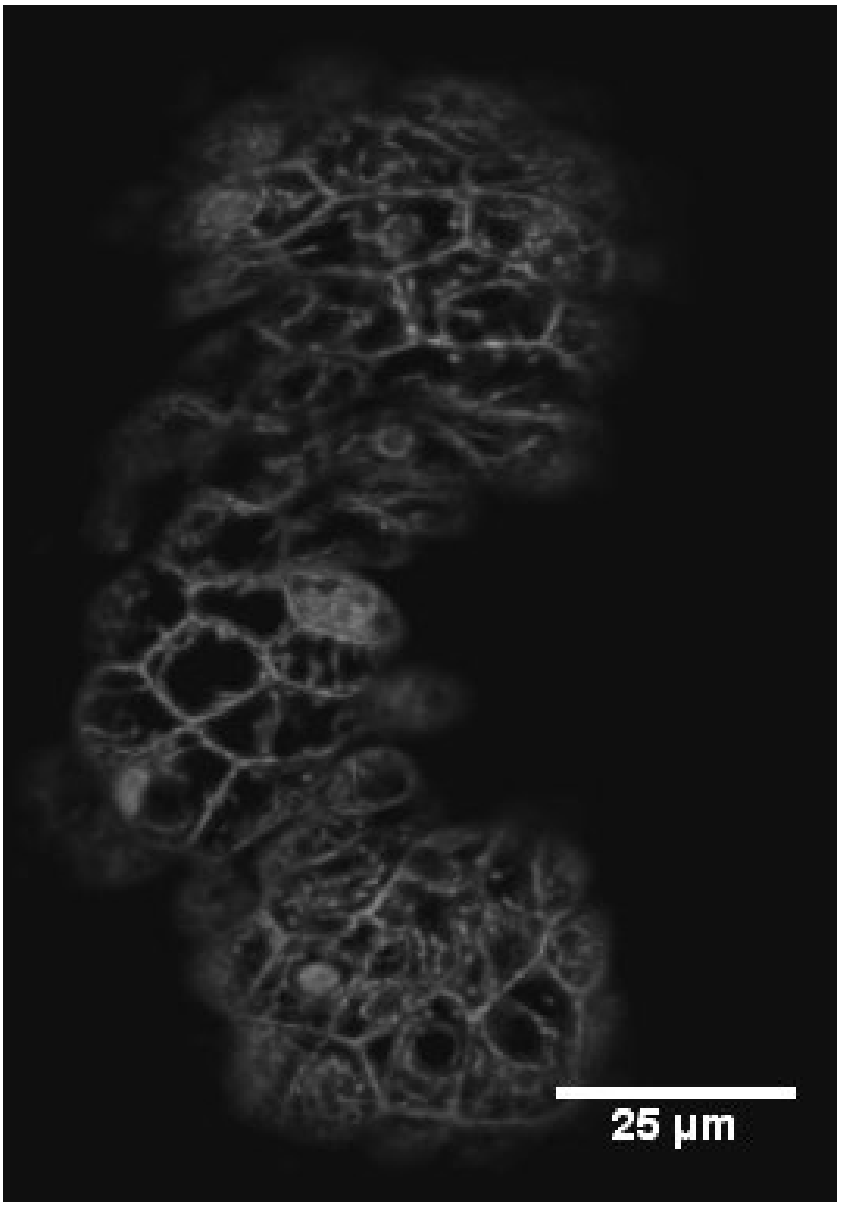

FIGURE 4.40: *Hydra* actin 1 hour after cutting. The cortical actin is still visible, while the stress fibers are only seen as recoiled residue at the cortex of the cell.

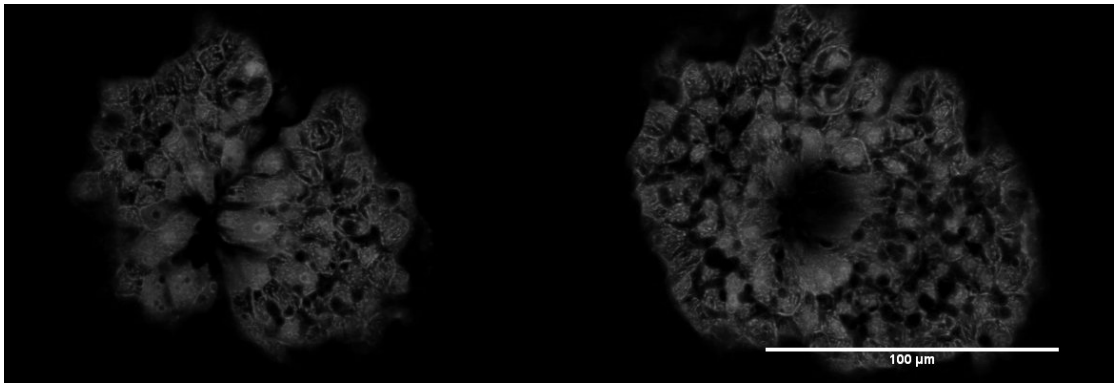

FIGURE 4.41: Mouth opening of *hydra* regenerate 20 hours after cutting in two focal planes. The left image shows the ectoderm and the outer surface of the mouth opening, the right image shows the endoderm. The cytosol of cells surrounding the opening in both focal planes seems diffuse, contrary to the remaining cells, which are clearly structured. In addition, the cells have an elongated and asymmetric shape that differs from the surrounding cells.

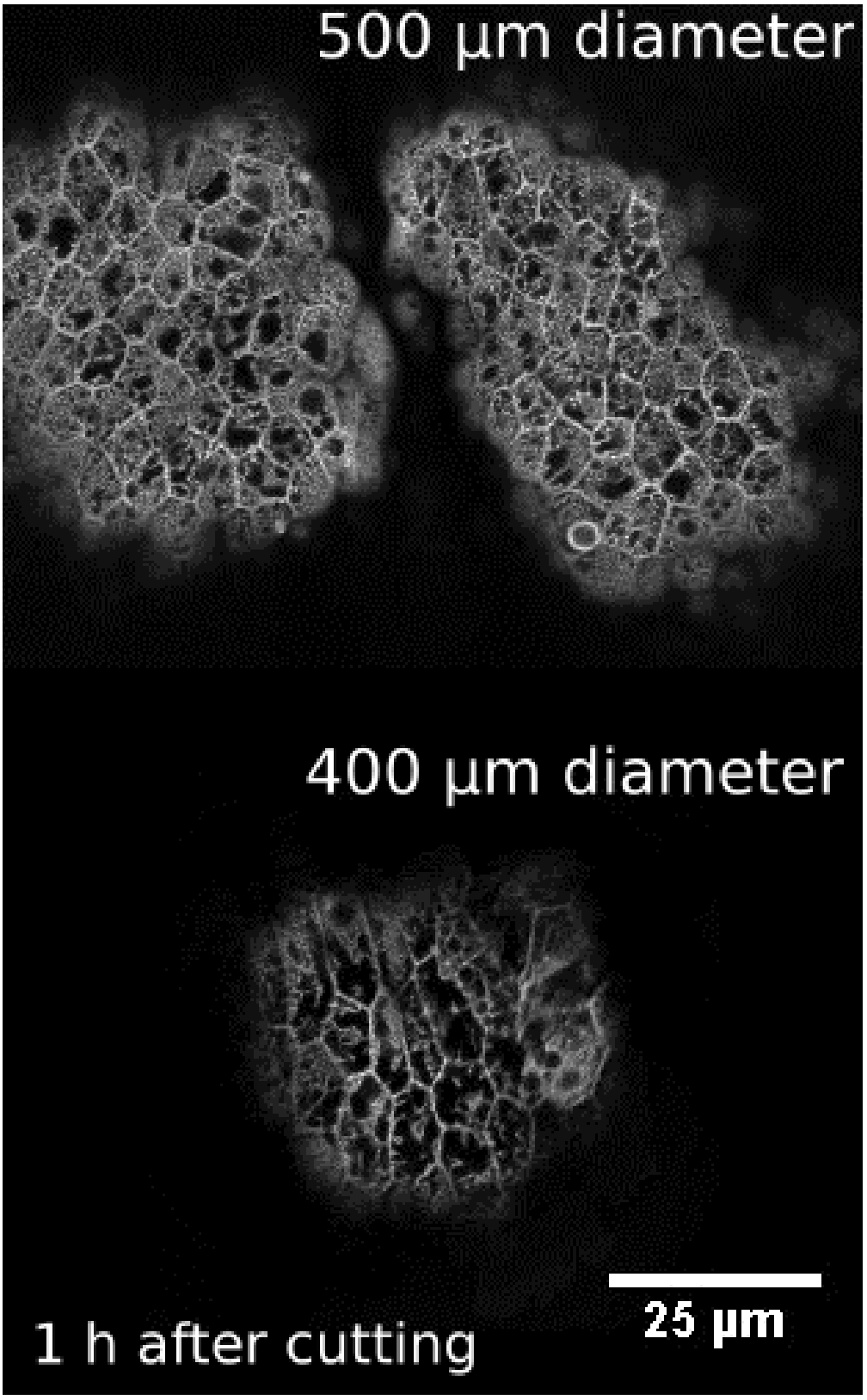

FIGURE 4.42: Confocal images of transgenic life-act regenerates. Both pictures display regenerates 1 hour after cutting. Upper panel shows a regenerate larger than 500 μm. The actin network is visible within the cells. The lower panel shows a medium (400 μm in diameter) sized regenerate. The cortical actin is visible, stress fibers are only seen as residues attached to the cortical actin.

FIGURE 4.43: Confocal imaging of life-act GFP transgenic *hydra*, 1 hour after cutting. The left panel shows the dissolving actin structures, recoiled and visible as small residues attached to the cortical actin. Center panel shows the total size of the regenerate. Right panel shows an overlay of both pictures to visualize the cell/regenerate ratio.

4.6.1.3 Summary and Discussion

In all observed regeneration of regenerates less than 500 μm in diameter(N=9), all visible large contractile actin structures except cortical actin disappear during the first large oscillation. A reorganization of myonemes in *hydra* toroids upon cutting has been observed by [129].
Regenerates undergo significant mechanical stimuli during the oscillation. Individual cells are stretched approximately 6 times their area during the large oscillations.The amount of stretch the *hydra* cells receive was approximated by measuring the size of cells before the first large inflation from the confocal imaging (12 μm in diameter) and calculating the average size increase of the sphere (60%). In addition, after cutting, the turgor pressure is lost until the regenerate heals into a sphere (approximately after 1 hour). This and the loss of tension resulting from the fast deflations is substantial and could be responsible for the loss of stress fibers in the cells.

The behavior of actin around the mouth opening is different from the behavior in the surrounding cells, indicating divergent mechanical properties in this area upon symmetry breaking. This appearance of actin can occur either due to a local change in biochemistry or, more directly, due to a change in mechanical stress surrounding this location, or both. A similar appearance of actin was observed during sea urchin gastrulation, as shown by [130]. During gastrulation in sea urchins, the vegetal plate (the first pole of the embryo) exhibits increased actin concentration and a change in cell shape, comparable to the cells seen in figure 4.41.
Actin stress fiber degradation probably occurs due to the quick change in substrate stiffness after cutting and during the deflations (see Tojkander et al. for substrate stiffness dependent stress fiber behavior [131]). The process of stress fiber and myoneme degradation after cutting is probably a part of the symmetry loss mechanism in *hydra* regenerates. The symmetry loss after cutting can therefore also be interpreted as a loss of mechanical symmetry, in addition to the loss of biochemical gradients described by [124].

4.6.2 Vimentin

Vimentin was investigated as it is a representative of the intermediate filaments and important in cell adhesion and wound-healing. A BLAST (Basic Local Alignment Search Tool, an algorithm to compare gene sequences) genome search revealed that *hydra vulgaris* contains vimentin-like sequences at the Locus100199525 (Gene ID: 100199525), although the protein itself has never been verified. An anti-Human vimentin Antibody staining demonstrates that vimentin epitopes are present in the cnidocytes of the *hydra* in the tail and harpoon of the nettles (see figure 4.44 and 4.45).

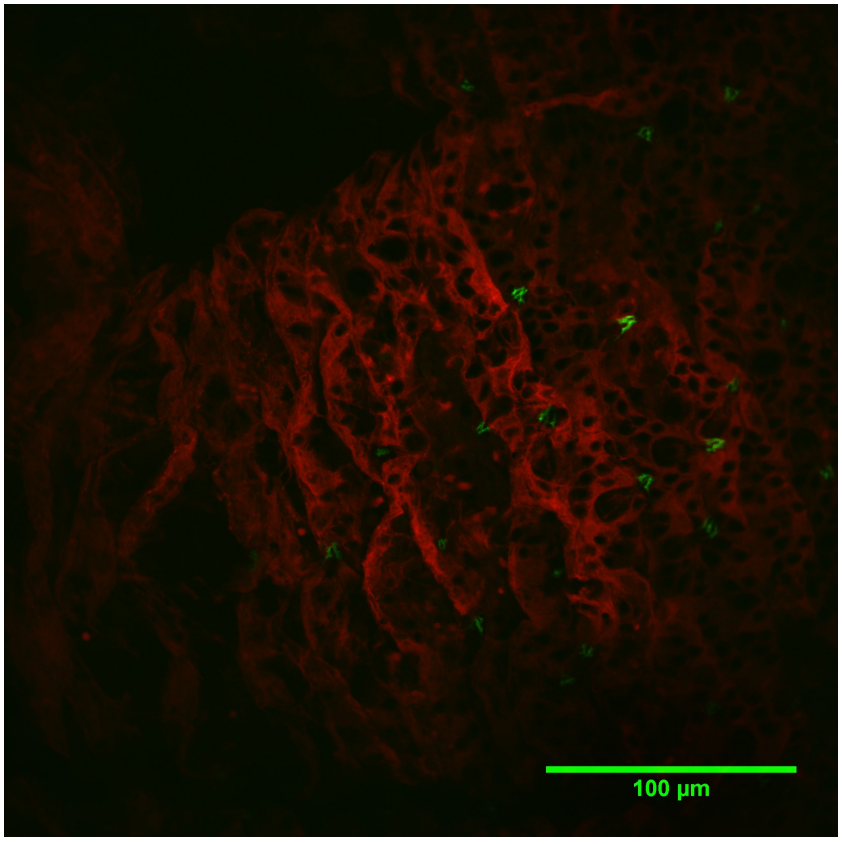

FIGURE 4.44: The body of an adult *hydra*. Vimentin is labeled in green, actin in red. The fork-like vimentin structures are part of the nettle apparatus within the Cnidocytes. All nettle-cells are discharged.

4.6.2.1 Summary and Discussion:

The nettle cells are too low in number and differentiated to play a role in symmetry breaking. Therefore the observed vimentin-like structures are unlikely to play a role in the change of the mechanical properties during regeneration. This does not exclude a participation of other intermediate filaments, which could not be investigated here.

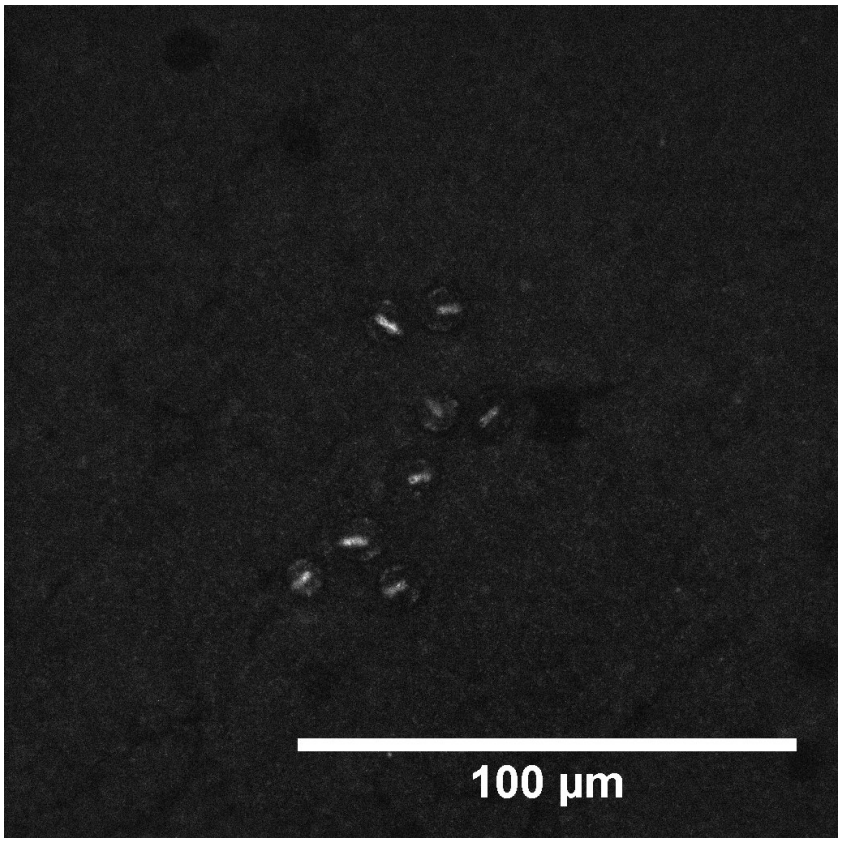

FIGURE 4.45: Charged Vimentin stained nettle cells.

Nevertheless, the presence of vimentin-like structures in specialized cells is a very interesting result since most publications only stated collagen-like proteins in the harpoon apparatus [132]. Further characterization of the vimentin-like protein and confirmation of its nature are necessary.

4.6.3 Summary and Conclusion

Major reorganization of the intra-and intercellular actin cytoskeleton takes place during *hydra* regeneration. This indicates that bio-mechanics or cytoskeletally transmitted signalling plays a role during regeneration. Large contractile actin structures are mostly absent during the symmetry breaking.
Actin structures are a large contributor to the mechanical asymmetry of the regenerates. Symmetry breaking itself however seems to depend on additional components, such as microtubules. Microtubule staining was not possible with available protocols, the effect of microtubules has been indirectly investigated in 4.7. After symmetry breaking, the cells surrounding the mouth opening have a different morphology and cytoskeletal structure than surrounding cells, even before the emergence of head and foot, indicating a role of actin structures after symmetry breaking. The role of actin as well as microtubules

during the regeneration process is investigated more closely using cytoskeletal drugs and is discussed in section 4.7.

4.7 Microtubules need to be present and contractile actin structures need to be absent for successful symmetry breaking

The results presented in the previous chapter indicate a strong correlation between the symmetry breaking and the mechanical behavior of the regenerate. The disappearance of the actin structures after cutting (described in chapter 4.6.1.2) disagrees with the involvement of large contractile actin structures in the regeneration process. However, short lived cellular actin structures would be invisible due to the indirect staining of the actin-gfp transgenic *hydrae* or destroyed during the rhodamin-phalloidin staining. To determine which cytoskeletal components play a role in symmetry breaking, the influence of cytoskeletal drugs on the regenerates was investigated. All drugs were tested for lethality on adult animals, and the highest non-lethal dosage was used (for exact dosage see section 3.2). The drugs are either involved in the control and modulation of actin (phalloidin, actin stabilizing agent), actin associated proteins (Y-27632, inhibits the Rho Kinase, part of the ROCK pathway and leads to decomposition of stress fibers, contractile actin-myosin fibers within cells; SMIFH2, an inhibitor of stress fiber connecting protein formin, see 2.5.4 in fundamentals), or in the modulation of microtubule polymerization (Nocodazole, inhibitor of tubulin polymerization, and paclitaxel, microtubule stabilizing agent).

4.7.1 Actin does not play a role in symmetry breaking but is important for the subsequent elongation of the regenerates

As visual investigation of large actin structures revealed their absence during symmetry breaking (see section 4.6), cytoskeletal drugs were used to further investigate the role of the actin cytoskeleton during regeneration.

4.7.1.1 Inhibition of actin contractility does not inhibit regeneration.

As regenerates exhibit rhythmical inflations and contractions within one oscillation phase, the influence of the Rho Kinase, which play a role in the regulation of the shape and movement of cells, was investigated using Y-27632 as an inhibitor. All three regeneration phases are present in the regenerations with Y-27632 (see figure 4.46). Y-27632 treated animals exhibit a sigmoidal inflation, indicating that the mechanical properties of the regenerates are influenced by some components of the Rho-kinase pathways. In all

phases the angle is more scattered throughout the whole regeneration compared to control regenerations. However, axis stability and instability can be clearly distinguished. The fluctuation behavior does not differ from untreated animals (see figure 4.32). The elongation of the regenerate after symmetry breaking, indicated by the Circularity, is less pronounced, however the regenerated animals are viable. The rhythmical trembling of the regenerate did neither change qualitatively nor quantitatively compared to the control (compare to section 4.2 for a detailed analysis of untreated regenerations).

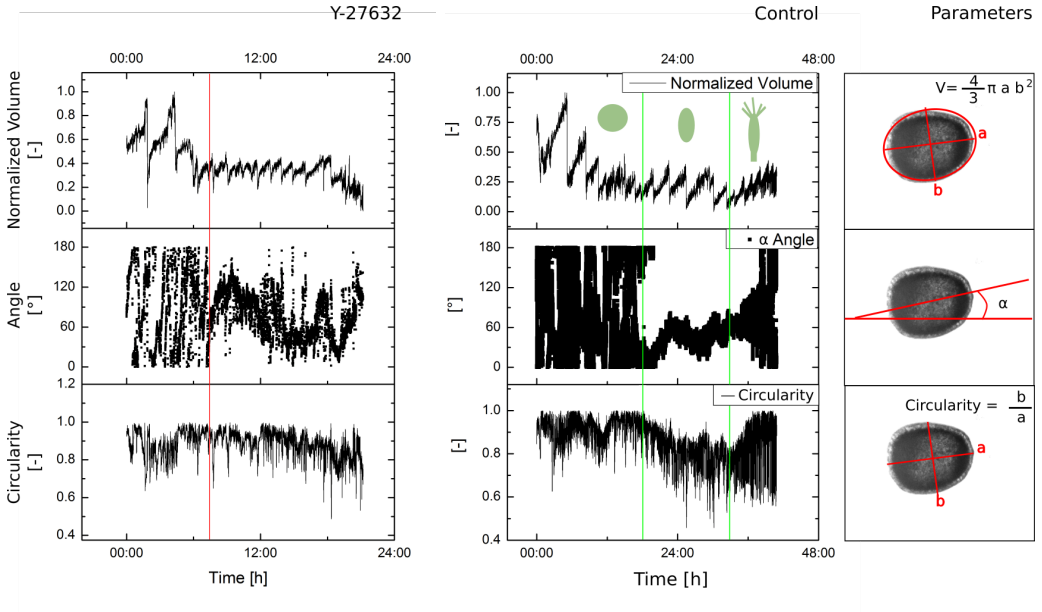

(a) y27632 (b) Control

FIGURE 4.46: Example of a regeneration under the influence of Y-27632 (a) compared to control (b). The investigated parameters are schematically displayed in the outer right panel. Y-27632 inhibits p160ROCK. In *hydra* y-27632causes a visible disassembly of stress fibers within 15 minutes (see section 4.6). The angle exhibits more pronounced scattering than control. Nevertheless, symmetry breaking takes place, as indicated by the red line. The elongation, as pictured by the Circularity, is less pronounced than in the control. The regenerate developed into a viable animal.

4.7.1.2 Formin-inhibitor SMIFH2 does not influence symmetry breaking, but inhibits the elongation of the regenerate

To investigate whether the *de novo* formation of stress fibers plays a role during symmetry breaking formin inhibitor SMIFH2 was used. Regenerates exhibit mechanical symmetry breaking as well as fluctuations and trembling (see figures 4.47 and 4.32 in section 4.5.3). The oscillation pattern is atypical. Large oscillations start late during the regeneration. The elongation of the regenerate after symmetry breaking does not take place. Foot, mouth and tentacles do not appear. The fluctuation behavior of the angle stays the same as in the control group.

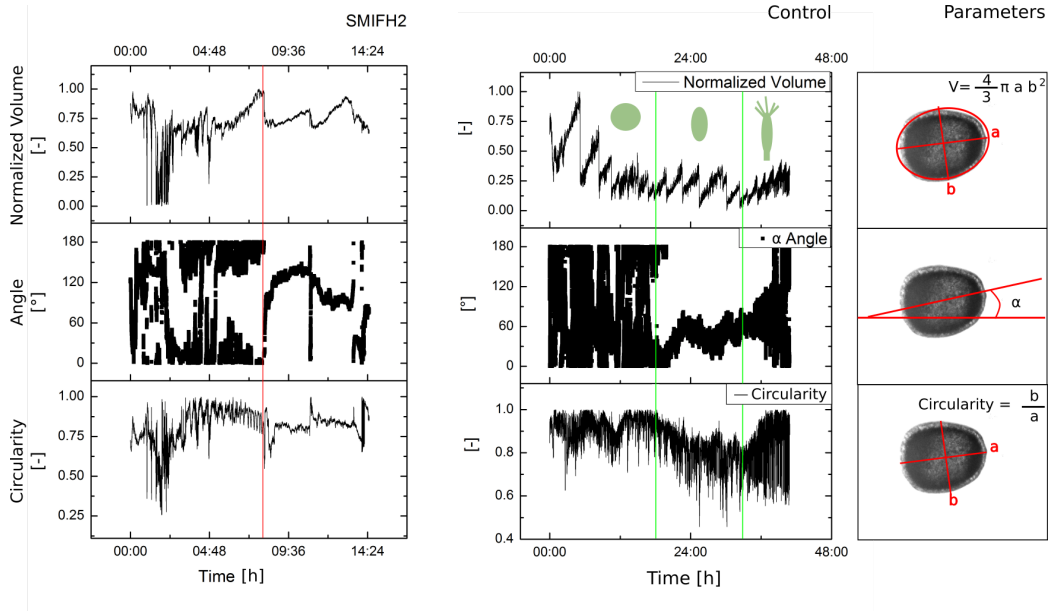

(a) SMIFH2 (b) Control

FIGURE 4.47: Example of a regeneration under the influence of SMIFH2 (a) compared to control (b). The investigated parameters are schematically displayed in the outer right panel. SMIFH2 inhibits formin, a protein necessary for stress-fiber formation. The mechanical symmetry breaking takes place (indicated in red), but no elongation of the sphere occurs. Inflation rate varies within the regeneration. Regeneration was not successful. The drop in normalized volume as well as circularity between 1 and 2 hours is an artifact due to image analysis.

4.7.1.3 Stabilizing polymerized actin inhibits regeneration and large oscillations of the regenerate.

Phalloidin was used to stabilize all actin structures in the regenerate. No shape fluctuations or angle scattering are observed, apparently the symmetry is not lost. Despite the inhibition of the inflations by phalloidin, deflation-like behavior is visible. However, the shape of the deflations is different than in control regenerations.

4.7.1.4 Cytochalasin B is lethal to regenerates in small dosages

Treatment with cytochalasin B to dissolve actin structures proved to be lethal in very small dosages. A concentration assay was performed to investigate the viable dosage, concentrations above 0.05 μM were lethal, concentrations below did not show any effect on symmetry breaking or oscillation patterns.

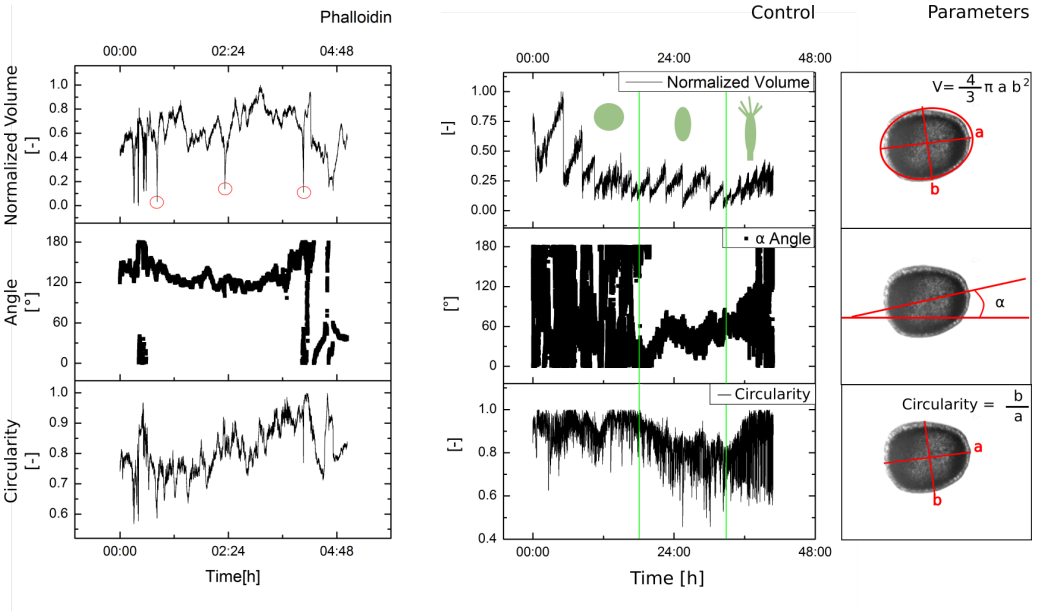

(a) Phalloidin (b) Control

FIGURE 4.48: Example of a regeneration under the influence of Phalloidin (a) compared to control (b). The investigated parameters are schematically displayed in the outer right panel. Phalloidin inhibits oscillations of the regenerating sphere. Stable angle indicates that the asymmetry is not lost. Strong deflation-like behavior is observed and indicated with red circles. The shape of the deflations is different, the deflation process itself is much slower than in control regenerations. Circularity rises. Regeneration was not successful.

4.7.2 Summary and Discussion

Actin contractility does not influence the symmetry breaking dynamics. Inhibition of actin contractility neither prevents symmetry breaking nor changes the timescale of the oscillations. However, the shape of the large inflations is different than in control regenerations without drugs, indicating that Rho kinase dependent activity, probably *de novo* stress fiber formation, takes place during the regeneration and is visible in the mechanical properties of the regenerates.

Symmetry loss depends on the degradation of actin structures, which supports the idea that the body axis is, among other factors (see section 2.3 in fundamentals), encoded in directional actin structures, as investigated in section 4.6. Experiments show that the fast trembling of the regenerate that correlates with symmetry breaking (see section 4.5) takes place even if contractile stress fibers are not present. Contrary to that, the elongation of the regenerate after symmetry breaking seems to depend on *de novo* formation of contractile actin structures via formin (see 2.5.4 in fundamentals). The fluctuations leading to symmetry breaking itself do not require polymerized actin stress fibers.

A stress fiber degradation due to the changing directionality of the stress due to the shape fluctuations during the large inflations (see section 4.5.1) could take place. Another possible cause for degradation could be the absence of mechanical cues after deflation [131]. A cell polarization using the stabilization of stress fibers therefore can only occur if the isotropic stress during shape fluctuations and inflations becomes continuously directional, as only uniaxial stress polarizes actin filaments [98]. The differently shaped inflations during Y-27632 treatment of the regenerates can be the manifestation of the supressed short-lived actin stress fibers formed during the stable phases of the shape fluctuations. However, surprisingly, the presence or the *de novo* formation of stress fiber is not a prerequisite for symmetry breaking.
Supported by the absence of visible cellular and supercellular actin structures during regeneration presented in 4.6 conclude that the symmetry breaking process or the establishment of the main axis are not directly associated with actin stress fibers. However, the stabilization of the symmetry and the subsequent shape change in the regenerate depend on stress-fibers.

4.7.3 Symmetry breaking depends on microtubule polymerization status

To investigate the influence of microtubules on the symmetry breaking, the microtubule stabilizing agent paclitaxel and the destabilizing agent nocodazole (see section 2.7) were used in the highest viable concentration, as tested on adult animals.

4.7.3.1 Suppressing microtubule polymerization using Nocodazole inhibits symmetry breaking

Nocodazole inhibits symmetry breaking. The *hydra* follows large clearly defined oscillations as found in phase 1 without establishing a new axis (see figure 4.49). The longest process recorded is 75 hours of continuous large oscillations with a duration of 4.5 hours on average. Neither an elongation of the regenerate nor the development of a head or a foot were observed. Shape fluctuations were less pronounced (see section 4.5.1), no fluctuations of the main axis orientation were observed and the characteristics of the *hydra* oscillation patterns was fundamentally different (see section 4.5.2). No symmetry loss nor symmetry breaking was observed.

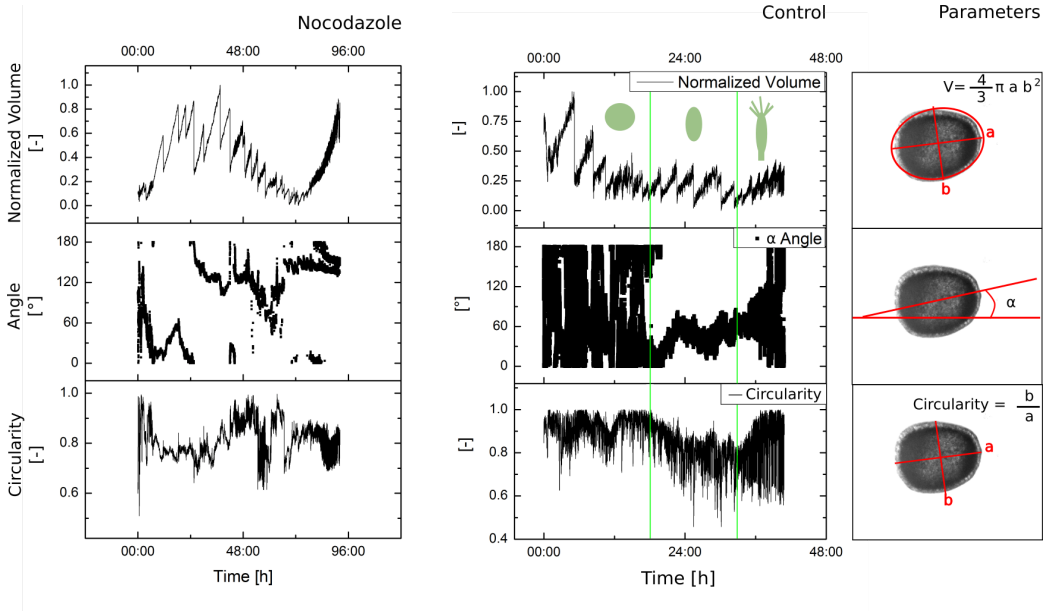

(a) Nocodazole (b) Control

FIGURE 4.49: Example of a regeneration under the influence of Nocodazole (a) compared to control (b). The investigated parameters are schematically displayed in the outer right panel. Nocodazole inhibits microtubule polymerization. No loss of symmetry nor symmetry breaking is observed. The regenerate seems to expand during the first 6 inflations. The trembling of the sphere during the large oscillations is almost absent and does not exhibit any visible regularity (see figure 4.51 and sections 4.5.5 and 4.5.2). After 40 hours, trembling starts, indicating that the drug effect wears off. A process that could be a size correction takes place. After 62 hours, *hydra* starts to disassemble.

4.7.3.2 Stabilizing polymerized microtubules using paclitaxel does not inhibit symmetry breaking

Paclitaxel treatment does not prevent symmetry breaking. The average time until symmetry breaking occurs does not change compared to controls. The angle scattering is stronger than in controls. The fluctuation behavior of the axis stability is present, the frequency distribution follows a power law with a different power exponent than the control (see figure 4.32). The trembling is much stronger. As described in section 4.5.2, the spectral analysis of the *hydra* trembling does not change. However, in control regenerations the trembling occurs in positive and negative direction with respect to the average linear inflation, while in paclitaxel treated animals only negative peaks can be observed (see figure 4.51).

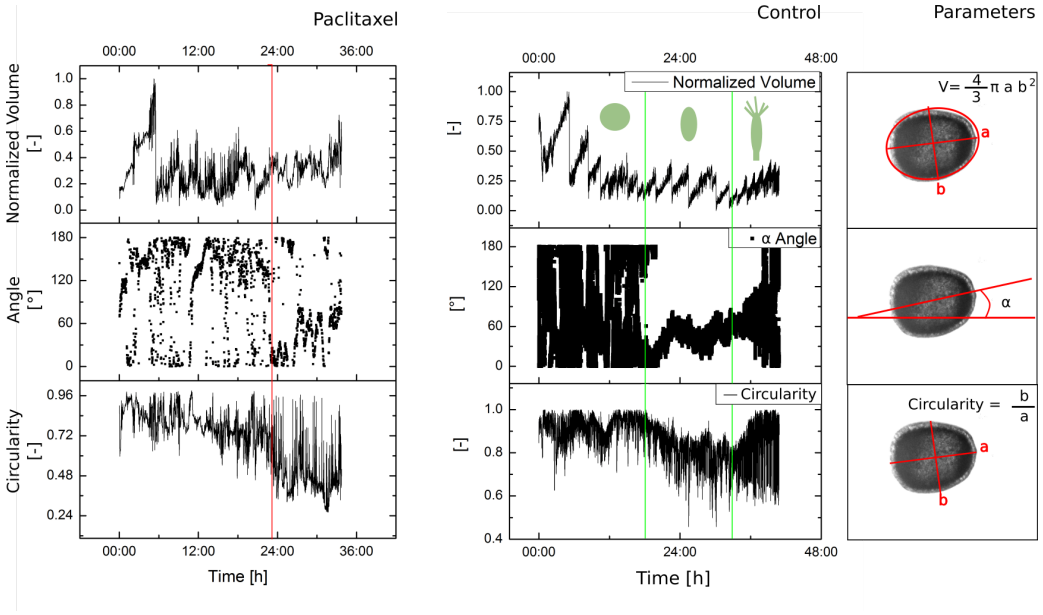

(a) Paclitaxel (b) Control

FIGURE 4.50: Example of a regeneration under the influence of paclitaxel (a) compared to control (b). The investigated parameters are schematically displayed in the outer right panel. Paclitaxel stabilizes polymerized microtubules. The regeneration with paclitaxel follows a typical regeneration pattern with 3 phases. The mechanical symmetry breaking is indicated by the red line. The symmetry breaking cannot be directly seen in the amplitude of the angle fluctuations, as in other regenerations, but can be observed by the elongation of the sphere.

4.7.3.3 Summary and Discussion

Both nocodazole and paclitaxel changed the trembling behavior of the *hydra* regenerates (see figure 4.51). Paclitaxel is causing a more pronounced rhythmical deflating trembling. Inhibiting microtubule polymerization inhibits trembling, fluctuations and symmetry breaking, while stabilizing polymerized microtubules reinforces trembling and allows symmetry breaking. This indicates that the trembling is at least partially dependent on the presence of polymerized microtubules. In addition, symmetry breaking seems to depend on the presence of polymerized microtubules, but the degree of the polymerization does not play a role, since stabilization of microtubules does not inhibit symmetry breaking despite a change in the dynamics of the process.

Stability of polymerized microtubules is temperature dependent [133]. In vitro, cooling polymerized microtubules leads to disassembly into individual subunits, heating microtubules up to 37 °C favors the polymerized state. The implication that polymerized microtubules play a crucial role in symmetry breaking therefore agrees with the results from the temperature gradient experiments in this work as well as in [23]. Different microtubule polymerization dynamics on the sphere (see section 4.1.1) during application of a temperature gradient could well be the cause of the induced axis orientation.

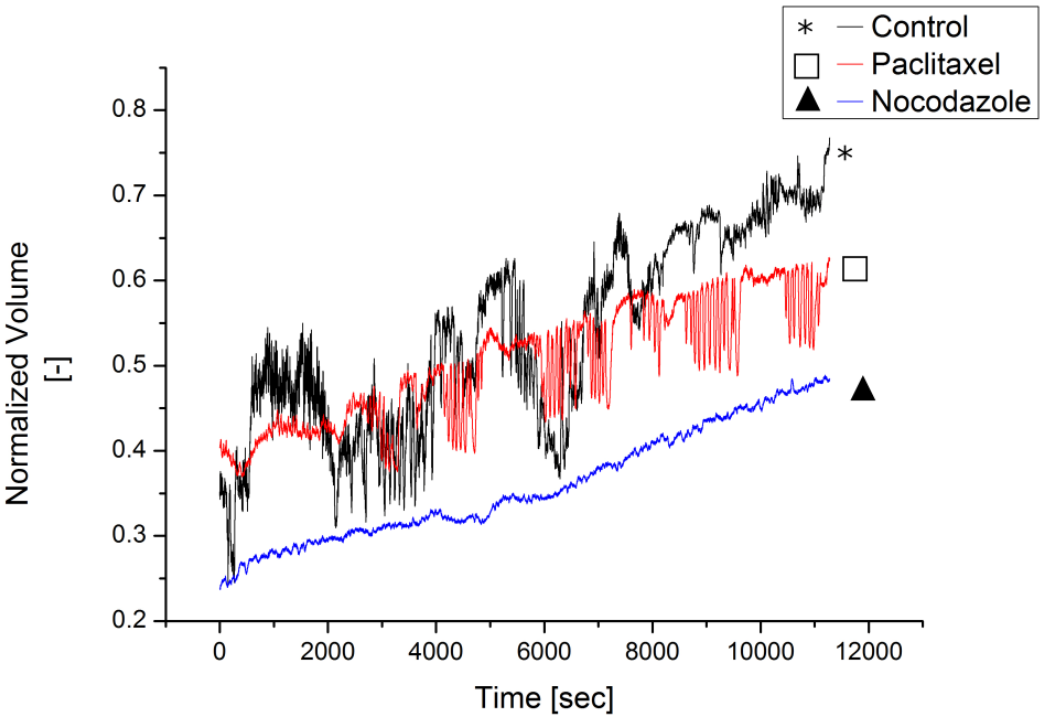

FIGURE 4.51: The normalized volume of the first large inflation of three different experiments are shown. Normalization was performed with respect to the maximum regenerate size. Control shows an untreated animal, paclitaxel and nocodazol show drug experiments. In nocodazole treated animals, the trembling almost completely vanishes. In paclitaxel treated animals, the rhythmical deflations are more pronounced than in control, rhythmical inflations are not present. Microtubules seem to play a role in the presence and modulation of the trembling.

4.7.4 Conclusion

The presence of polymerized microtubules is a prerequisite of symmetry breaking while stress fiber formation is crucial for the elongation of the regenerates after symmetry breaking.

Chapter 5

Discussion

. In this work the hydra motion and shape change during regeneration has been investigated in detail. Morphogenetic motion on several timescales has been observed and analyzed. The mechanical symmetry breaking instant manifests as an irreversible transition from a spherical to an oblong average shape.

After cutting, hydra fragments heal into hollow tissue spheres made of a cell bilayer. After healing, tissue fragments of hydra undergo periodic volume changes that follow a sawtooth-like course over time, described by Fuetterer et al [125]. The osmotic pressure inducing these cycles is caused by the regenerate itself [14]. The duration of these cycles depends on the size of the regenerate (see section 4.2).

The size of the regenerates yields a narrow size range of the regenerate that break symmetry successfully, not matter the initial size after the cutting by the experimentator, see section 4.2.5. The dependence of regeneration time on size, as observed by [51, 52, 124], could depend on the time that the regenerates need for their size correction.

In artificial aggregates that are larger than the regenerates in this work, a regeneration with multiple heads and probably without size correction occurs (the size at the symmetry breaking moment was not explicitly mentioned, only the initial size)[124]. Artificially created aggregates made of individual hydra cells can result in much larger regenerates. In this case multiple heads are observed. A possible effect of the size correction would be to ensure that only one head can emerge. It is possible that the size correction requires an at least partially connected mesoglea, as mechanical deformation applied on a tissue is transmitted through the extracellular matrix [134]. Therefore, the process cannot take place in artificial aggregates.

The question remains: How do the regenerates perceive and modify their own size?

Allometric changes can influence metabolic rate, genetic behavior and morphology [135]. It is not surprising that the size also plays a role during symmetry breaking in *hydra* regenerates, especially if the process affects the regenerates globally and synchronizes

their mechanical properties.

Tissue size control during embryonic development is a very robust process. It is controlled via a coordination of growth, proliferation, apoptosis and movement and mechanically regulated [136]. [137] and [138] presented models to explain a mechanical regulation of tissue size in embryonic development, the former based on a mechanical vertex model and the latter based on self-similarity in tissue. However, the question of how tissues and organs perceive their own size remains unsolved [139].

Strain rate dependent apoptosis as described by [140] for astrocytes, induced by a size dependent change in the large sawtooth oscillations, could be the explanation of the size correction mechanism in *hydra*. A possible mechanism could be that in larger regenerates with lower strain rate the stimulus received by the individual cells is not sufficient for all cells to survive[26].

In vascular endothelial cells, a change in applied shear stress modulates endothelial function. A lack of mechanical stimuli, in this case shear stress, induces apoptosis, indicating that a constantly present mechanical stimulus is essential for the maintenance of the endothelial structures[141].

Considering the correlation between size and duration of inflation of the regenerates, a strain rate dependent cell survival would explain how the regenerate "knows" when size correction is achieved. The large oscillations can therefore provide a defined strain with a specific strain rate (automatically adjusted via size correction) which points to a strain rate dependent symmetry breaking process. However, this cannot explain how symmetry breaking in larger artificial regenerates, that experience a different mechanical stimulus due to their sawtooth inflations, occurs.

Besides the sawtooth oscillations, regenerates exhibit a variety of oscillations on shorter timescales. The observed size independent frequency of 0.001 hz is within the range where the cytoskeleton responds readily to a mechanical stimulus[142]. The observed mechanical stimulus of this frequency could serve the purpose of preparing the individual cells for a mechanical reaction.

A large-scale sinusoidal superposition of the volume over time behavior is observed. A regenerate seems to undergo a defined series of oscillations from fully deflated to fully inflated. The repeating normalized values indicate an internal timer or oscillator.

In other words, every sawtooth inflation cycle follows the same course. There was no apparent change in the Fourier spectra of the trembling over the course of the regeneration, except during the phase with undefined oscillations before symmetry breaking, see section 4.2. Here the signals are more difficult to analyze due to undefined beginning and end of the oscillations, so no conclusion could be drawn. The inflation rate (dV/dt, volume change over time) during the inflations has been considered to be linear [14, 23]. The Fourier analysis revealed a size independent course of the regenerations (short inflations follow the same course as long inflations, scaled to their duration), which is

probably a manifestation of both the reaction of the *hydra* tissue to strain and the work of ion channels that provide the osmotic potential causing the inflation in response to this strain. As described in the reviews by [143, 144], the work of ion channels can be influenced by several factors, including mechano-sensitivity. Therefore the stress exercised on the regenerates is probably not constant in the course of an inflation. In addition, the active behavior of the regenerate has to be taken into account, especially considering the lower-frequent signals. The current knowledge about the inflation of the regenerates therefore does not give enough evidence to further characterize or discuss its nature and course during a cycle. There is no possibility to differentiate between the influence of stress generated by ion pump activity and a strain-specific reaction of the tissue.
The conclusion that can be drawn from the low-frequent Fast Fourier Transformation signals found during the inflations is that the inflation progress of the regenerates is non-linear, more complex than the inflation of, for example, rubber balloons [145] and that the regeneration process exhibits mechanical size (and time)-independent oscillations.
The fast oscillations on shorter timescales of each detrended inflation also exhibit a $1/f^{\alpha}$ noise behavior, the values of α indicating a noise between pink and red. Pink, or $1/f^{\alpha}$ with $1 \leq \alpha \leq 2$ noise is a frequently occurring phenomenon in biological systems[146]. Self organized criticality generates 1/f behavior[146] as well, which is ubiquitous in natural as well as in artificial complex systems[147].
In nocodazole treated animals, the noise exponent is closer to 1, indicating that the processes underlying the mechanical behavior are different from those in untreated regenerations. This indicates that the molecular basis for the non-equilibrium mechanical behavior in *hydra* regenerates may be stongly related to microtubule polymerization. In addition, it is striking that all regenerations that exhibit symmetry breaking (including drug-treated, yet successful ones) exhibit a noise with an exponent that is between 1 and two. In contrast, nocodazole regenerations, despite showing large inflations and deflations, do not regenerate and yield an exponent closer to 1. This indicates that the microtubule dependent noise is a manifestation of the symmetry breaking process and that symmetry breaking correlates with a part of the oscillations.
The power law fit of the angle fluctuations described in chapter 4.5.3 revealed scale free behavior as well. Scale free behavior in the context of symmetry breaking in regenerating hydra fragments has been described by Soriano et al, who observed scale free distribution of ks1 mRNA expression patterns at the symmetry breaking instant. The observed ks1 expression patterns have been reproduced by a self-organized criticality model, specifically a next neighbor coupled lattice model based on dynamic non-equilibrium processes.
What is the possible role of the observed rhythmical oscillations on several timescales? Oscillations are common in biological systems, as described in chapter Fundamentals (see 2). Examples are neural oscillations in the central nervous system, periodically changing cell signaling with positive or negative feedback loops, circadian and genetic

oscillations. However, the question of what drives the high amplitude fluctuating oscillations remains difficult to answer: is it either an external, neural or biochemical stimulus, or are the oscillations intrinsically driven?

In some systems, such as in wing beating of some insects [148], the oscillations are too fast to be driven by neural or biochemical signals. Models for oscillations without inducing stimuli exist for chromosome oscillations during mitosis [149], spindle oscillations during asymmetric cell division [150] and spontaneous oscillations of muscle sarcomeres [151]. However, the experimental proof of the absence of external stimuli inducing the oscillations remains elusive.

Other examples for oscillations during embryonic development are pulsed contractions during apical constriction in *Drosophila* [152], gastrulation in *Drosophila* [153] and sea urchin [130].

Mechanical oscillations allow cells to constantly probe the mechanical properties of their surroundings and react by changing either their own cytoskeletal structure, the attachment to the substrate or their differentiation status [121, 154]. Local mechanical changes induce localized changes in gene expression, which can lead to gastrulation events [7], section 2.6.

Global morphological changes as convergent extension of embryonic tissue can be induced by pulsed contractions, as demonstrated for Drosophila by [152].

Mechanical oscillations of tissue can also occur as a reaction to a mechanical stimulus, as observed by [153]. The oscillations exhibited by *hydra* could well be reactions to the mechanical stimulus created by the inflation. The oscillatory behavior correlates with polymerized microtubules, which indicates that the cytoskeleton plays a role during this process.

It is also possible that the oscillations are not inherently mechanical, but electrophysiological, or any combination of it. Thuret-Carnahan et al demonstrated that paclitaxel has not only an effect on microtubule polymerization, but on the catecholamine release from secretory cells. Catecholamines are neural regulators. On the timescales used in the *hydra* experiments (hours), Paclitaxel has been shown to completely inhibit catecholamin release and to provoke an augmentation of free Ca^{++} in the cytoplasm [114, 155]. The activity of K^+ channels are determined by cytoskeletal interactions as well [156]. Thus, even if there is no superordinate neurological structure, the oscillations can well result from an interdependent effect of the cytoskeleton, the mechanical stimulus and the electro-physiology of the regenerates. As reported in section 4.5.1, the regenerates fluctuate between different asymmetric shapes during regeneration. The fluctuations correlate with the fluctuations of the spatial orientation of the ellipsoid shapes over time. Several transition from a state with an unstable angle to a state with a stable angle occurred. The last transition marked the moment of irreversible symmetry breaking The abruptness of the transition and its correlation with the shape and volume

oscillations suggests that a global mechanical synchronization of the regenerate takes place. Therefore, prior to symmetry breaking, the regenerates fluctuate between states of mechanical symmetry and asymmetry. Axis formation is indicated by a stabilized mechanical asymmetry. Creating and stabilizing an asymmetry in the regenerate do not always appear together and are probably two different processes. A similar concept was proposed by Bode et al., who hypothesized that the biochemical *de-novo* creation and the maintenance of the head organizer are two different processes [157].

While the sawtooth-like oscillations due to osmotic inflations provide isotropic mechanical stimulus, shape fluctuations of the regenerate seem to translate this isotropic stimulus into a transient anisotropic stimulus. Cells and tissue react to anisotropic directional stimuli by polarizing and changing their mechanical properties related to the stimulus (see chapter 2.5). Eventually, this interaction between shape fluctuations and directional mechanical stimulus leads to an elongation of the tissue. Thus, the vesicle fluctuation is translated into a mechanical asymmetry of the tissue. However, the regenerate can still fluctuate if the asymmetry is not pronounced enough to induce a subsequent biochemical stabilization. Therefore, a beginning mechanical asymmetry can still be overwritten by a stochastic shape fluctuation, an event that explains the multiple transitions between a state with a pronounced main axis orientation and elongation and a state without.

Boulbitch et al. demonstrated that shape instabilities of biomembranes depend on the state of the cytoskeleton and are driven by a local softening of the underlying actin cortex [158]. However, the influence of microtubule polymerization was not investigated in this publication. However, microtubule polymerization status changes the bending rigidity of biomembranes [159], a parameter important for vesicle fluctuations. A microtubule dependent stiffening has been observed in embryonic tissue [160].

The strong influence of the mechanical stimulus induced by a micropipette on the body axis suggests a mechano-sensitive process of axis orientation. The axis orientation that is oriented with respect to the stimulus, but not at the spot of the stimulus itself, points to a mechanism that is communicating the effect that determines head orientation in a circular orientation around the stimulus.

In symmetrical balloons, the strain rate during inflation and deflation is evenly distributed. Introduction of an asymmetry by a local opening induced a difference of the strain rate in circular geometry around the asymmetry [161]. The asymmetry induces a directional strain as well, since the centrosymmetric area cannot expand. The effect of the micropipette stimulation of *hydra* could well be to introduce such a strain asymmetry. Head determining processes could be mechanically induced by either strain rate or directional strain.

Brunet et al. demonstrated that a local mechanical stimulus can induce mesoderm invagination, a polarizing process dependent on the wnt/beta catenin pathway (see section 2.4 in fundamentals). This effect has been found in *Drosophila* as well as *Danio rero*

(Zebrafish) and can be rescued by a mechanical stimulus [7]. The subsequent nuclear translocation of beta catenin can also take place without wnt expression. A possible interpretation is that the cytoskeleton provides a directional mechanical stimulus during this polarization process. This stimulus is responsible for induction of the canonical wnt pathway via nuclear translocation of beta-catenin, which in turn activates the wnt expression. A similar process could well be responsible for *hydra* axis determination which uses the same biochemical pathways [157]. However, while Brunet et al. observed a local effect [7], the axis induction observed here in *hydra* is not at the point of the stimulus. A possible reason for this difference is that the micropipette used by Brunet et al. has a diameter of 40 μm, while in this work the pipette was much larger and aspired about a substantial part of the regenerate. The distribution of the strain was different in both cases.

In addition, the absence of *hydrae* regenerating facing head down indicates a mechanism that detects either the direction of the light or gravity.

The induction of the axis via micropipette aspiration points to symmetry breaking as a bio-mechanical process which depends on the direction of strain and/or strain rate.

Regeneration usually takes place without significant and stable external mechanical stimulus. As the outcome of the regeneration is robust, the *hydra* regenerates need to be able to translate a non-directional mechanical stimulus provided by either the oscillations or the surrounding or other mechanical processes into a directional one to induce beta-catenin nuclear translocation. Mechanotransduction in cells is mediated via the cytoskeleton (see also fundamentals 2.5 and 2.6). Upon mechanical stimulation, cells can react in multiple ways, depending on the nature of the stimulus. The reaction depends on the directionality[162], the strain rate [163, 164] and frequency [163] and on the initial condition of the cells[165]. Despite the presence of large sawtooth oscillations, symmetry breaking does not take place in regenerates with inhibited microtubule polymerization. Mickey et al. demonstrated that microtubules and their polymerization status influence stiffness of cardiomyocytes submitted to directional shear stress [159]. Bundled microtubules exhibit a strain rate dependent reorientation and microtubule breaking [166, 167]. Microtubule polymerization status influences the mechanical properties of embryonic tissue. In *Xenopus* embryonic tissue, Zhou et al. [160] found that depolymerization of microtubules leads to a 3-4 fold tissue stiffening. This effect is attributed to a ligand of the Rho GTPase pathway called XLfc. XLfc regulates the actomyosin cytoskeleton and binds microtubules.

A process that can be described as convergent extension takes place correlated with the stable phases of the fluctuations of the angle in *hydra*. Convergent extension is also observed during the process of elongation and simultaneous convergence in direction of the anterioposterior axis of the embryo. Convergent extension depends on microtubule polymerization and the early stages can be inhibited by nocodazole [168]. Kwan et

al. proposed that initiation of convergent extension in *Xenopus laevis*, a process that is sensitive to microtubule polymerization inhibition but not microtubule stabilization, depends on the mass of polymerized microtubules. Convergent extension in animals is mediated by Rho-kinase controlled wnt activity [169]. Both the canonical and the non-canonical [62–64] wnt pathways are involved [68]. During polarization of cells, Rho acts as a switch between dynamic and stable states of the microtubule cytoskeleton [170]. The Rho mediated microtubule regulation [103] turned out to be actin stress fiber independent [102].

The results presented in sections 4.2 and 4.7 point to a microtubule mediated tissue- polarization and -elongation that requires the presence of actively polarizing microtubules, which corresponds to the results presented in section 4.5.3 and 4.7. This establishes a connection between mechanical properties of tissue, microtubule polymerization status and the well established wnt pathway which plays a crucial role in *hydra* head formation (see [27] for a review). The elongation of the regenerates depends on a change of mechanical properties of individual cells. In general, mechanical and biochemical polarization of cells is mediated by the cytoskeleton. The polarization of individual cells as a reaction to a mechanical stimulus with constant frequency depends on the amplitude of the strain applied which is applied and the strain rate [171]. Malek et al. demonstrated that the microtubule cytoskeleton plays a fundamental role in the cytoskeletal remodeling in endothelial cells exposed to fluid shear stress [104]. However, the actin cytoskeleton is also thought to drive a symmetry breaking process in cells, enables a polarized distribution of regulatory molecules and allows microtubules to build on this symmetry (see [96] for review).

Microtubules play a crucial role in the initial polarization of fertilized oocytes. In *Xenopus laevis* [30] as well as *C.Elegans*[8], the initial polarization of the fertilized egg is microtubule mediated. (For more details see fundamentals, sections 2.2 (embryonic development), 2.5.4(polarization), 2.6(mechanotransduction) and 2.5.5 for the role of microtubules in symmetry breaking.)

The change in FFT spectra of the inflations upon microtubule polymerization inhibition described in section 4.5.2 supports the microtubule dependent change of mechanical properties in the regenerate. The spectra of the short timescale oscillations change if microtubule polymerization is inhibited. They do not change if microtubules are stabilized. Both, the signals as well as the higher frequent noise, are affected. This implies a process that depends on the presence of polymerized microtubules, but not on the degree of polymerization or the polymerization process itself. A mechanical fracturing of polymerized microtubules, which can only happen if microtubules are polymerized, could be the cause of the mechanical trembling observed in the FFT transformation. Odde et al. observed that microtubule breaking in fibroblasts depends on the bending

of the microtubules [172]. This could explain a bending-dependent microtubule polymerization/depolymerization dynamic caused by the global shape fluctuations of the regenerates that feeds back on the bending rigidity of the membrane.
While the elongation of the regenerates after symmetry breaking seems to be actin dependent as well, the fluctuations leading to symmetry breaking itself do not require polymerized actin stress fibers. The induction of stress fiber formation and actin-myosin interaction are both, among others, depending on the Rho-associated protein kinase (ROCK) and can occur as a response to as well as independently of a mechanical stimulus [86]. The Rho-Kinase pathway and mechanical stimuli have been found to work cooperatively in stress fiber organization [104, 173]. Depending on the frequency [126, 174], cells subjected to a cyclic mechanical stretch orient their stress fibers perpendicularly to the stretch direction. The stretch frequencies observed in regenerates have been demonstrated to cause this stress fiber orientation, see [126] for theoretical model, [174] for experimental data. Treatment with with Y-27632 (a Rho-kinase inhibitor found not to interfere with symmetry breaking in *hydra* in this work) causes the stress fibers to orient in parallel to the stretch direction [98], therefore inducing a polarization. Completely inhibiting *de novo* stress fiber formation with SMIFH2 [117], (section 4.7) does not inhibit symmetry breaking, but inhibits elongation of the regenerate after symmetry is broken. He et al. proposed an acto-myosin dependent mechanism of tissue elongation that depends on oscillating contractions [175]; similar to the ones exhibited by the *hydra* regenerate after symmetry breaking.
Stress fibers constantly organize and reorganize depending on mechanical cues [176]. At least for short times on the scale of minutes, one can assume that stress fibers develop in regenerating *hydra* even before symmetry breaking.
The extracellular matrix plays a role in the mechanical properties of tissue as well. The cytoskeleton is connected to the extracellular matrix via cell-substrate adhesions. This allows the cells to directly respond to mechanical cues from the environment. Cells can exhibit multiple responses to changes in substrate. Stress fibers reorganize in response to changing substrate stiffness [98, 177] and cells differentiate depending on the substrate stiffness [109]. Cells can also actively exert mechanical stimuli on the extracellular matrix via the myosin induced contractility [178]. Tissue, a group of mechanically and biochemically connected cells and extracellular matrix, has the capability to react collectively to mechanical stimuli. Cells in tissues are mechanically connected to the extracellular matrix via cell-matrix adhesions and to one another via cell-cell adhesions. All cytoskeletal components are connected with the environment of the cell [133]. A local mechanical stimulus applied to cells in a tissue or a mechanical stimulation of the extracellular matrix affects neighboring cells as well. Adherens junctions, one type of cell-cell adhesions, allow neighboring cells to connect mechanically by locally inducing microtubule polymerization and stabilization [95, 179]. Similar structures exist for actin

structures and intermediate filaments as well. A mechanical stimulus can cause a reorganization of the adherens junctions [84]. The reorganization of the adherens junctions following a mechanical stimulus is mediated by the Rho associated kinase pathway [84], a key mediator of the wnt pathways [68].

Hydra tissue is not only connected by cell-cell and cell-matrix adhesions, but a supercellular filament assembly as well (see section 4.6). The myonemes in *hydra* are actin bundles that span several cells and build a polarized rectangular mesh within the animal that allows it to move in a synchronized way, see 2.3 in fundamentals. Myonemes provide a strong tissue connection within the animal. Actin and microtubule structures work together to allow quick elongation and retraction of the animal [48].

The size dependence of the actin structure disappearance is in agreement with literature that states a size dependence of symmetry loss. This result shows that the regenerates used in this as well as in other experiments [14, 22] loose the symmetry of the actin components. The the size of the regenerates was about 250 μm, which is well within the area of symmetry loss.

Loss of cellular contractile actin structures occurs in larger regenerates than expected. The loss of the actin structures coincides with a loss of activity in the regenerates. However, large successfully regenerating fragments that are 400 μm in diameter do not occur as often as smaller ones, regardless of the apparent loss of symmetry, see section 4.2.5.

Gupta et al. described a substrate stiffness dependent actin filament ordering, with the absence of stress fibers on very soft substrates and a change from isotropic to nematic ordering of stress fibers with increasing substrate stiffness [180]. The loss of turgor pressure affects the tensional state of the mesoglea, effectively changing its stiffness (among other properties). Several publications [173, 180, 181] described the phenomenon that cells develop an actin cytoskeleton with stress fibers only on substrates with sufficient stiffness. The actin stress fibers disappear if the counteracting force disappears as well. In addition to this, biochemical cues could lead to the deterioration of stress fibers in the regenerates.

Recoiled actin structures, as observed in the cells (see figure 4.40), also appear after local severing of stress fibers and are indicators of their contractility [182].

Substrate stiffness dependent actin remodeling could be responsible for the disappearance of the actin stress fibers observed here. Not much is known about the molecular structure and the biomechanical assembly and disassembly mechanisms of the myonemes (supercellular actin structures). However, a similar mechanism of dissolving and reassembly as in the stress fibers can be assumed.

The mechanism behind the actin remodeling in *hydra* regenerates needs further investigation.

During regeneration until symmetry breaking, no visible stress fibers or myonemes seem

to play a exist. Due to the indirect actin fiber staining caused by the actin-gfp colocalisation in the transgenic *hydra* it is possible that the transient structures are not visible under a 20x magnification and very short lived. In support of this, the shape of the large inflations under the influence of Y-27632 is different (although the regenerations are successful), indicating that either stress fibers, stress fiber contractility or other elements of the Rho-kinase pathway reorganize during regeneration.

A common model for head formation in *hydra* is the the set up of the head organizer due to expression of the HyWnt genes, starting with HyWnt3 [157]. The canonical wnt pathway then stabilizes beta-catenin. Stabilized beta-catenin is transported into the nucleus (nuclear translocation) and subsequently induces changes in gene expression. Upon these changes, the affected cells change their fate and differentiate into cells with head organizer potential. A group of these cells acts as a head organizer.

Artificial stabilization of beta-catenin itself by alsterpaullone induces head organizer activity in cells throughout the *hydra* [183, 184]. Mesodermal invagination is a process that takes place during gastrulation in vertebrate embryos. This step requires the setup of the speman organizer [185], an organizing center of several differentiated cells. For this process, the activation of the canonical wnt pathway in the organizer with subsequent beta-catenin nuclear translocation is involved [186]. The process is analogous to the setup of the *hydra* head organizer [17]. However, Brunet et al. demonstrated that mesodermal invagination can be inhibited by suppressing either *de novo* stress fiber formation or microtubule polymerization. This effect can be rescued by application of a local mechanical stimulus, which directly activates beta-catenin nuclear translocation independently of wnt. Wnt is expressed only after the start of the invagination process [7], indicating the possibility that the initial setup and the maintenance of the head organizer function are controlled by different processes.

This idea has been proposed for *hydra* symmetry breaking by Bode et al. and Broun et al [18, 157].

The results of this work support this idea. The setup of the organizer (symmetry breaking) depends on the mechanical status of the tissue. The subsequent steps (elongation of the regenerate, differentiation of head and foot) require restructuring of the cytoskeleton as well. The maintenance of the head activator however has been demonstrated to be based on the subsequently expressed canonical wnt pathway [27].

The necessity of a mechanical stimulus to differentiate cells into a head organizer could also explain the maintenance of the head organizer in adult *hydra* despite constant tissue loss at the hypostome: The mechanical context at this location induces the differentiation of cells into a head organizer. In other words, just the position around the mouth opening and the specific mechanical stimulus provided in this area is sufficient to change undifferentiated cells into members of the head organizer.

If this is true, the head organizer activity would start after mechanical symmetry breaking by the nuclear translocation of beta-catenin, not by wnt activation. Fluctuations of beta-catenin nuclear translocation can be expected. Further experiments are necessary to determine the exact location of the head organizer development, the nature of its induction, and the behavior of beta-catenin during the shape fluctuations.

However, the exact connection between the nature of the mechanical, externally or internally generated, stimulus and the location of the head organizer is not clear. As discussed earlier in this chapter, the morphogenetic motion of the hydra regenerates creates local, transient asymmetries in the regenerate. An overview of the wnt pathways

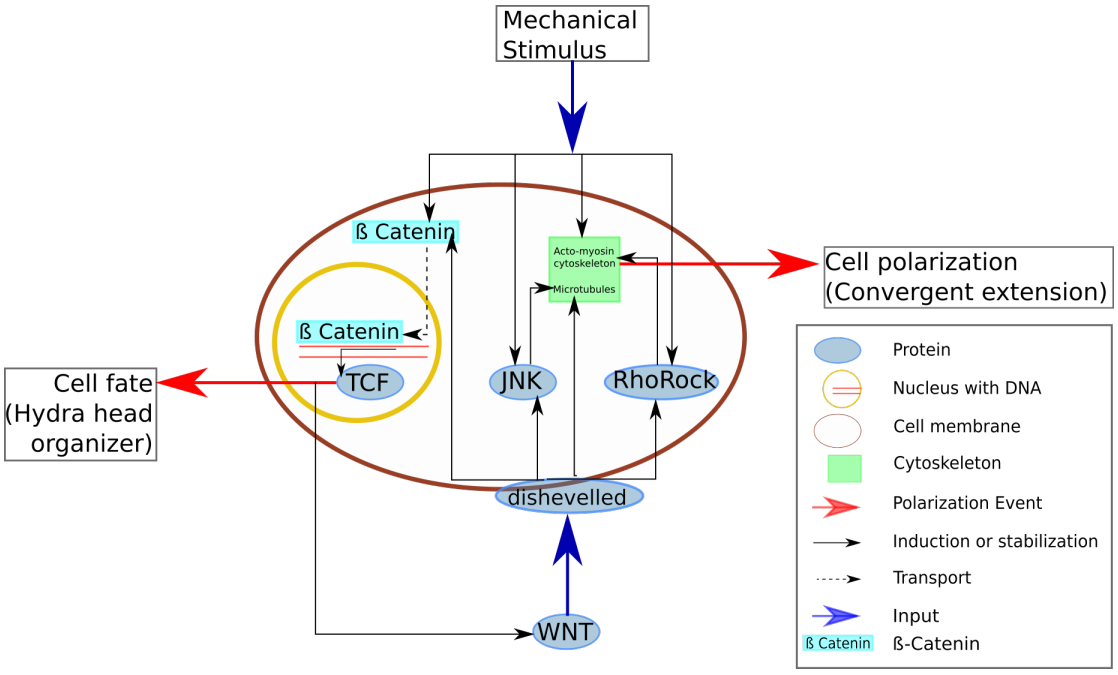

FIGURE 5.1: Wnt pathways, embryonic development and mechanical stimulus are connected. The wnt-dishevveled complex stabilizes cytosolic beta catenin , which can the be translocated into the nucleus and activate the transcription of TCF(T-Cell factor)[187]. TCF leads to the formation of the head organizer in *hydra* [15, 27] or the mesoderm invagination during Drosophila [62] and Zebrafish [7] gastrulation. Beta catenin nuclear translocation in turn can induce wnt expression [188]. On the other hand, wnt controls acto-myosin contraction via ROCK, Rho dependent protein kinase[68]. Wnt-dishevveled can locally act to stabilize microtubules [70]. In addition, wnt-dishevveled complex can act via JNK (c-Jun N terminal kinase, involved in cell polarization) to reorganize the microtubule cytoskeleton [66]. JNK mediated cell polarization is also induced vie mechanical stimulus [176], leading to cell polarization. Wnt controlled JNK activity mediates convergent extension during embryonic development [10, 63]

that play a role in cell polarization and the setup of the head organizer and their connection with the cytoskeleton and mechanical stimuli is shown in figure 5.1.

In the regenerating hydra, a possible location of the head organizer would be the tip of the observed bulges. It is possible that the ideal strain rate occurs in a circle surrounding the tip of these bulges. This agrees with the findings of Brunet et al., who discovered

that beta-catenin nuclear translocation is induced at the area of the indentation with a micropipette [7].

At the bottom of the indentation as well as on the tip of the bulge the cells do not receive a directional strain. In *hydra* regenerates this could lead to a mechanical weakening of the cells inducing the formation of a weak spot which later becomes the mouth opening. In contrast, the surrounding cells receive directional strain, which can activate the wnt-cascade (see sections 2.4 and 2.5.4). This would suggest that only the cells very close to the tip of the bulge receive a stimulus adequate for symmetry breaking and the cells around the later mouth opening develop into the head organizer.

Therefore, not the tip but the area surrounding the bulges is the head forming location. The micropipette aspiration can shift the head forming area. However, the different actin conformations observed around the later mouth opening (see section 4.6) indicate that an almost circular patch of cells receives a different mechanical stimulus than their neighbors. A model for morphogen mediated curvature changes as a mediator in *hydra* symmetry breaking was proposed by [189]. If the mechanical asymmetry of the regenerate is pronounced enough, a local activation of the head inducing pathway via mechanotransduction is possible in areas with stronger mechanical strain, like the observed small bulges.

5.1 Summary

I investigated the symmetry breaking as inferred from changes in the mechanical properties of the cell sphere of *hydra* regenerates from the isotropic spherical to the polarized elongated state. After cutting of tissue pieces from the body column of an adult polyp, they heal into tissue spheres. If initially small enough, symmetry in these tissue pieces is lost (see section 4.4).

Observing polarized actin structure integrity as indicator for mechanical asymmetry reveals that regenerates up to 400 μm in diameter loose their symmetry on a molecular level. The probability for a successful regeneration increases in regenerates closer to 200 μm in diameter (see section 4.6.1.2). All regenerating spheres exhibit oscillatory behavior showing large slow inflations with constant inflation rate and short fast deflations[14]. During the first oscillation cycles, regenerates adjust to an ideal regeneration size prior to symmetry breaking (see section 4.2.5).

A variety of oscillation patterns regarding number and process were observed. Oscillation patterns change upon mechanical symmetry breaking (see section 4.2) . On average, large inflations exhibit an increase of sphere volume with a constant rate. Closer investigation reveals that they are superimposed by sinusoid signals and 1/f scaling behavior that changes with respect to symmetry breaking. Inflations exhibit rhythmical trembling that is visible by eye. The regenerate exhibits fluctuations of the angle between a state with a stable main axis and a state without a stable main axis. Regenerates switch between mechanical symmetry and asymmetry (see section 4.5.5). Terminal symmetry breaking manifests as a stable mechanical asymmetry (see section 4.2). The frequency distribution of the fluctuations follows a power law that changes upon microtubule stabilization (see section 4.5.3). The fluctuations are the result of different distinct shapes that the regenerate adopts (see section 4.5.1).

Symmetry breaking induces the emergence of a body axis. Gamba et al. demonstrated experimentally that small temperature gradients affect the axis orientation of regenerating *hydra* and predicted the influence of even smaller gradients [22]. This work confirmed this prediction (see section 4.1.1), demonstrating the extremely sensitive nature of the symmetry breaking process.

Constant mechanical stimulus via micropipette aspiration induces head position in a plane perpendicular to the stimulus, indicating a mechanosensitive process of symmetry breaking (see section 4.3). Mechanotransduction is a cytoskeleton mediated process. Drug experiments demonstrate that actin stress fibers do not play a direct role in symmetry breaking. Instead they seem crucial to the elongation of the sphere and to the

definition of the mouth area after symmetry breaking (see section 4.7). Stabilizing microtubule polymerization does not inhibit symmetry breaking, however, contrary to suppressing of microtubule polymerization (see section 4.7). Signals derived by Fast Fourier transform disappear and the exponent of the 1/f scaling behavior changes if microtubule polymerization is inhibited (see section 4.5.2). The high correlation and sensitivity to microtubule polymerization inhibiting drugs indicate that trembling, shape fluctuations and symmetry breaking depend on the presence of polymerized microtubules.

5.1.1 Possible process of regeneration:

Based on the results discussed above one can assume that regeneration and symmetry breaking of *hydra* tissue pieces are not only mechanically manifest but mechanically driven processes as well. Symmetry breaking relies on a feedback mechanism between global shape fluctuations and microtubule driven local cell polarization.
I propose the following process for a regeneration:
1. First, a preexisting symmetry from the adult polyp, which is stored in the supercellular and cellular actin cytoskeleton, is deleted (discussed in sections 4.4, 4.6, 4.2.3).
2. During the large inflations, cells are destroyed and disgorged until an ideal regeneration size is reached (discussed in sections 4.2.5 and 4.5.2).
3. Inflation- and deflation cycles apply an oscillating mechanical stimulus with a size dependent strain rate (discussed in section 4.5.2).
4. Due to the mechanical properties of the cell bilayer, regenerates fluctuate between different shapes, comparable to membrane vesicles. In addition, the regenerates oscillate rhythmically on the timescale of minutes.
5. Meanwhile, microtubule polymerization and -breakdown on different timescales, lead to trembling behavior. The combination of global shape fluctuations of the regenerate, microtubule dynamics, next-neighbor cytoskeleton orientation synchronization and periodically provided strain of a specific rate allow the regenerates to fluctuate between different polarized states. These states either break down (leading to shape fluctuations) or are terminally stabilized (discussed in section 4.2).
6. The stabilization of the microtubule induced polarization occurs via the re-establishment of contractile actin structures, leading to a final elongation of the regenerate (discussed in section 4.6). The canonical wnt pathway is activated and allows the emergence of a head organizer.

Chapter 6

Conclusion

Symmetry breaking in hydra tissue is a mechanical process mediated by the microtubule cytoskeleton and stabilized by the actin cytoskeleton

In this thesis I addressed the role of the cytoskeleton in symmetry breaking of isotropic spherical tissue during regeneration of *hydra vulgaris*. It was undertaken to understand the role of mechanics in intrinsically driven tissue polarization processes, as during embryonic development. In addition, this thesis hoped to gain insight into the evolutionary origin of tissue symmetry breaking and the development of body axes.

I could confirm the observation that the mechanical behavior of regenerating *hydra* spheres plays a major role in the symmetry breaking process. Shape fluctuations and 1/f scaling behavior of the mechanical oscillations suggest a non-equilibrium process. The initiation and the maintenance of an asymmetry are two different processes. The results in this work imply a symmetry breaking process in hydra based on inherent properties of the microtubule cytoskeleton that is stabilized by the subsequent polarization of the actin cytoskeleton. Based on this, *Hydra* regenerates can translate an nondirectional mechanical stimulus into a directional one, which in turn allows the emergence of a head organizer.

My work contributes to the current knowledge by showing the importance of mechanotransduction in tissue polarization. While microtubule mediated cell- polarization in embryonic development was already known [8], the role of microtubules in tissue polarization and the process itself have not been investigated yet. In addition, the assumption of Bode et al., that the establishment and maintenance of the polarization of *hydrae* are possible two different processes [49], could be confirmed.

The cytoskeleton is evolutionary very old and almost identical in all animal species. A

process based on this structure is likely to be a universal one and not a speciality of one species.
Therefore, from an evolutionary point of view the results in this work suggests that the cytoskeleton contributed in an essential manner to the emergence of complex body plans.

Emergence of complex body plans is enabled by the cytoskeleton

Between 3900 and 2500 million years ago the first cells resembling prokaryotes appeared. 1850 million years ago, the first eukaryotic cells appear. 600 million years ago, the first complex multicellular organisms that feed on others (metazoans) appear and dramatically change the life on earth. The evolution of multicellular organisms from this point on was faster than ever before, new species emerged very quickly. The emergence of multicellularity was an evolutionary advantage for organisms. It allowed the division of labor between cells and therefore more efficient means of nutrient intake and procreation.
Still, it took about 3000 million years for this advantageous characteristic to evolve.
Two main requirements are given for the emergence of multicellular organisms from singe cells. First, the cells need to stick together even during and after cell division. Second, the connected cells need to synchronize their behavior in order to cooperate, a crucial requirement for the division of labor.
To explain the quick appearance of metazoans these two capabilities must have either evolved synchronously or be linked to each other, or one of the capabilities must have been present before.
The findings in this work point to the synchronization of cells as the prior silent ability that emerged only after cells connected in a specific way. The synchronization of the polarity is based on the cytoskeleton, an evolutionary very old structure. Most of its properties and capabilities predate the last common ancestor (1200 million years ago) [9]. The capability of beta-catenin nuclear translocation dependent mesoderm specification can be dated at least to the last bilaterian common ancestor 570 million years ago [7]. However, simple aggregates of cells have already existed about 1200 million years ago. They possessed a cytoskeleton that was very similar to the cytoskeleton of contemporary animals. So what caused the new ability to polarize synchronously?
According to the findings in my work, cells need a rhythmical mechanical stimulus and a specific substrate stiffness in order to polarize synchronously. This can be provided by the attachment of the cells to a matrix that can change its rigidity. In cnidarians, this matrix is the mesoglea. The cells therefore must not grow as an aggregate, but as a cell layer (hydra aggregates always change to a hollow sphere before regeneration, [51]).

If a critical size is reached, cells attached to the mesoglea create their own mechanical stimulus due to shape fluctuations. The emergence of an extracellular matrix could be the precondition for complex organisms. The cells produce their own flexible substrate to grow on and collectively either generate an intrinsic mechanical stimulus or translate an isotropic external stimulus into a directional one. This is supported by the findings that the extracellular matrix evolved simultaneously with the metazoa [190].

Further research possibilities

As a result of my study, further research might well be conducted in order to investigate the microtubule based symmetry breaking process further and to verify the proposed mechanism *in silico*. Directly observing the actual microtubule symmetry fluctuations *in vivo* would grant insight into the underlying processes. In addition, the maintenance of the new symmetry and the differentiation of cells into a head organizer need to be verified as a product of mechanically induced nuclear translocation of β-catenin in hydra. The implications about the role of mechanotransduction in embryonic development as well as in the evolutionary origin of tissue polarization need to be verified by using different models. Either existing ones, like the process of zebrafish gastrulation, or artificial ones, like the embryoid bodies that polarize presented by van den Brink et al. [34]. Another experiment to verify the assumption that tissue can break its polarity based on inherent cytoskeletal properties of the individual cells would be the creation of artificial tissue sheets of epithelial cells submitted to isotropic stress to see whether a polarization takes place. In single cells, the contribution of microtubules in response to an external mechanical stimulus is not fully understood yet.

Further implications

The emergence of complex body plans based on cytoskeleton properties shows that biological structures can take up new roles leading to complex outcomes in a changed context. Instead of the slow emergence of biochemical pathways that will eventually lead to a new function, the new function arises based on existing structures and is cemented by the newly developing pathways. The emergence of tissue polarity based on structures that developed to function in single cells shows impressively that evolution can, indeed, take place in leaps without the need to develop everything from scratch and that the potential of seemingly simple structures cannot be overestimated.
For biological research, this implies that an integrative global approach to investigate the synergistic abilities of a specimen complements the investigation of biochemical details.

The global and local mechanisms as well as their interactions need to be taken into account to truly understand a system.

Bibliography

[1] John Gerhart, Michael Danilchik, T Doniach, S Roberts, B Rowning, and R Stewart. Cortical rotation of the xenopus egg: consequences for the anteroposterior pattern of embryonic dorsal development. *Development*, 107(Supplement):37–51, 1989.

[2] Siegfried Roth and Jeremy A Lynch. Symmetry breaking during drosophila oogenesis. *Cold Spring Harbor Perspectives in Biology*, 1(2):a001891, 2009.

[3] Sebastian Wennekamp, Sven Mesecke, François Nédélec, and Takashi Hiiragi. A self-organization framework for symmetry breaking in the mammalian embryo. *Nat Rev Mol Cell Biol*, 14(7):452–459, Jul 2013. doi: 10.1038/nrm3602. URL `http://dx.doi.org/10.1038/nrm3602`.

[4] Jens-Erik Dietrich and Takashi Hiiragi. Stochastic patterning in the mouse preimplantation embryo. *Development*, 134(23):4219–4231, Dec 2007. doi: 10.1242/dev.003798. URL `http://dx.doi.org/10.1242/dev.003798`.

[5] Tibor Kalmar, Chea Lim, Penelope Hayward, Silvia Muñoz-Descalzo, Jennifer Nichols, Jordi Garcia-Ojalvo, and Alfonso Martinez Arias. Regulated fluctuations in nanog expression mediate cell fate decisions in embryonic stem cells. *PLoS Biol*, 7(7):e1000149, Jul 2009. doi: 10.1371/journal.pbio.1000149. URL `http://dx.doi.org/10.1371/journal.pbio.1000149`.

[6] Dmitry Krotov, Julien O. Dubuis, Thomas Gregor, and William Bialek. Morphogenesis at criticality. *Proc Natl Acad Sci U S A*, 111(10):3683–3688, Mar 2014. doi: 10.1073/pnas.1324186111. URL `http://dx.doi.org/10.1073/pnas.1324186111`.

[7] Thibaut Brunet, Adrien Bouclet, Padra Ahmadi, Démosthène Mitrossilis, Benjamin Driquez, Anne-Christine Brunet, Laurent Henry, Fanny Serman, Gaëlle Béalle, Christine Ménager, Frédéric Dumas-Bouchiat, Dominique Givord, Constantin Yanicostas, Damien Le-Roy, Nora M. Dempsey, Anne Plessis, and Emmanuel Farge. Evolutionary conservation of early mesoderm specification by

mechanotransduction in bilateria. *Nat Commun*, 4:2821, 2013. doi: 10.1038/ncomms3821. URL `http://dx.doi.org/10.1038/ncomms3821`.

[8] Bob Goldstein. Embryonic polarity: a role for microtubules. *Current Biology*, 10 (22):R820–R822, 2000.

[9] Bill Wickstead and Keith Gull. The evolution of the cytoskeleton. *J Cell Biol*, 194 (4):513–525, Aug 2011. doi: 10.1083/jcb.201102065. URL `http://dx.doi.org/10.1083/jcb.201102065`.

[10] S. Sokol. A role for wnts in morpho-genesis and tissue polarity. *Nat Cell Biol*, 2 (7):E124–E125, Jul 2000. doi: 10.1038/35017136. URL `http://dx.doi.org/10.1038/35017136`.

[11] Jenifer C Croce and David R McClay. Evolution of the wnt pathways. In *Wnt Signaling*, pages 3–18. Springer, 2009. URL `http://link.springer.com/protocol/10.1007/978-1-60327-469-2_1`.

[12] Xiaoyan Ge, Danielle Grotjahn, Elaine Welch, Jamie Lyman-Gingerich, Christiana Holguin, Eva Dimitrova, Elliot W. Abrams, Tripti Gupta, Florence L. Marlow, Taijiro Yabe, Anna Adler, Mary C. Mullins, and Francisco Pelegri. Hecate/grip2a acts to reorganize the cytoskeleton in the symmetry-breaking event of embryonic axis induction. *PLoS Genet*, 10(6):e1004422, Jun 2014. doi: 10.1371/journal.pgen.1004422. URL `http://dx.doi.org/10.1371/journal.pgen.1004422`.

[13] Alfred Gierer. The hydra model-a model for what? *International Journal of Developmental Biology*, 2012. doi: doi:10.1387/ijdb.113458ag.

[14] Michael Kücken, Jordi Soriano, Pramod A. Pullarkat, Albrecht Ott, and Ernesto M. Nicola. An osmoregulatory basis for shape oscillations in regenerating hydra. *Biophys J*, 95(2):978–985, Jul 2008. doi: 10.1529/biophysj.107.117655. URL `http://dx.doi.org/10.1529/biophysj.107.117655`.

[15] Günter Plickert, Vered Jacoby, Uri Frank, Werner A. Müller, and Ofer Mokady. Wnt signaling in hydroid development: formation of the primary body axis in embryogenesis and its subsequent patterning. *Dev Biol*, 298(2):368–378, Oct 2006. doi: 10.1016/j.ydbio.2006.06.043. URL `http://dx.doi.org/10.1016/j.ydbio.2006.06.043`.

[16] Bert Hobmayer, Fabian Rentzsch, Kerstin Kuhn, Christoph M Happel, Christoph Cramer von Laue, Petra Snyder, Ute Rothbächer, and Thomas W Holstein. Wnt signalling molecules act in axis formation in the diploblastic metazoan hydra. *Nature*, 407(6801):186–189, 2000. URL `http://www.nature.com/nature/journal/v407/n6801/abs/407186a0.html`.

[17] Tobias Lengfeld, Hiroshi Watanabe, Oleg Simakov, Dirk Lindgens, Lydia Gee, Lee Law, Heiko A. Schmidt, Suat Ozbek, Hans Bode, and Thomas W. Holstein. Multiple wnts are involved in hydra organizer formation and regeneration. *Dev Biol*, 330(1):186–199, Jun 2009. doi: 10.1016/j.ydbio.2009.02.004. URL `http://dx.doi.org/10.1016/j.ydbio.2009.02.004`.

[18] Mariya Broun, Lydia Gee, Beate Reinhardt, and Hans R Bode. Formation of the head organizer in hydra involves the canonical wnt pathway. *Development*, 132(12):2907–2916, 2005. URL `http://dev.biologists.org/content/132/12/2907.short`.

[19] René Augustin, André Franke, Konstantin Khalturin, Rainer Kiko, Stefan Siebert, Georg Hemmrich, and Thomas C G. Bosch. Dickkopf related genes are components of the positional value gradient in hydra. *Dev Biol*, 296(1):62–70, Aug 2006. doi: 10.1016/j.ydbio.2006.04.003. URL `http://dx.doi.org/10.1016/j.ydbio.2006.04.003`.

[20] Corina Guder, Sonia Pinho, Tanju G. Nacak, Heiko A. Schmidt, Bert Hobmayer, Christof Niehrs, and Thomas W. Holstein. An ancient wnt-dickkopf antagonism in hydra. *Development*, 133(5):901–911, Mar 2006. doi: 10.1242/dev.02265. URL `http://dx.doi.org/10.1242/dev.02265`.

[21] U. Technau, C. Cramer von Laue, F. Rentzsch, S. Luft, B. Hobmayer, H. R. Bode, and T. W. Holstein. Parameters of self-organization in hydra aggregates. *Proc Natl Acad Sci U S A*, 97(22):12127–12131, Oct 2000. doi: 10.1073/pnas.97.22.12127. URL `http://dx.doi.org/10.1073/pnas.97.22.12127`.

[22] Andrea Gamba, Mario Nicodemi, Jordi Soriano, and Albrechts Ott. Critical behavior and axis defining symmetry breaking in hydra embryonic development. *Physical Review Letters*, 108(15):158103, 2012. URL `http://prl.aps.org/abstract/PRL/v108/i15/e158103`.

[23] Jordi Soriano, Cyril Colombo, and Albrecht Ott. Hydra molecular network reaches criticality at the symmetry-breaking axis-defining moment. *Phys Rev Lett*, 97(25):258102, Dec 2006.

[24] Moritz Mercker, Alexandra Köthe, and Anna Marciniak-Czochra. Mechanochemical symmetry breaking in hydra aggregates. *Biophys J*, 108(9):2396–2407, May 2015. doi: 10.1016/j.bpj.2015.03.033. URL `http://dx.doi.org/10.1016/j.bpj.2015.03.033`.

[25] Donald E. Ingber. Cellular mechanotransduction: putting all the pieces together again. *FASEB J*, 20(7):811–827, May 2006. doi: 10.1096/fj.05-5424rev. URL http://dx.doi.org/10.1096/fj.05-5424rev.

[26] JANE B. REECE NEIL A. CAMPBELL. *Biologie*. Pearson; Auflage: 8., aktualisierte Auflage (1. Juni 2009), 2009.

[27] Hans Bode. Axis formation in hydra. *Annu Rev Genet*, 45:105–117, 2011. doi: 10.1146/annurev-genet-102209-163540. URL http://dx.doi.org/10.1146/annurev-genet-102209-163540.

[28] Ray Keller, Lance A. Davidson, and David R. Shook. How we are shaped: the biomechanics of gastrulation. *Differentiation*, 71(3):171–205, Apr 2003. doi: 10.1046/j.1432-0436.2003.710301.x. URL http://dx.doi.org/10.1046/j.1432-0436.2003.710301.x.

[29] Stefano Piccolo. b. *Nature*, 504(7479):223–225, Dec 2013. doi: 10.1038/504223a. URL http://dx.doi.org/10.1038/504223a.

[30] G. A. Ubbels, K. Hara, C. H. Koster, and M. W. Kirschner. Evidence for a functional role of the cytoskeleton in determination of the dorsoventral axis in xenopus laevis eggs. *J Embryol Exp Morphol*, 77:15–37, Oct 1983.

[31] A. K. Tarkowski and J. Wróblewska. Development of blastomeres of mouse eggs isolated at the 4- and 8-cell stage. *J Embryol Exp Morphol*, 18(1):155–180, Aug 1967.

[32] Matteo Rauzi, Pascale Verant, Thomas Lecuit, and Pierre-François Lenne. Nature and anisotropy of cortical forces orienting drosophila tissue morphogenesis. *Nat Cell Biol*, 10(12):1401–1410, Dec 2008. doi: 10.1038/ncb1798. URL http://dx.doi.org/10.1038/ncb1798.

[33] L Solnica-Krezel and W Driever. Microtubule arrays of the zebrafish yolk cell: organization and function during epiboly. *Development*, 120(9):2443–2455, 1994.

[34] Susanne C. van den Brink, Peter Baillie-Johnson, Tina Balayo, Anna-Katerina Hadjantonakis, Sonja Nowotschin, David A. Turner, and Alfonso Martinez Arias. Symmetry breaking, germ layer specification and axial organisation in aggregates of mouse embryonic stem cells. *Development*, 141(22):4231–4242, Nov 2014. doi: 10.1242/dev.113001. URL http://dx.doi.org/10.1242/dev.113001.

[35] & Eric Bonabeau Scott Camazine & Jean-Louis Deneubourg & Nigel R. Franks & James Sneyd & Guy Theraulaz. *Self-Organization in Biological Systems*. Princeton University Press, 2001.

[36] Eric Karsenti. Self-organization in cell biology: a brief history. *Nat Rev Mol Cell Biol*, 9(3):255–262, Mar 2008. doi: 10.1038/nrm2357. URL `http://dx.doi.org/10.1038/nrm2357`.

[37] Immanuel Kant. *Critique of Judgement*. Riga, 1790.

[38] E. M. Mandelkow and E. Mandelkow. Microtubule oscillations. *Cell Motil Cytoskeleton*, 22(4):235–244, 1992. doi: 10.1002/cm.970220403. URL `http://dx.doi.org/10.1002/cm.970220403`.

[39] Per Bak. *How nature works*. Oxford university press Oxford, 1997.

[40] C. N. David and S. Murphy. Characterization of interstitial stem cells in hydra by cloning. *Dev Biol*, 58(2):372–383, Jul 1977.

[41] H. R. Bode and C. N. David. Regulation of a multipotent stem cell, the interstitial cell of hydra. *Prog Biophys Mol Biol*, 33(2):189–206, 1978.

[42] E. Trenkner, K. Flick, G. Hansmann, H. Bode, and P. Bode. Studies on hydra cells in vitro. *J Exp Zool*, 185(3):317–326, Sep 1973. doi: 10.1002/jez.1401850306. URL `http://dx.doi.org/10.1002/jez.1401850306`.

[43] Brigitte Galliot. Hydra, a fruitful model system for 270 years. *Int J Dev Biol*, 56 (6-8):411–423, 2012. doi: 10.1387/ijdb.120086bg. URL `http://dx.doi.org/10.1387/ijdb.120086bg`.

[44] Anna-Marei Boehm and Thomas C G. Bosch. Migration of multipotent interstitial stem cells in hydra. *Zoology (Jena)*, 115(5):275–282, Oct 2012. doi: 10.1016/j.zool.2012.03.004. URL `http://dx.doi.org/10.1016/j.zool.2012.03.004`.

[45] T. Fujisawa. Role of interstitial cell migration in generating position-dependent patterns of nerve cell differentiation in hydra. *Dev Biol*, 133(1):77–82, May 1989.

[46] Scorr E Fraser, Colin R Green, Hans R Bode, and Norton B Gilula. Selective disruption of gap junctional communication interferes with a patterning process in hydra. *Science*, 237(4810):49–55, 1987. URL `http://www.sciencemag.org/content/237/4810/49.short`.

[47] M. Sakaguchi, A. Mizusina, and Y. Kobayakawa. Structure, development, and maintenance of the nerve net of the body column in hydra. *J Comp Neurol*, 373(1): 41–54, Sep 1996. doi: gt;3.0.CO;2-D. URL `http://dx.doi.org/gt;3.0.CO;2-D`.

[48] Yasuharu Takaku, Hiroshi Shimizu, and Toshitaka Fujisawa. Microtubules are involved in regulating body length in hydra. *Dev Biol*, 350(1):228–237, Feb 2011. doi: 10.1016/j.ydbio.2010.10.035. URL `http://dx.doi.org/10.1016/j.ydbio.2010.10.035`.

[49] Hans R Bode. Axial patterning in hydra. *Cold Spring Harbor perspectives in biology*, 1(1), 2009. URL `http://cshperspectives.cshlp.org/content/1/1/a000463.short`.

[50] Kengo Yoshida, Toshitaka Fujisawa, Jung Shan Hwang, Kazuho Ikeo, and Takashi Gojobori. Degeneration after sexual differentiation in hydra and its relevance to the evolution of aging. *Gene*, 385:64–70, Dec 2006. doi: 10.1016/j.gene.2006.06.031. URL `http://dx.doi.org/10.1016/j.gene.2006.06.031`.

[51] A. Gierer, S. Berking, H. Bode, C. N. David, K. Flick, G. Hansmann, H. Schaller, and E. Trenkner. Regeneration of hydra from reaggregated cells. *Nat New Biol*, 239(91):98–101, Sep 1972.

[52] Hiroshi Shimizu, Yasuji Sawada, and Tsutomu Sugiyama. Minimum tissue size required for hydra regeneration. *Developmental biology*, 155(2):287–296, 1993.

[53] Florence Peebles. The effect of temperature on the regeneration of hydra. *Zoological Bulletin*, Vol. 2, No. 3 (Dec., 1898), pp. 125-128.

[54] Ruth Weinziger, Luis M Salgado, Charles N David, and TC Bosch. Ks1, an epithelial cell-specific gene, responds to early signals of head formation in hydra. *Development*, 120(9):2511–2517, 1994. URL `http://dev.biologists.org/content/120/9/2511.short`.

[55] Lydia Gee, Julia Hartig, Lee Law, Jörg Wittlieb, Konstantin Khalturin, Thomas C G. Bosch, and Hans R. Bode. beta-catenin plays a central role in setting up the head organizer in hydra. *Dev Biol*, 340(1):116–124, Apr 2010. doi: 10.1016/j.ydbio.2009.12.036. URL `http://dx.doi.org/10.1016/j.ydbio.2009.12.036`.

[56] Waldo Cerpa, Elena Latorre-Esteves, and Andres Barria. Ror2 functions as a noncanonical wnt receptor that regulates nmdar-mediated synaptic transmission. *Proc Natl Acad Sci U S A*, 112(15):4797–4802, Apr 2015. doi: 10.1073/pnas.1417053112. URL `http://dx.doi.org/10.1073/pnas.1417053112`.

[57] Christer Larsson. Protein kinase c and the regulation of the actin cytoskeleton. *Cell Signal*, 18(3):276–284, Mar 2006. doi: 10.1016/j.cellsig.2005.07.010. URL `http://dx.doi.org/10.1016/j.cellsig.2005.07.010`.

[58] Jung Shan Hwang, Yasuharu Takaku, Jarrod Chapman, Kazuho Ikeo, Charles N. David, and Takashi Gojobori. Cilium evolution: identification of a novel protein, nematocilin, in the mechanosensory cilium of hydra nematocytes. *Mol Biol Evol*, 25(9):2009–2017, Sep 2008. doi: 10.1093/molbev/msn154. URL `http://dx.doi.org/10.1093/molbev/msn154`.

[59] Ken M Cadigan and Roel Nusse. Wnt signaling: a common theme in animal development. *Genes & development*, 11(24):3286–3305, 1997. URL `http://genesdev.cshlp.org/content/11/24/3286.short`.

[60] L. Zeng, F. Fagotto, T. Zhang, W. Hsu, T. J. Vasicek, WL Perry, 3rd, J. J. Lee, S. M. Tilghman, B. M. Gumbiner, and F. Costantini. The mouse fused locus encodes axin, an inhibitor of the wnt signaling pathway that regulates embryonic axis formation. *Cell*, 90(1):181–192, Jul 1997.

[61] Julia Christina Gross, Varun Chaudhary, Kerstin Bartscherer, and Michael Boutros. Active wnt proteins are secreted on exosomes. *Nature cell biology*, 14 (10):1036–1045, 2012.

[62] Roel Nusse and Harold Varmus. Three decades of wnts: a personal perspective on how a scientific field developed. *EMBO J*, 31(12):2670–2684, Jun 2012. doi: 10.1038/emboj.2012.146. URL `http://dx.doi.org/10.1038/emboj.2012.146`.

[63] Hiroaki Yamanaka, Tetsuo Moriguchi, Norihisa Masuyama, Morioh Kusakabe, Hiroshi Hanafusa, Ritsuko Takada, Shinji Takada, and Eisuke Nishida. Jnk functions in the non-canonical wnt pathway to regulate convergent extension movements in vertebrates. *EMBO Rep*, 3(1):69–75, Jan 2002. doi: 10.1093/embo-reports/kvf008. URL `http://dx.doi.org/10.1093/embo-reports/kvf008`.

[64] Yuko Komiya and Raymond Habas. Wnt signal transduction pathways. *Organogenesis*, 4(2):68–75, 2008.

[65] Vanessa Daire, Julien Giustiniani, Ingrid Leroy-Gori, Mélanie Quesnoit, Stéphanie Drevensek, Ariane Dimitrov, Franck Perez, and Christian Poüs. Kinesin-1 regulates microtubule dynamics via a c-jun n-terminal kinase-dependent mechanism. *J Biol Chem*, 284(46):31992–32001, Nov 2009. doi: 10.1074/jbc.M109.007906. URL `http://dx.doi.org/10.1074/jbc.M109.007906`.

[66] Lorenza Ciani and Patricia C Salinas. c-jun n-terminal kinase (jnk) cooperates with gsk3β to regulate dishevelled-mediated microtubule stability. *BMC cell biology*, 8 (1):27, 2007.

[67] Diane S Sepich, Mohsinah Usmani, Staci Pawlicki, and Lila Solnica-Krezel. Wnt/pcp signaling controls intracellular position of mtocs during gastrulation convergence and extension movements. *Development*, 138(3):543–552, 2011.

[68] Karni Schlessinger, Alan Hall, and Nicholas Tolwinski. Wnt signaling pathways meet rho gtpases. *Genes Dev*, 23(3):265–277, Feb 2009. doi: 10.1101/gad.1760809. URL `http://dx.doi.org/10.1101/gad.1760809`.

[69] Michael D. Gordon and Roel Nusse. Wnt signaling: multiple pathways, multiple receptors, and multiple transcription factors. *J Biol Chem*, 281(32):22429–22433, Aug 2006. doi: 10.1074/jbc.R600015200. URL `http://dx.doi.org/10.1074/jbc.R600015200`.

[70] Lorenza Ciani, Olga Krylova, Matthew J. Smalley, Trevor C. Dale, and Patricia C. Salinas. A divergent canonical wnt-signaling pathway regulates microtubule dynamics: dishevelled signals locally to stabilize microtubules. *J Cell Biol*, 164(2): 243–253, Jan 2004. doi: 10.1083/jcb.200309096. URL `http://dx.doi.org/10.1083/jcb.200309096`.

[71] E. M. De Robertis, J. Larraín, M. Oelgeschläger, and O. Wessely. The establishment of spemann's organizer and patterning of the vertebrate embryo. *Nat Rev Genet*, 1(3):171–181, Dec 2000. doi: 10.1038/35042039. URL `http://dx.doi.org/10.1038/35042039`.

[72] Renée van Amerongen and Roel Nusse. Towards an integrated view of wnt signaling in development. *Development*, 136(19):3205–3214, 2009.

[73] Renée van Amerongen, Christophe Fuerer, Makiko Mizutani, and Roel Nusse. Wnt5a can both activate and repress wnt/β-catenin signaling during mouse embryonic development. *Developmental biology*, 369(1):101–114, 2012.

[74] Janet Heasman. Patterning the early xenopus embryo. *Development*, 133(7): 1205–1217, Apr 2006. doi: 10.1242/dev.02304. URL `http://dx.doi.org/10.1242/dev.02304`.

[75] Robert D. Goldman, Boris Grin, Melissa G. Mendez, and Edward R. Kuczmarski. Intermediate filaments: versatile building blocks of cell structure. *Curr Opin Cell Biol*, 20(1):28–34, Feb 2008. doi: 10.1016/j.ceb.2007.11.003. URL `http://dx.doi.org/10.1016/j.ceb.2007.11.003`.

[76] Mark S. Longtine and Erfei Bi. Regulation of septin organization and function in yeast. *Trends Cell Biol*, 13(8):403–409, Aug 2003.

[77] Elias T. Spiliotis, Stephen J. Hunt, Qicong Hu, Makoto Kinoshita, and W James Nelson. Epithelial polarity requires septin coupling of vesicle transport to polyglutamylated microtubules. *J Cell Biol*, 180(2):295–303, Jan 2008. doi: 10.1083/jcb.200710039. URL `http://dx.doi.org/10.1083/jcb.200710039`.

[78] Brandon E. Kremer, Laura A. Adang, and Ian G. Macara. Septins regulate actin organization and cell-cycle arrest through nuclear accumulation of nck mediated by socs7. *Cell*, 130(5):837–850, Sep 2007. doi: 10.1016/j.cell.2007.06.053. URL `http://dx.doi.org/10.1016/j.cell.2007.06.053`.

[79] P. B. Moore, H. E. Huxley, and D. J. DeRosier. Three-dimensional reconstruction of f-actin, thin filaments and decorated thin filaments. *J Mol Biol*, 50(2):279–295, Jun 1970.

[80] Ana Sarasa-Renedo, Vildan Tunç-Civelek, and Matthias Chiquet. Role of rhoa/rock-dependent actin contractility in the induction of tenascin-c by cyclic tensile strain. *Experimental cell research*, 312(8):1361–1370, 2006.

[81] Marie Evangelista, Sally Zigmond, and Charles Boone. Formins: signaling effectors for assembly and polarization of actin filaments. *J Cell Sci*, 116(Pt 13):2603–2611, Jul 2003. doi: 10.1242/jcs.00611. URL `http://dx.doi.org/10.1242/jcs.00611`.

[82] A. J. Ridley and A. Hall. The small gtp-binding protein rho regulates the assembly of focal adhesions and actin stress fibers in response to growth factors. *Cell*, 70 (3):389–399, Aug 1992.

[83] K. Katoh, Y. Kano, M. Amano, K. Kaibuchi, and K. Fujiwara. Stress fiber organization regulated by mlck and rho-kinase in cultured human fibroblasts. *Am J Physiol Cell Physiol*, 280(6):C1669–C1679, Jun 2001.

[84] Kazuo Katoh, Yumiko Kano, and Yasuko Noda. Rho-associated kinase-dependent contraction of stress fibres and the organization of focal adhesions. *J R Soc Interface*, 8(56):305–311, Mar 2011. doi: 10.1098/rsif.2010.0419. URL `http://dx.doi.org/10.1098/rsif.2010.0419`.

[85] Tony J C. Harris and Mark Peifer. Decisions, decisions: beta-catenin chooses between adhesion and transcription. *Trends Cell Biol*, 15(5):234–237, May 2005. doi: 10.1016/j.tcb.2005.03.002. URL `http://dx.doi.org/10.1016/j.tcb.2005.03.002`.

[86] Stéphanie Pellegrin and Harry Mellor. Actin stress fibres. *J Cell Sci*, 120(Pt 20): 3491–3499, Oct 2007. doi: 10.1242/jcs.018473. URL `http://dx.doi.org/10.1242/jcs.018473`.

[87] M. F. Olson, N. G. Pasteris, J. L. Gorski, and A. Hall. Faciogenital dysplasia protein (fgd1) and vav, two related proteins required for normal embryonic development, are upstream regulators of rho gtpases. *Curr Biol*, 6(12):1628–1633, Dec 1996.

[88] D. L. West. The epitheliomuscular cell of hydra: its fine structure, three-dimensional architecture and relation to morphogenesis. *Tissue Cell*, 10(4):629–646, 1978.

[89] Michael Krahe, Iris Wenzel, Kao-Nung Lin, Julia Fischer, Joseph Goldmann, Markus Kästner, and Claus Fütterer. Fluctuations and differential contraction during regeneration of hydra vulgaris tissue toroids. *New Journal of Physics*, 15 (3):035004, 2013.

[90] illustrated by Nigel Orme Ron Milo, Rob Philips. *Cell biology by the numbers*. Garland Science Taylor and Francis Group, 2015.

[91] A Hall. Rho gtpases and the control of cell behaviour. *Biochemical Society Transactions*, 33(5):891–895, 2005.

[92] G. A. Dunn, D. Zicha, and P. E. Fraylich. Rapid, microtubule-dependent fluctuations of the cell margin. *J Cell Sci*, 110 (Pt 24):3091–3098, Dec 1997.

[93] E. Mandelkow, E. M. Mandelkow, H. Hotani, B. Hess, and S. C. Müller. Spatial patterns from oscillating microtubules. *Science*, 246(4935):1291–1293, Dec 1989.

[94] P Huang, T Senga, and M Hamaguchi. A novel role of phospho-β-catenin in microtubule regrowth at centrosome. *Oncogene*, 26(30):4357–4371, 2007.

[95] Lee A Ligon, Sher Karki, Mariko Tokito, and Erika LF Holzbaur. Dynein binds to β-catenin and may tether microtubules at adherens junctions. *Nature cell biology*, 3(10):913–917, 2001.

[96] Rong Li and Gregg G. Gundersen. Beyond polymer polarity: how the cytoskeleton builds a polarized cell. *Nat Rev Mol Cell Biol*, 9(11):860–873, Nov 2008. doi: 10.1038/nrm2522. URL `http://dx.doi.org/10.1038/nrm2522`.

[97] Athanassios Dovas, Bojana Gligorijevic, Xiaoming Chen, David Entenberg, John Condeelis, and Dianne Cox. Visualization of actin polymerization in invasive structures of macrophages and carcinoma cells using photoconvertible β-actin–dendra2 fusion proteins. *PloS one*, 6(2):e16485, 2011.

[98] Roland Kaunas and Hui-Ju Hsu. A kinematic model of stretch-induced stress fiber turnover and reorientation. *J Theor Biol*, 257(2):320–330, Mar 2009. doi: 10.1016/j.jtbi.2008.11.024. URL `http://dx.doi.org/10.1016/j.jtbi.2008.11.024`.

[99] Franziska Lautenschläger, Stephan Paschke, Stefan Schinkinger, Arlette Bruel, Michael Beil, and Jochen Guck. The regulatory role of cell mechanics for migration of differentiating myeloid cells. *Proc Natl Acad Sci U S A*, 106(37):15696–15701, Sep 2009. doi: 10.1073/pnas.0811261106. URL `http://dx.doi.org/10.1073/pnas.0811261106`.

[100] Nicolas Minc, David Burgess, and Fred Chang. Influence of cell geometry on division-plane positioning. *Cell*, 144(3):414–426, Feb 2011. doi: 10.1016/j.cell.2011.01.016. URL `http://dx.doi.org/10.1016/j.cell.2011.01.016`.

[101] G. G. Gundersen and J. C. Bulinski. Selective stabilization of microtubules oriented toward the direction of cell migration. *Proc Natl Acad Sci U S A*, 85(16): 5946–5950, Aug 1988.

[102] T. A. Cook, T. Nagasaki, and G. G. Gundersen. Rho guanosine triphosphatase mediates the selective stabilization of microtubules induced by lysophosphatidic acid. *J Cell Biol*, 141(1):175–185, Apr 1998.

[103] Gregg G. Gundersen, Edgar R. Gomes, and Ying Wen. Cortical control of microtubule stability and polarization. *Curr Opin Cell Biol*, 16(1):106–112, Feb 2004. doi: 10.1016/j.ceb.2003.11.010. URL `http://dx.doi.org/10.1016/j.ceb.2003.11.010`.

[104] A. M. Malek and S. Izumo. Mechanism of endothelial cell shape change and cytoskeletal remodeling in response to fluid shear stress. *J Cell Sci*, 109 (Pt 4): 713–726, Apr 1996.

[105] Sarah E. Siegrist and Chris Q. Doe. Microtubule-induced cortical cell polarity. *Genes Dev*, 21(5):483–496, Mar 2007. doi: 10.1101/gad.1511207. URL `http://dx.doi.org/10.1101/gad.1511207`.

[106] V. I. Rodionov, F. K. Gyoeva, E. Tanaka, A. D. Bershadsky, J. M. Vasiliev, and V. I. Gelfand. Microtubule-dependent control of cell shape and pseudopodial activity is inhibited by the antibody to kinesin motor domain. *J Cell Biol*, 123(6 Pt 2):1811–1820, Dec 1993.

[107] Michele A. Wozniak and Christopher S. Chen. Mechanotransduction in development: a growing role for contractility. *Nat Rev Mol Cell Biol*, 10(1):34–43, Jan 2009. doi: 10.1038/nrm2592. URL `http://dx.doi.org/10.1038/nrm2592`.

[108] Frederick H Silver and Lorraine M Siperko. Mechanosensing and mechanochemical transduction: how is mechanical energy sensed and converted into chemical energy in an extracellular matrix? *Critical Reviews^{TM} in Biomedical Engineering*, 31(4), 2003.

[109] Jennifer S. Park, Julia S. Chu, Anchi D. Tsou, Rokhaya Diop, Zhenyu Tang, Aijun Wang, and Song Li. The effect of matrix stiffness on the differentiation of mesenchymal stem cells in response to tgf-?. *Biomaterials*, 32(16):3921–3930, Jun 2011. doi: 10.1016/j.biomaterials.2011.02.019. URL `http://dx.doi.org/10.1016/j.biomaterials.2011.02.019`.

[110] Jérémie Dalous, Emmanuel Burghardt, Annette Müller-Taubenberger, Franz Bruckert, Günther Gerisch, and Till Bretschneider. Reversal of cell polarity and actin-myosin cytoskeleton reorganization under mechanical and chemical stimulation. *Biophys J*, 94(3):1063–1074, Feb 2008. doi: 10.1529/biophysj.107.114702. URL `http://dx.doi.org/10.1529/biophysj.107.114702`.

[111] Rebecca G. Wells. Tissue mechanics and fibrosis. *Biochim Biophys Acta*, 1832(7): 884–890, Jul 2013. doi: 10.1016/j.bbadis.2013.02.007. URL `http://dx.doi.org/10.1016/j.bbadis.2013.02.007`.

[112] Isabelle Arnal and Richard H Wade. How does taxol stabilize microtubules? *Current Biology*, 5(8):900–908, 1995.

[113] Mary Ann Jordan and Leslie Wilson. Microtubules as a target for anticancer drugs. *Nature Reviews Cancer*, 4(4):253–265, 2004.

[114] JOSETTE Thuret-Carnahan, Jean-Louis Bossu, Anne Feltz, Keith Langley, and Dominique Aunis. Effect of taxol on secretory cells: functional, morphological, and electrophysiological correlates. *The Journal of cell biology*, 100(6):1863–1874, 1985.

[115] Masayoshi Uehata, Toshimasa Ishizaki, Hiroyuki Satoh, Takashi Ono, Toshio Kawahara, Tamami Morishita, Hiroki Tamakawa, Keiji Yamagami, Jun Inui, Midori Maekawa, et al. Calcium sensitization of smooth muscle mediated by a rho-associated protein kinase in hypertension. *Nature*, 389(6654):990–994, 1997.

[116] Nicola Rath and Michael F Olson. Rho-associated kinases in tumorigenesis: reconsidering rock inhibition for cancer therapy. *EMBO reports*, 13(10):900–908, 2012.

[117] Syed A. Rizvi, Erin M. Neidt, Jiayue Cui, Zach Feiger, Colleen T. Skau, Margaret L. Gardel, Sergey A. Kozmin, and David R. Kovar. Identification and characterization of a small molecule inhibitor of formin-mediated actin assembly. *Chem Biol*, 16(11):1158–1168, Nov 2009. doi: 10.1016/j.chembiol.2009.10.006. URL `http://dx.doi.org/10.1016/j.chembiol.2009.10.006`.

[118] S. MacLean-Fletcher and T. D. Pollard. Mechanism of action of cytochalasin b on actin. *Cell*, 20(2):329–341, Jun 1980.

[119] WO Friesen and GD Block. What is a biological oscillator? *American Journal of Physiology-Regulatory, Integrative and Comparative Physiology*, 246(6):R847–R853, 1984.

[120] Till Roenneberg, Zdravko Dragovic, and Martha Merrow. Demasking biological oscillators: properties and principles of entrainment exemplified by the neurospora circadian clock. *Proc Natl Acad Sci U S A*, 102(21):7742–7747, May 2005. doi: 10.1073/pnas.0501884102. URL `http://dx.doi.org/10.1073/pnas.0501884102`.

[121] Karsten Kruse and Daniel Riveline. Spontaneous mechanical oscillations: implications for developing organisms. *Curr Top Dev Biol*, 95:67–91, 2011. doi: 10.1016/B978-0-12-385065-2.00003-7. URL `http://dx.doi.org/10.1016/B978-0-12-385065-2.00003-7`.

[122] Sven K. Vogel, Nenad Pavin, Nicola Maghelli, Frank Jülicher, and Iva M. Toli?-Nørrelykke. Self-organization of dynein motors generates meiotic nuclear oscillations. *PLoS Biol*, 7(4):e1000087, Apr 2009. doi: 10.1371/journal.pbio.1000087. URL `http://dx.doi.org/10.1371/journal.pbio.1000087`.

[123] James W Cooley, Peter AW Lewis, and Peter D Welch. The fast fourier transform and its applications. *Education, IEEE Transactions on*, 12(1):27–34, 1969.

[124] Jordi Soriano, Sten Rüdiger, Pramod Pullarkat, and Albrecht Ott. Mechanogenetic coupling of hydra symmetry breaking and driven turing instability model. *Biophys J*, 96(4):1649–1660, Feb 2009. doi: 10.1016/j.bpj.2008.09.062. URL `http://dx.doi.org/10.1016/j.bpj.2008.09.062`.

[125] F. Jülicher2 C. Fütterer1, C. Colombo1 and A. Ott3. Morphogenetic oscillations during symmetry breaking of regenerating hydra vulgaris cells. *EUROPHYSICS LETTERS*, 64(1):pp. 137–143, 2003.

[126] Hui-Ju Hsu, Chin-Fu Lee, and Roland Kaunas. A dynamic stochastic model of frequency-dependent stress fiber alignment induced by cyclic stretch. In *ASME 2009 Summer Bioengineering Conference*, pages 95–96. American Society of Mechanical Engineers, 2009.

[127] Celina E Juliano and Bert Hobmayer. Meeting report on "animal evolution: New perspectives from early emerging metazoans", tutzing, september 14–17, 2015. *BioEssays*, 2016.

[128] Udo Seifert, Karin Berndl, and Reinhard Lipowsky. Shape transformations of vesicles: Phase diagram for spontaneous-curvature and bilayer-coupling models. *Physical Review A*, 44(2):1182, 1991.

[129] Michael Krahe, Claus Fütterer, Kao-Nung Lin, Iris Wenzel, and Julia Fischer. Fluctuations and symmetry breaking during regeneration of hydra vulgaris tissue toroids. Technical report, Institut für Experimentelle Physik I, Universität Leipzig, Linnéstrasse 5, 04103 Leipzig, Germany, 2012.

[130] Y. Nakajima and R. D. Burke. The initial phase of gastrulation in sea urchins is accompanied by the formation of bottle cells. *Dev Biol*, 179(2):436–446, Nov 1996. doi: 10.1006/dbio.1996.0273. URL `http://dx.doi.org/10.1006/dbio.1996.0273`.

[131] Sari Tojkander, Gergana Gateva, and Pekka Lappalainen. Actin stress fibers–assembly, dynamics and biological roles. *Journal of cell science*, 125(8):1855–1864, 2012.

[132] Suat Ozbek. The cnidarian nematocyst: a miniature extracellular matrix within a secretory vesicle. *Protoplasma*, 248(4):635–640, Oct 2011. doi: 10.1007/s00709-010-0219-4. URL `http://dx.doi.org/10.1007/s00709-010-0219-4`.

[133] Harvey Lodish and S Lawrence Zipursky. Molecular cell biology. *Biochemistry and Molecular Biology Education*, 29:126–133, 2001.

[134] Woojin M Han, Su-Jin Heo, Tristan P Driscoll, Lachlan J Smith, Robert L Mauck, and Dawn M Elliott. Macro-to microscale strain transfer in fibrous tissues is heterogeneous and tissue-specific. *Biophysical journal*, 105(3):807–817, 2013.

[135] A Shingleton. Allometry: the study of biological scaling. *Nature Education Knowledge*, 3(10):2, 2010.

[136] Tadanori Mammoto and Donald E Ingber. Mechanical control of tissue and organ development. *Development*, 137(9):1407–1420, 2010.

[137] Jochen Kursawe, Pavel A Brodskiy, Jeremiah J Zartman, Ruth E Baker, and Alexander George Fletcher. Capabilities and limitations of tissue size control through passive mechanical forces. *bioRxiv*, page 023184, 2015.

[138] Davide Ambrosi, Viola Pettinati, and Pasquale Ciarletta. Active stress as a local regulator of global size in morphogenesis. *International Journal of Non-Linear Mechanics*, 2014.

[139] Gretchen Vogel. Mysteries of development. how do organs know when they have reached the right size? *Science*, 340(6137):1156–1157, Jun 2013. doi: 10.1126/science.340.6137.1156-b. URL `http://dx.doi.org/10.1126/science.340.6137.1156-b`.

[140] D Kacy Cullen, Crystal M Simon, and Michelle C LaPlaca. Strain rate-dependent induction of reactive astrogliosis and cell death in three-dimensional neuronal–astrocytic co-cultures. *Brain research*, 1158:103–115, 2007.

[141] Dirk Kaiser, Mark-Andre Freyberg, and Peter Friedl. Lack of hemodynamic forces triggers apoptosis in vascular endothelial cells. *Biochemical and biophysical research communications*, 231(3):586–590, 1997.

[142] Brenton D Hoffman, Gladys Massiera, Kathleen M Van Citters, and John C Crocker. The consensus mechanics of cultured mammalian cells. *Proc Natl Acad Sci U S A*, 103(27):10259–10264, Jul 2006. doi: 10.1073/pnas.0510348103. URL `http://dx.doi.org/10.1073/pnas.0510348103`.

[143] Catherine E Morris. Mechanosensitive ion channels. *Journal of Membrane Biology*, 113(2):93–107, 1990.

[144] Boris Martinac, J Adler, and C Kung. Mechanosensitive ion channels. *Part A*, 58: 29–57, 2007.

[145] Ingo Müller and Henning Struchtrup. Inflating a rubber balloon. *Mathematics and Mechanics of Solids*, 7(5):569–577, 2002.

[146] Per Bak, Chao Tang, Kurt Wiesenfeld, et al. Self-organized criticality: An explanation of 1/f noise. *Physical Review Letters*, 59(4):381–384, 1987.

[147] Jean-René Huynh and Daniel St Johnston. The origin of asymmetry: early polarisation of the drosophila germline cyst and oocyte. *Current Biology*, 14(11): R438–R449, 2004.

[148] R. K. Josephson, J. G. Malamud, and D. R. Stokes. Power output by an asynchronous flight muscle from a beetle. *J Exp Biol*, 203(Pt 17):2667–2689, Sep 2000.

[149] Otger Campàs and Pierre Sens. Chromosome oscillations in mitosis. *Phys Rev Lett*, 97(12):128102, Sep 2006.

[150] Cleopatra Kozlowski, Martin Srayko, and Francois Nedelec. Cortical microtubule contacts position the spindle in c. elegans embryos. *Cell*, 129(3):499–510, May 2007. doi: 10.1016/j.cell.2007.03.027. URL `http://dx.doi.org/10.1016/j.cell.2007.03.027`.

[151] Stefan Günther and Karsten Kruse. Spontaneous sarcomere dynamics. *Chaos*, 20(4):045122, Dec 2010. doi: 10.1063/1.3523283. URL `http://dx.doi.org/10.1063/1.3523283`.

[152] Adam C. Martin, Matthias Kaschube, and Eric F. Wieschaus. Pulsed contractions of an actin-myosin network drive apical constriction. *Nature*, 457(7228): 495–499, Jan 2009. doi: 10.1038/nature07522. URL `http://dx.doi.org/10.1038/nature07522`.

[153] Karine Guevorkian, David Gonzalez-Rodriguez, Camille Carlier, Sylvie Dufour, and Françoise Brochard-Wyart. Mechanosensitive shivering of model tissues under controlled aspiration. *Proc Natl Acad Sci U S A*, 108(33):13387–13392, Aug 2011. doi: 10.1073/pnas.1105741108. URL `http://dx.doi.org/10.1073/pnas.1105741108`.

[154] Adam J. Engler, Shamik Sen, H Lee Sweeney, and Dennis E. Discher. Matrix elasticity directs stem cell lineage specification. *Cell*, 126(4):677–689, Aug 2006. doi: 10.1016/j.cell.2006.06.044. URL `http://dx.doi.org/10.1016/j.cell.2006.06.044`.

[155] Jeremy T Smyth, Wayne I DeHaven, Gary S Bird, and James W Putney. Role of the microtubule cytoskeleton in the function of the store-operated ca2+ channel activator stim1. *Journal of cell science*, 120(21):3762–3771, 2007.

[156] Javier Camacho, Araceli Sánchez, Walter Stühmer, and Luis A Pardo. Cytoskeletal interactions determine the electrophysiological properties of human eag potassium channels. *Pflügers Archiv*, 441(2-3):167–174, 2000.

[157] Hans R Bode. The head organizer in hydra. *International Journal of Developmental Biology*, 56(6):473, 2012.

[158] A Boulbitch, R Simson, DA Simson, R Merkel, W Häckl, M Bärmann, and E Sackmann. Shape instability of a biomembrane driven by a local softening of the underlying actin cortex. *Physical review E*, 62(3):3974, 2000.

[159] Brian Mickey and Jonathon Howard. Rigidity of microtubules is increased by stabilizing agents. *The Journal of cell biology*, 130(4):909–917, 1995.

[160] Jian Zhou, Hye Young Kim, James H-C Wang, and Lance A Davidson. Macroscopic stiffening of embryonic tissues via microtubules, rhogef and the assembly of contractile bundles of actomyosin. *Development*, 137(16):2785–2794, 2010.

[161] Xiaowei Deng and Sergio Pellegrino. Wrinkling of orthotropic viscoelastic membranes. *AIAA journal*, 50(3):668–681, 2012.

[162] RC Geiger, W Taylor, MR Glucksberg, and DA Dean. Cyclic stretch-induced reorganization of the cytoskeleton and its role in enhanced gene transfer. *Gene therapy*, 13(8):725–731, 2006.

[163] Simon Jungbauer, Huajian Gao, Joachim P Spatz, and Ralf Kemkemer. Two characteristic regimes in frequency-dependent dynamic reorientation of fibroblasts on cyclically stretched substrates. *Biophysical journal*, 95(7):3470–3478, 2008.

[164] Pablo Fernández and Albrecht Ott. Single cell mechanics: stress stiffening and kinematic hardening. *Phys Rev Lett*, 100(23):238102, Jun 2008.

[165] Pablo Fernández, Pramod A Pullarkat, and Albrecht Ott. A master relation defines the nonlinear viscoelasticity of single fibroblasts. *Biophysical journal*, 90(10):3796–3805, 2006.

[166] Hossein Ahmadzadeh, Douglas H Smith, and Vivek B Shenoy. Viscoelasticity of tau proteins leads to strain rate-dependent breaking of microtubules during axonal stretch injury: predictions from a mathematical model. *Biophysical journal*, 106 (5):1123–1133, 2014.

[167] Hossein Ahmadzadeh, Douglas H Smith, and Vivek B Shenoy. Mechanical effects of dynamic binding between tau proteins on microtubules during axonal injury. *Biophysical journal*, 109(11):2328–2337, 2015.

[168] Mary Constance Lane and Ray Keller. Microtubule disruption reveals that spemann's organizer is subdivided into two domains by the vegetal alignment zone. *Development*, 124(4):895–906, 1997.

[169] M Kühl. The wnt/calcium pathway: biochemical mediators, tools and future requirements. *Frontiers in bioscience: a journal and virtual library*, 9:967–974, 2004.

[170] Kristen M Kwan and Marc W Kirschner. A microtubule-binding rho-gef controls cell morphology during convergent extension of xenopus laevis. *Development*, 132 (20):4599–4610, 2005.

[171] Virginia Ballotta, Anita Driessen-Mol, Carlijn VC Bouten, and Frank PT Baaijens. Strain-dependent modulation of macrophage polarization within scaffolds. *Biomaterials*, 35(18):4919–4928, 2014.

[172] David J Odde, Le Ma, Amelie H Briggs, Alyssa DeMarco, and Marc W Kirschner. Microtubule bending and breaking in living fibroblast cells. *Journal of cell science*, 112(19):3283–3288, 1999.

[173] Dennis E Discher, Paul Janmey, and Yu-li Wang. Tissue cells feel and respond to the stiffness of their substrate. *Science*, 310(5751):1139–1143, 2005.

[174] James H-C Wang, Pascal Goldschmidt-Clermont, Jeremiah Wille, and Frank C-P Yin. Specificity of endothelial cell reorientation in response to cyclic mechanical stretching. *Journal of biomechanics*, 34(12):1563–1572, 2001.

[175] Li He, Xiaobo Wang, Ho Lam Tang, and Denise J. Montell. p. *Nat Cell Biol*, 12 (12):1133–1142, Dec 2010. doi: 10.1038/ncb2124. URL `http://dx.doi.org/10.1038/ncb2124`.

[176] Roland Kaunas, Shunichi Usami, and Shu Chien. Regulation of stretch-induced jnk activation by stress fiber orientation. *Cell Signal*, 18(11):1924–1931, Nov 2006. doi: 10.1016/j.cellsig.2006.02.008. URL `http://dx.doi.org/10.1016/j.cellsig.2006.02.008`.

[177] Roland Kaunas, Phu Nguyen, Shunichi Usami, and Shu Chien. Cooperative effects of rho and mechanical stretch on stress fiber organization. *Proc Natl Acad Sci U S A*, 102(44):15895–15900, Nov 2005. doi: 10.1073/pnas.0506041102. URL `http://dx.doi.org/10.1073/pnas.0506041102`.

[178] Keith Burridge and Christophe Guilluy. Focal adhesions, stress fibers and mechanical tension. *Experimental cell research*, 2015.

[179] Lee A. Ligon and Erika L F. Holzbaur. Microtubules tethered at epithelial cell junctions by dynein facilitate efficient junction assembly. *Traffic*, 8(7):808–819, Jul 2007. doi: 10.1111/j.1600-0854.2007.00574.x. URL `http://dx.doi.org/10.1111/j.1600-0854.2007.00574.x`.

[180] Mukund Gupta, Bibhu Ranjan Sarangi, Joran Deschamps, Yasaman Nematbakhsh, Andrew Callan-Jones, Felix Margadant, René-Marc Mège, Chwee Teck Lim, Raphaël Voituriez, and Benoît Ladoux. Adaptive rheology and ordering of cell cytoskeleton govern matrix rigidity sensing. *Nature communications*, 6, 2015.

[181] Jérôme Solon, Ilya Levental, Kheya Sengupta, Penelope C Georges, and Paul A Janmey. Fibroblast adaptation and stiffness matching to soft elastic substrates. *Biophysical journal*, 93(12):4453–4461, 2007.

[182] Matthew R Stachowiak and Ben O'Shaughnessy. Recoil after severing reveals stress fiber contraction mechanisms. *Biophysical journal*, 97(2):462–471, 2009.

[183] Maryse Leost, Christiane Schultz, Andreas Link, Yong-Zhong Wu, Jacek Biernat, Eva-Maria Mandelkow, James A Bibb, Gretchen L Snyder, Paul Greengard, Daniel W Zaharevitz, et al. Paullones are potent inhibitors of glycogen synthase kinase-3β and cyclin-dependent kinase 5/p25. *European Journal of Biochemistry*, 267(19):5983–5994, 2000.

[184] Jenny Bain, Lorna Plater, Matt Elliott, Natalia Shpiro, C James Hastie, Hilary Mclauchlan, Iva Klevernic, J Simon C Arthur, Dario R Alessi, and Philip Cohen. The selectivity of protein kinase inhibitors: a further update. *Biochemical Journal*, 408(3):297–315, 2007.

[185] Richard Harland and John Gerhart. Formation and function of spemann's organizer. *Annual review of cell and developmental biology*, 13(1):611–667, 1997.

[186] Clemens Kiecker and Christof Niehrs. The role of wnt signaling in vertebrate head induction and the organizer-gradient model dualism. *Madame Curie Bioscience Database*, 2000.

[187] Catriona Y Logan and Roel Nusse. The wnt signaling pathway in development and disease. *Annu. Rev. Cell Dev. Biol.*, 20:781–810, 2004.

[188] Yukio Nakamura, Charisios D Tsiairis, Suat Özbek, and Thomas W Holstein. Autoregulatory and repressive inputs localize hydra wnt3 to the head organizer. *Proceedings of the National Academy of Sciences*, 108(22):9137–9142, 2011.

[189] Moritz Mercker, Dirk Hartmann, and Anna Marciniak-Czochra. A mechanochemical model for embryonic pattern formation: coupling tissue mechanics and morphogen expression. *PLoS One*, 8(12):e82617, 2013. doi: 10.1371/journal.pone.0082617. URL `http://dx.doi.org/10.1371/journal.pone.0082617`.

[190] Suat Özbek, Prakash G Balasubramanian, Ruth Chiquet-Ehrismann, Richard P Tucker, and Josephine C Adams. The evolution of extracellular matrix. *Molecular biology of the cell*, 21(24):4300–4305, 2010.